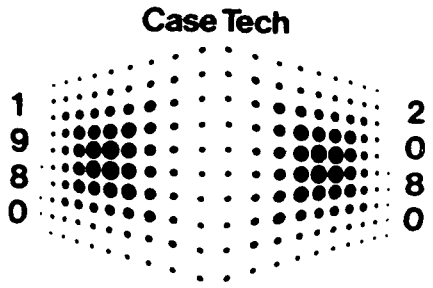

MUTUAL COUPLING EFFECTS
IN ANTENNA ARRAYS

FINAL TECHNICAL REPORT
Vol. I of 2

Prepared For
NASA LEWIS RESEARCH CENTER
Cleveland, Ohio

REPORT WGR-86-4: GRANT NAG3-291. Mar. 1986

ELECTROMAGNETIC WAVES AND WAVE PROPAGATION REPORT

(NASA-CR-176699) MUTUAL COUPLING EFFECTS IN ANTENNA ARRAYS, VOLUME 1 Final Technical Report, 15 May 1982 - 31 Mar. 1986 (Case Western Reserve Univ.) 178 p EC A09/MF A01 CSCL 20N G3/32

N86-22782

Unclas
05885

Department of Electrical Engineering
and
Applied Physics
Case Institute of Technology
Case Western Reserve University
University Circle
Cleveland, Ohio 44106

MUTUAL COUPLING EFFECTS IN ANTENNA ARRAYS

FINAL TECHNICAL REPORT
Vol. I of 2

Prepared For
NASA LEWIS RESEARCH CENTER
Cleveland, Ohio

REPORT WGR-86-4: GRANT NAG3-291. Mar. 1986

PRINCIPAL INVESTIGATOR: R.E.Collin
CASE WESTERN RESERVE UNIVERSITY
CLEVELAND, OHIO, 44106

NASA TECHNICAL MONITOR: Jerry Smetana
Period Covered: 5/15/82 to 3/31/86

MUTUAL COUPLING IN FINITE

ARRAYS OF RECTANGULAR APERTURES

Abstract

by

JOHN WILLIAM SILVESTRO

The mutual coupling between rectangular apertures in a finite antenna array, in an infinite ground plane, is analyzed using the vector potential approach. The method of moments is used to solve the equations that result from setting the tangential magnetic fields across each aperture equal. The approximation uses a set of vector potential modal functions to solve for equivalent magnetic currents. A computer program was written to carry out this analysis and the resulting currents were used to determine the co- and cross-polarized far zone radiation patterns.

Numerical results for various arrays using several modes in the approximation are presented. Results for one and two aperture arrays are compared against published data to check on the agreement of this model with previous work. Computer derived results are also compared against experimental results to test the model's accuracy. These tests of the program's accuracy showed that it yields valid data.

A look at the effects of mutual coupling in modest sized arrays and a short discussion on the beam scanning properties of three aperture arrays are also presented. Included with this data are results

for the first order coupling theory for small arrays. This theory assumes that the coupling of energy back to the source due to the re-radiation of nearby undriven apertures is small enough to be dropped from the analysis. The tests showed good agreements with the theory and are presented here for future use in the study of possible approximation techniques.

ACKNOWLEDGEMENT

I would like to express sincere appreciation to my advisor, Dr. R.E. Collin, whose help and immense mathematical knowledge were invaluable to this work. A good deal of the theoretical and mathematical manipulation, especially the change of variable used in the integral reduction and the general Fourier transform method, were either his or brought to my attention by him.

I also wish to thank Dr. J. Mathews who allowed me access to his computer terminals and equipment at all hours and to his graduate students Jim Breakall, Tim Tucker and Wen-Ping Ying and also Georg Karawas whose computer expertise was of considerable help in the writing of the computer program. I also want to thank my Thesis Committee, Dr. J. Mathews and Dr. A. Ferendeci for taking the time to review this document. This work was done under a grant from NASA-Lewis Research Center. I am also thankful to Vicki Gilbert who typed this document.

Finally I am most grateful to my wife for her support and inspiration which enabled me to return to school and also to my parents whose guidance made this all possible.

TABLE OF CONTENTS

LIST OF SYMBOLS

$\underline{a}_x$, $\underline{a}_y$, $\underline{a}_z$	Unit vectors in x, y, z direction
β_{nm}	Waveguide propagation constant
$\underline{\nabla}_t$	$\underline{a}_x \frac{\partial}{\partial x} + \underline{a}_y \frac{\partial}{\partial y}$
δ_{pn}	Kronecker Delta = $1 \begin{cases} p = n \\ 0 \begin{cases} p \neq n \end{cases} \end{cases}$
ϵ_{0n}	Neuman Factor = $1 \begin{cases} n = 0 \\ 2 \begin{cases} n > 0 \end{cases} \end{cases}$
ϵ_0	Permittivity in Free space
$\underline{E}$	Electric field vector
$\underline{e}_{e,nm}$	TE Modal function
$\underline{e}_{h,nm}$	TM Modal function
$\underline{H}$	Magnetic field vector
$\underline{J}_m$	Equivalent magnetic current
$\underline{J}_e$	Electric current
j	$\sqrt{-1}$
k_0	Free space wave number
k_x	Fourier transform variable with respect to x
k_y	Fourier transform variable with respect to y
λ	Free space wavelength
μ_o	Permeability in free space
S_{ij}	Scattering matrix parameter

Γ	Reflection coefficient
ω	Angular frequency in radians per second
$Y_{e,nm}$	TE Waveguide admittance
$Y_{h,nm}$	TM Waveguide admittance

CHAPTER 1

INTRODUCTION AND REVIEW OF PAST WORK

1.1 Introduction

It is projected that the growth of the satellite communication service will result in saturation of the existing frequency bands (C through Ku), by the end of this decade. In hopes of relieving this situation NASA is currently supporting research into the development of a 30/20 GHz satellite communication system. The aim of this work is to develop the technology necessary to make the use of these higher frequencies possible and at the same time to develop a more efficient system. In order to accomplish the latter, the satellite's antenna will have to provide narrow spot beams that are either fixed or scanned. With these spot beams, the antenna can service small areas individually, instead of targeting the entire country. This way each frequency can be reused in non-adjacent areas and thus increase the system's capacity. The projected antenna would allow for individual control of the phase and power level of each array element. The objective is to produce a scanning spot beam that has low sidelobe levels, sufficient gain, minimum cross polarization and with minimum cross talk between beams. To aide in this design work, a considerable amount of computer modeling is needed in order to evaluate the effects of mutual coupling between the array elements on the above characteristics. This report presents a model developed to analyze the effects of mutual coupling in arrays of rectangular waveguides. The computer codes that were developed can be used to

aid in the design and development of modest array systems by solving for the radiation patterns, reflection coefficient and inter-element coupling coefficients.

One of the problems that arises in the design of array antennas is that as radiating elements are placed close together the mutual coupling will change the radiation characteristic of each element. The effects of this coupling on an array are threefold: 1) changes in the total radiation pattern, 2) changes in the radiation impedance of the elements and, 3) variations in the polarization characteristics (Amitay, Galindo and Wu, 1972). The pattern affects can be very pronounced. Sharp spurious nulls have been found experimentally in large arrays (ibid) at certain scan angles.

There are several techniques or approaches that may be used for solving for mutual coupling and each has it's own strengths and weaknesses. In this report the vector potential approach is used. This method is described in Chap. 2 along with a brief overview of some of the other approaches that may also be used. The vector potential method, as presented, uses the method of moments solution with vector potential modal functions as both basis and testing functions. These modal functions are used to approximate the equivalent surface magnetic currents in the apertures. Once these currents are known, the radiation patterns and scattering parameters can be solved for.

The numerical results from computer analysis of various sized antenna arrays with mutual coupling are presented in later chapters. The single aperture antenna is used to determine the number of modes

necessary for reasonable accuracy. The two and three aperture array results illustrate the coupling effects and are used as a basis for a first order coupling theory. Modest sized arrays are briefly looked at to consider the problem of coupling in larger arrays. Finally, results from experimental tests that were performed on a 2 element array are compared against computed data to verify the accuracy of the analytical work. Much of the computer data presented in this report deals with the testing of the first order coupling hypothesis. This hypothesis assumes that for a given array the mutual coupling can be solved for by assuming only coupling from a driven guide to it's undriven neighboring guides and not back again. With this approximation it should be possible to reduce the computational time needed to analyze large arrays. These results are presented here and will be used at a later time to formulate a technique for use in analyzing large arrays.

The numerical and experimental results that have been obtained here are compared against both published and experimental results obtained by others. The validity of the analysis and the numerical results was thereby established. It appears that acceptable accuracy can be obtained using relatively few modes for the expansion of the magnetic current in each aperture.

1.2 Review of Past Work

A number of authors have studied mutual coupling effects in finite arrays composed of circular or rectangular waveguide apertures in a large ground plane. Mailloux (Mailloux, Jan. 1969) studied the

coupling between two rectangular waveguides using a vector potential approach. He assumed that no cross polarized aperture fields were excited. The self-admittance of a single waveguide and the coupled power between two waveguides were solved for and for some cases were compared against experimental data.

The Fourier transform method (solving for the fields in the transform domain) was used by Borgiotti (Borgiotti, May, 1968) and then expanded on by Bailey (Bailey, 1972). The former obtained an expression for the mutual admittance between two identical apertures in the form of a Fourier transform of a function related to the radiation pattern of each element. Bailey started with the same basic coupling equation as used by Borgiotti and developed a general expression that is applicable to apertures that are not identical in shape or excitation. He also included the case where a planar stratified region outside the aperture existed (i.e. a plasma layer). He computed the TE_{11} to TE_{11} mode coupling between two circular apertures as a function of spacing. The reflection coefficient for a central and edge element in an array of 183 elements was also evaluated as a function of scan angle. Higher order mode coupling was treated in a limited way.

Cha and Hsiao considered the coupling between rectangular apertures in terms of an aperture field expansion in TE_{nm} and TM_{nm} modes (Cha and Hsiao, 1974). The reflection coefficient for a central element in a 19 x 19 array was evaluated.

Luzwick and Harrington also considered the problem of coupling between rectangular guides and used an expansion of the aperture field

in terms of TE_{nm} and TM_{nm} modes (Luzwick and Harrington, 1982). They present some numerical results based on a single basis function in each aperture with the aperture and waveguide of different sizes. The coupling between 2 identical apertures and the coupled power in a 49 element array with a single driven element were evaluated.

Steyskal (Steyskal, 1974) used a method similar to that of Luzwick and Harrington to solve for the coupling between circular apertures. The coupling coefficients for the center element of a 127 element array were evaluated and compared against measured values.

Fenn, Thiele and Munk studied the coupling in rectangular aperture arrays using pulse and peice-wise continuous sinusoidal localized basis functions (Fenn, Thiele and Munk, 1982). Cross polarized basis functions were also included. The numerical computations were limited to the calculation of the input reflection coefficient for a single waveguide in an infinite ground plane, and for the edge and center elements of an 11 x 11 array as a function of scan angle for both E and H plane scans.

Mailloux (Mailloux, Nov. 1969) studied the coupling of cross-polarized radiation between two square apertures and found that for certain orientations this is as large as the co-polarized coupling. The results for two aperture coupling were compared against experimental data.

The above investigations have provided an excellent theoretical foundation for the analysis of mutual coupling effects. However, the numerical results were limited in both accuracy and scope and did not provide sufficient data for the design of high performance arrays.

Some of the major deficiences in much of this work are:

1. Limited number of modes in aperture field expansions.
2. Cross-polarization aperture fields are neglected.
3. Lack of analysis of the beam forming properties of the array and the beam patterns.
4. Lack of analysis of the effect of mutual coupling on the co-polarization and the cross-polarization of the beam.
5. No consideration of the effects of mismatched waveguide sources on the radiation patterns.

CHAPTER 2

ANALYSIS OF MUTUAL COUPLING

2.1 Introduction

This chapter will present an overview of various methods that have been used to solve for mutual coupling in antenna arrays that have a finite number of apertures. The method chosen for use in the computer model described here, the vector potential approach, will be discussed in detail (Sec. 2.4) along with a brief look at three other techniques that were considered. The overview of these three methods, included here for completeness, will include a short discussion of their respective strengths and weaknesses, and the reasons why each wasn't chosen. The three are: Fourier transform approach (Sec. 2.2), expansion in terms of TE or TM modes and piece-wise sinusoidal patches (Sec. 2.3) The latter two use the method of moments, much like the vector potential approach, to solve the $\underline{H}$ field equations. The Fourier transform approach solves for the modal amplitudes in the transform domain.

Following the discussion of the vector potential approach there will be a section on the needed mathematical techniques used to reduce the integral equations, along with one on the method used to derive the scattering parameters and radiation patterns. There will also be a section on a possible technique for approximating the mutual coupling. It solves for the first order coupling between a driven element and it's neighboring elements. Its use could reduce the computational time necessary to solve a coupling problem.

Figure 2.1 shows the basic problem to be analyzed in the following sections along with it's coordinate system. A perfectly conducting

ground plane that covers the entire z=0 plane has a finite set of apertures cut in it. The apertures have H-plane lengths of a and E-plane widths of b. These apertures are waveguides terminating on the ground plane. The waveguides are individually driven by matched sources in the z<0 region. The z>0 space is assumed to be free of reflecting obstructions.

The assumption of matched sources will be relaxed later on. Also in practice a finite ground plane is used. The affects associated with a finite ground plane are not treated in this report.

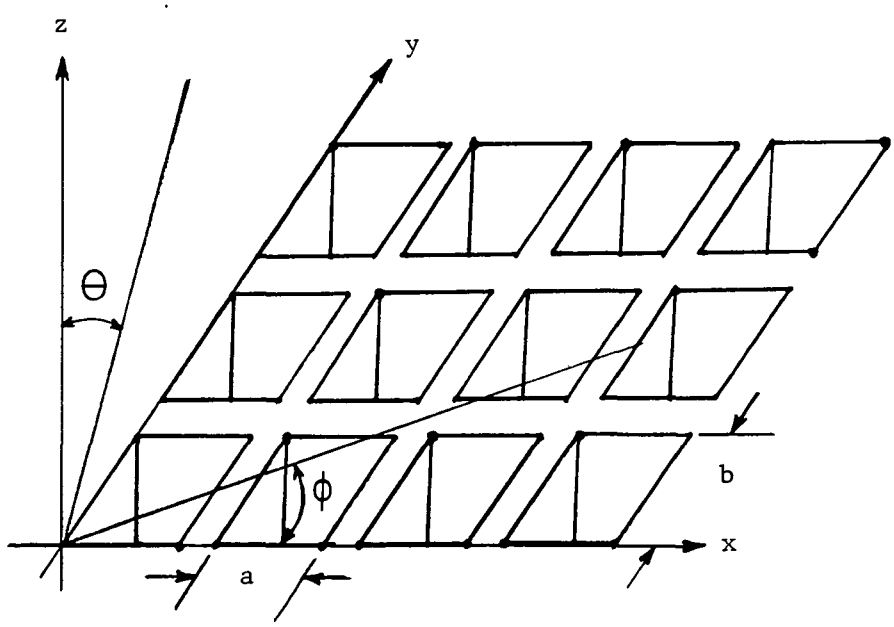

Figure 2.1 General Problem

2.2 Fourier Transform Approach

The Fourier transform approach solves for the aperture fields in the transform domain. The reason for using this method is that it results in some simplification of the equations to a form that is easier to work with from an analytical point of view. Since there are several approaches to the problem, a brief overview of one that appeared in the literature will be presented along with a general procedure that matches free space fields to the guide fields.

The first approach is the one used by Bailey to solve for the coupling between circular apertures (Bailey, 1972). It starts by representing the transverse aperture fields as the sum of waveguide modal fields:

$$\underline{E}_t = \sum_q V_q' \underline{e}_q' + \sum_q V_q'' \underline{e}_q'' \qquad (2.1)$$

$$\underline{H}_t = \sum_q I_q' \underline{h}_q' + \sum_q I_q'' \underline{h}_q''$$

The $\underline{h}_q'$ and $\underline{e}_q'$ are the TE modal functions and the $\underline{h}_q''$ and $\underline{e}_q''$ are the TM functions. Using the fact that the energy for each mode propagates independently the equations are set up by assuming that each modal field is fed by a seperate source. This corresponds to an equivalent microwave network of N ports where N equals the product of the number of modes per aperture and the number of apertures. In matrix form the coupling is represented as:

$$[I]_{NX1} = [Y]_{NXN}[V]_{NX1} \qquad (2.2)$$

from which the scattering matrix is readily found to be given by:

$$[S] = \left[[Y_0] - [Y]\right] \left[[Y_0] + [Y]\right]^{-1} \tag{2.3}$$

where

$[Y_0]$ = diagonal matrix of waveguide mode characteristic admittances.

$[Y]$ = coupling admittance matrix.

$[V]$ = equivalent voltage vector.

$[I]$ = equivalent current vector.

Once the admittance matrix [Y] has been determined, the scattering matrix can be found.

The elements of the admittance matrix are found by solving the electromagnetic reaction integral (Harrington, 1961).

$$Y_{i,j} = \frac{1}{V_i V_j} \iint_{S_i} [\underline{E}^i \times \underline{H}^j] \cdot \underline{a}_z \, dS_i \tag{2.4}$$

where $Y_{i,j} = \frac{I_i}{V_j}$ = coupling between the i and j modes

S_i = surface of the aperture in i^{th} waveguide

When the Fourier transform of the terms in the integral are introduced it is found that:

$$Y_{i,j} = \frac{1}{V_i V_j} \frac{1}{(2\pi)^2} \int_{-\infty}^{\infty}\int_{-\infty}^{\infty} [\underline{E}^i(k_x,k_y) \times \underline{H}^j(-k_x,k_y)] \cdot \underline{a}_z \, dk_x dk_y \tag{2.5}$$

where $\underline{E}(k_x,k_y)$ and $\underline{H}(-k_x,-k_y)$ are the Fourier transforms of the $\underline{E}$ and $\underline{H}$ fields. By solving for $\underline{H}$ and $\underline{E}$ in terms of their vector

potentials, a double integral of a term composed of only the transformed E field results. After further manipulation the final integral for Y_{ij} must generally then be evaluated numerically.

After numerically solving these equations for the admittance matrix, Bailey substituted it into (2.3) to find the scattering matrix [S]. Then using the S_{ij} terms ($i \neq j$), the coupled power between the array elements can be found.

The second method illustrating a general approach to the mutual coupling problem using Fourier transforms is outlined below. Some of the steps and procedures outlined here can also be found in the references (Collin and Zucker, 1969).

Initially, we consider a single aperture and define the transverse fields of the aperture in terms of modal functions in the following form (where R is the reflection coefficient):

$$\underline{E}_a(x,y)=V^+_{e,10}(1+R)\underline{e}_{e,10}+ \sum_{n,m}{}'' \; V^-_{e,nm}\underline{e}_{e,nm} + \sum_{n,m} V^-_{h,nm}\,\underline{e}_{h,nm} \qquad (2.6)$$

where $V^+_{e,10}$ is the amplitude of the incident dominant mode, and $V^-_{e,nm}$, $V^-_{h,nm}$ are amplitudes of the reflected TE and TM modes, also $\sum_{nm}{}''$ signifies the sum over all nm except n=1, m=0. The free space ($z>0$) field is a solution of:

$$(\underline{\nabla}^2 + k_0^2)\,\underline{E} = 0 \qquad (2.7)$$

which in the transform domain is:

$$(k_0^2 - k_t^2 + \frac{\partial^2}{\partial z^2})\,\underline{E}(k_x,k_y,z) = 0$$

where $k_t^2 = k_x^2 + k_y^2$ and $\underline{E}(k_x, k_y, z)$ is the transform of $\underline{E}(x,y,z)$. This gives $\underline{E}$ in the form:

$$\underline{E}(k_x, k_y, z) = \underline{F}(k_x, k_y)\, e^{-jk_z z},\ z \geq 0 \tag{2.8}$$

where $k_z = \sqrt{k_0^2 - k_t^2}$. At $z = 0$ the transverse part $\underline{F}_t(k_x, k_y)$ equals the Fourier transform of the aperture field expressed by (2.6). The z component of $\underline{F}$ is obtained by using $\nabla \cdot \underline{E} = 0$ in the transform domain Thus,

$$\underline{k} \cdot \underline{F}(k_x, k_y) = \underline{k}_t \cdot \underline{F}_t + k_z F_z = 0$$

or

$$F_z = \frac{-\underline{k}_t \cdot \underline{F}_t}{k_z} \tag{2.9}$$

When we solve for the transformed $\underline{H}$ field using $\nabla \times \underline{E} = -j\omega\mu_0 \underline{H}$ we obtain

$$-jk_0 Z_0 \underline{H}(k_x, k_y) = -j\underline{k} \times \underline{F} \tag{2.10}$$

After further manipulation the transverse part is found to be

$$\underline{H}_a(k_x, k_y) = \frac{-Y_0 \left[k_0^2 - \underline{k}_t \underline{k}_t \cdot\right] \underline{F}_t \times \underline{a}_z}{k_0 k_z} \tag{2.11}$$

where $\underline{F}_t = \underline{E}_a(k_x, k_y)$. The transverse magnetic field on the $z = 0$ plane is given by

$$\underline{H}_t(x,y) = \frac{1}{4\pi^2} \int_{-\infty}^{\infty} \underline{H}_a(k_x, k_y)\, e^{-jk_x x - jk_y y} dk_x dk_y \tag{2.12}$$

The transverse magnetic field in the aperture may also be expressed in terms of the waveguide modes. When this is done and the Fourier transform is taken it is readily found that:

$$\underline{H}_a(k_x,k_y) = V^+_{e,10}(1-R)Y_{e,10}\left(\frac{2k_0Z_0}{ab\beta_{10}k^2_{c,10}}\right)^{1/2}\left[-\frac{\pi}{a}S_1(k_x)C_0(k_y)\underline{a}_y\right] -$$

$$\sum_{n,m}{}'' V^-_{e,nm}Y_{e,nm}\left(\frac{k_0Z_0\varepsilon_{0m}\varepsilon_{0m}}{ab\beta_{nm}k^2_{c,nm}}\right)^{1/2}\left[\frac{\pi m}{b}C_n(k_x)S_m(k_y)\underline{a}_x - \frac{n\pi}{a}S_n(k_x)\right.$$

$$\left.C_m(k_y)\,\underline{a}_y\right] - \sum_{n,m} V^-_{h,nm}Y_{h,nm}\left(\frac{\varepsilon_{0m}\varepsilon_{0m}\beta_{nm}}{abk_{c,nm}{}^2Z_0k_0}\right)^{1/2}\left[\frac{n\pi}{a}C_n(k_x)S_m(k_y)\right.$$

$$\left.\underline{a}_x + \frac{m\pi}{b}S_n(k_x)C_m(k_y)\underline{a}_y\right] \qquad (2.13)$$

where $S_n(k_x) = \mathcal{F}\left\{\sin\left(\frac{n\pi x}{a}\right)\right\}$ $\quad C_n(k_x) = \mathcal{F}\left\{\cos\left(\frac{n\pi x}{a}\right)\right\}$

$S_m(k_y) = \mathcal{F}\left\{\sin\left(\frac{m\pi y}{b}\right)\right\}$ $\quad C_m(k_y) = \mathcal{F}\left\{\cos\left(\frac{m\pi y}{b}\right)\right\}$

The $\mathcal{F}\{\ \}$ signifies the Fourier transform operator. The continuity of the tangential H field in the aperture then means that (2.13) equals the transform of $\underline{H}_t(x,y)$ over the aperture, i.e.

$$\frac{1}{4\pi^2}\int_{-\infty}^{\infty}\int_{-\infty}^{\infty}\int_0^b\int_0^a \underline{H}_a(k'_x,k'_y)\, e^{j(k_x-k_x')x + j(k_y-k'_y)y}\,dxdy\,dk'_xdk'_y$$

The function $\underline{H}_a(k_x,k_y)$ is given by (2.11) where $\underline{F}_t$ is the Fourier transform of $\underline{E}_a$, which is given by (2.13) after setting all admittance parameters equal to unity and taking the cross product with $-\underline{a}_z$. The integration over x and y is readily carried out and leaves a two dimensional convolution integral still to be done.

The above yields a system of equations with N unknowns (N = number of modes). The amplitude $V^-_{e,10}$ determines the dominant mode reflection coefficient. In solving for these unknowns the aperture field can be viewed as a band-limited function of extent a along x and b along y for a rectangular aperture. As such the aperture field can be recovered in terms of the sample values at points spaced by π/a along k_x and by

π/b along k_y in the transform domain. We may assume that the aperture field is adequately represented by a finite number of modes and enforce the continuity of $\underline{H}_a$ at the wave numbers corresponding to $k_x = n\pi/a$, $k_y = m\pi/b$ in k_x-k_y space. A total of N spectral points are thus matched. This point matching procedure is equivalent to assuming that the free space field can be adequately represented by a spectrum of plane waves having transverse wave numbers that closely match those of the finite number of waveguide modes that are included in the aperture field expansion.

For the multi-aperture case it is only necessary to add to the free space term of each aperture, the sum of the Fourier transforms of the other aperture fields, each multiplied by $e^{jk_xD_x + jk_yD_y}$, where $D_x\underline{a}_x + D_y\underline{a}_y$ is the seperation vector between the apertures involved.

This concludes the brief overview of two Fourier transform approaches, where the equations for the aperture fields or mutual admittances are solved for in the transform domain. The main disadvantage of the Fourier transform method is that the coupling integral (2.5) giving Y_{ij} or the matching condition (2.13) involves the infinite k_x-k_y domain. Thus the integral must be truncated or the matching must be limited to a finite part of the k_x-k_y plane. In view of this, there does not appear to be any numerical advantage in using the Fourier transform approach even though the analytical results do have a certain degree of formal simplicity.

2.3 Expansion in Terms of TM and TE Modes and Sinusoidal Patches

The approaches discussed in this section use the method of moments to solve the integral equation found by using the continuity of the H field in the aperture. Luzwick and Harrington (1982) use a single modal function per aperture as their expansion function. Fenn et al (1982) use piece-wise sinusoidal-uniform surface patches to solve a similar set of equations. A quick overview of these two approaches will be given here. Much of this material is taken directly from these two articles and the interested reader is referred to them for more detail. The equations and how they were derived are similar for both and start by looking at a single rectangular waveguide fed aperture in a ground plane. It should be noted at this point that both Luzwick and Harrington, and Fenn et al use a notation that is slightly different from that presented here. They both used $\underline{M}$ for $\underline{J}_m$, $\underline{F}$ for $\underline{A}_m$ and Harrington used $\underline{H}^{imp}$ in place of $\underline{H}^{INC}$.

First the equivalence principle is used (Harrington, 1961, Sec. 3-5) to split the problem into two seperate regions by covering the aperture with an electric conductor. To keep the tangential component of the E field continuous across the aperture, equivalent magnetic currents are placed on both sides of this conductor over the aperture areas as shown in Fig. 2.2. Since $\underline{J}_m = \underline{n} \times \underline{E}$, the currents on the half-space region are negatively directed. Next, due to continuity of the tangential $\underline{H}$ the magnetic fields on either side are set equal. The waveguide region H fields in $z \leq 0$ are

$$\underline{H}_t^{WG} = \underline{H}_t^{INC} + \underline{H}_t^{WG}(\underline{J}_m) \qquad (2.14)$$

where $\underline{H}_t^{WG}(\underline{J}_m)$ = tangential $\underline{H}$ due to the equivalent magnetic currents

$\underline{H}_t^{INC}$ = tangential $\underline{H}$ due to the sources ($\underline{J}_m'$ and $\underline{J}_e'$) under short circuit conditions at the aperture.

The half space region then has:

$$\underline{H}_t^{HS} = \underline{H}_t^{HS}(-\underline{J}_m) = -\underline{H}_t^{HS}(\underline{J}_m) \tag{2.15}$$

Setting (2.14) equal to (2.15) at z = 0 yields:

$$\underline{H}_t^{WG}(\underline{J}_m) + \underline{H}_t^{HS}(\underline{J}_m) = -\underline{H}_t^{INC} \text{ at } z = 0 \tag{2.16}$$

When N-1 apertures are added, we get for each aperture

$$\underline{H}_t^{WG}(\underline{J}_{m_i}) + \sum_{j=1}^{N} \underline{H}_{t_i}^{HS}(\underline{J}_{m_j}) = -\underline{H}_{t_i}^{INC} \quad i=1,2, \ldots N \tag{2.17}$$

The $\underline{H}_{t_i}^{HS}(\underline{J}_{m_j})$ term is the radiated field at the i^{th} aperture due to the j^{th} magnetic current and is derived from the vector potential $\underline{A}_{m_{ij}}$ and the scalar potential ϕ_{ij} where:

$$\underline{A}_{m_{ij}} = \frac{\varepsilon_0}{4\pi} \iint_{\text{apert.}} \underline{J}_{m_j} \frac{e^{-jk_0|\underline{r}-\underline{r}'|}}{|\underline{r}-\underline{r}'|} \, dS$$

$$\phi_{ij} = \frac{1}{4\pi\mu_0} \iint_{\text{apert.}} \rho_j \frac{e^{-jk_0|\underline{r}-\underline{r}'|}}{|\underline{r}-\underline{r}'|} \, dS \text{ where } \rho_j = \frac{\nabla \cdot \underline{J}_{m_j}}{-j\omega}$$

$$\underline{H}_{t_i}^{HS}(\underline{J}_{m_j}) = -j\omega \underline{A}_{m_{ij}} - \nabla\phi_{ij} \tag{2.18}$$

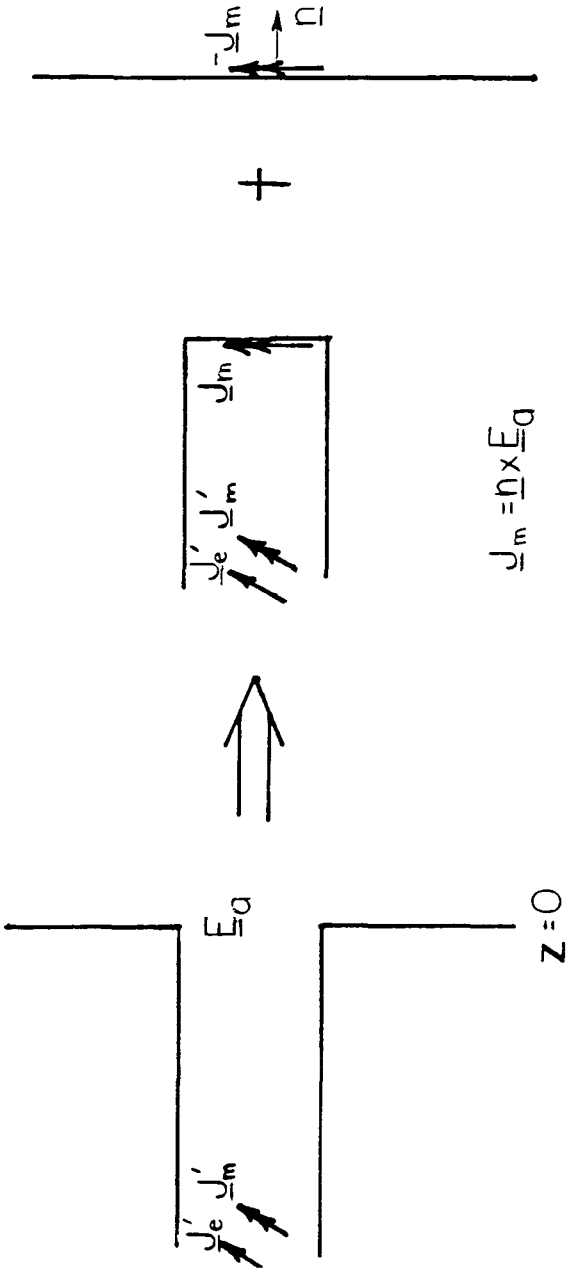

Figure 2.2 Closing the Aperture Using the Equivalence Principle.

In solving for the waveguide term $\underline{H}_t^{WG}(\underline{J}_m)$ due to the $\underline{J}_m$ the two articles take different approaches. Harrington and Luzwick express the field in modal form and solve for the mode amplitudes. The analysis is somewhat involved since they include the case where the guide dimensions are larger than the aperture dimension. Fenn et al use image theory to derive the field in their situation. Since both are quite lengthy, they will not be presented here.

It is relevant, at this point, to present a quick review of the method of moments, since it is used both here and again in the vector potential approach. The method of moments allows the user to solve the following equation for f:

$$L(f) = g \tag{2.19}$$

where L(), a linear operator, and g are known. The first step is to approximate f by:

$$f \cong \sum_{n=1}^{N} \alpha_n f_n \tag{2.20}$$

where α_n = unknown constants

f_n = suitably chosen basis or expansion functions

The f_n should be chosen so that if $N = \infty$ the two terms in (2.20) are equal. The substitution of (2.20) into (2.19) yields:

$$\sum_{n=1}^{N} \alpha_n L(f_n) \cong g \tag{2.21}$$

Next a suitable set of N testing functions W_n are chosen along with an inner product $\langle a,b \rangle$. Taking the inner product of each W_n, also

called testing with W_n, with both sides of (2.21) gives:

$$\sum_{n=1}^{N} \alpha_n < W_m, L(f_n) > = <W_m, g>, \quad m = 1, 2, \ldots N$$

$$[\ell]_{NxN}[\alpha]_{Nx1} = [g]_{Nx1} \tag{2.22}$$

where

$$[\ell]_{NxN} = \begin{bmatrix} < W_1, L(f_1) > & < W_1, L(f_2) > & \ldots \\ < W_2, L(f_2) > & < W_2, L(F_2) > & \ldots \\ \vdots & \vdots & \end{bmatrix}$$

$$[\alpha] = \begin{bmatrix} \alpha_1 \\ \alpha_2 \\ \vdots \end{bmatrix} \qquad [g] = \begin{bmatrix} <W_1, g> \\ <W_2, g> \\ \vdots \end{bmatrix}$$

Provided that $[\ell]$ is nonsingular then

$$[\alpha] = [\ell]^{-1}[g] \tag{2.23}$$

Proper choice of f_n, W_n and <a,b> dictates the accuracy of the solution. A more complete discussion of the method of moments is given in Harrington's book (Harrington, 1968).

The basic equation (2.16) is in a form that is readily solvable by the method of moments for the unknown $\underline{J}_m$ (which is related to the aperture field $\underline{E}$). Here again the two groups differ in the way

they approximate $\underline{J}_m$. Harrington and Luzwick use full domain functions analogous to the TE and TM modal functions with the TE mode functions having the form:

$$C\left[\underline{a}_x \frac{n}{b}\cos\left(\frac{m\pi x}{a}\right)\sin\left(\frac{n\pi y}{b}\right) - \underline{a}_y \frac{m}{a}\sin\left(\frac{m\pi x}{a}\right)\cos\left(\frac{n\pi y}{b}\right)\right]$$

In the work presented in their article only a single function was used. Fenn, et al used piecewise sinusoidal-uniform basis functions of the form:

$$\underline{a}_x K_n \frac{\sin[\beta(nL-|x|)]}{\sin(\beta L)} \qquad (n-1)L<x<(n+1)L, 0<y<W$$

for overlapping surface patches of length 2L and width W as shown in Fig. 2.3, where $\beta = 2\pi/\lambda$ and n = basis function number.

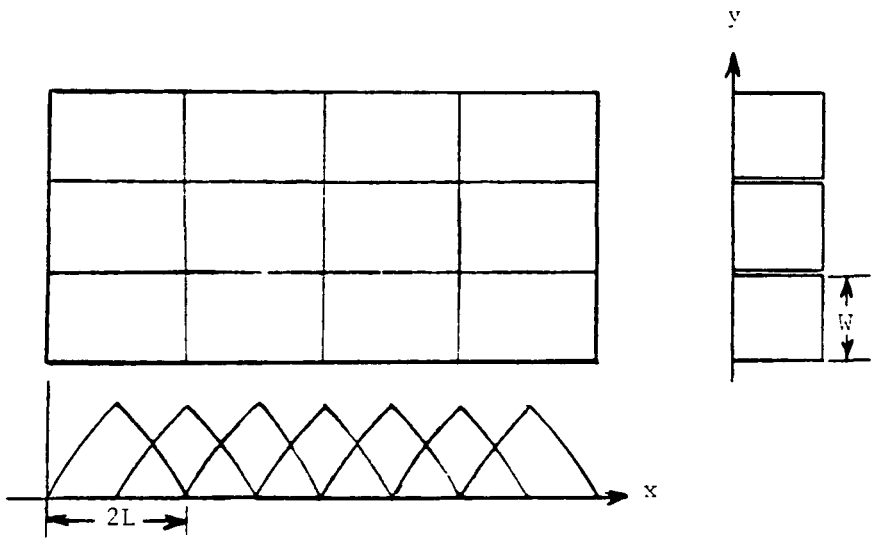

Figure 2.3 Piecewise Sinusoidal Basis Functions.

These can be used for both x and y directed currents. Seven sinusoids per aperture for rectangular apertures was found to give satisfactory results.

For the choice of testing function both Luzwick and Harrington and Fenn, et al used the same function as they used for their basis function. This technique is known as Galerkin's method and in the former case would allow for the use of the orthogonality of the modal functions to reduce the complexity of the integral equations. For the inner product both groups used:

$$\langle a,b \rangle = \iint \underline{a} \cdot \underline{b} \, dS$$

where the integration is over the aperture.

Once the $[\ell]$ matrix is solved for numerically it can be inverted and the amplitudes of the expansion functions determined. With these amplitudes the approximation for the equivalent current is complete and the scattering parameters can be found.

Fenn et al used their approximation to solve for the reflection coefficient of driven elements in several array situations while Harrington and Luzwick found the coupled power ($20 \log|S_{21}|$) between apertures in several configurations. Using the piecewise sinusoidal expansion approach, Fenn et al were also able to look at the edge singularity present in the aperture fields. Some of these results will be presented in Chapter 3 as a comparison with the results found with the method used in this report.

A good general reference covering the basic ideas presented here is the report by Harrington and Mautz (Harrington and Mautz, 1976)

It should be noted that the definition of the mutual admittance parameters is quite arbitrary. It can be chosen as the coupling coefficient between the n^{th} basis function in the aperture i and the m^{th} testing function in the aperture j. The various choices of basis and testing functions used will then give different expressions for the admittance parameters. As a general rule, the scattering matrix relating the amplitudes of the propagating modes in the waveguides is a desired end result so the evaluation of the admittance parameters is often only an intermediate step.

The main disadvantage of the TE and TM mode technique is the fact that each coefficient will have to be split into an $\underline{a}_x$ and an $\underline{a}_y$ term. As we will see in the next section, the vector potential approach overcomes this difficulty. The reason for not choosing the local basis functions is that the size of the matrix that would have to be inverted for arrays of square apertures would become very large for modest sized arrays. This would severly limit the cases that could be solved.

2.4 Vector Potential Approach

The vector potential approach is very similar to the methods discussed in the last section. The main difference is in the modal expansions used to determine the fields and the approximation for the magnetic currents. The approximation uses vector potential modes for basis functions. This allows the equations to be solved by first finding the magnetic vector potentials, which are more straight-forward and easier to work with. The TE and TM modes in the waveguides can be

found later if this information is required.

Consider again the single aperture case (see Fig. 2.2). There exists a $\underline{J}_m$ (magnetic current) on both sides of the aperture surface equal to $\underline{a}_z \times \underline{E}_a$, where $\underline{E}_a$ is the aperture E field. The form of this current using the vector potential modal functions (also called a hybrid mode set; Harrington, 1961, Sec. 4.4) is:

$$\underline{J}_m = \sum_{n=1}^{n_1} \sum_{m=0}^{m_1} C_{nm} \underline{\Psi}_{nm} + \sum_{n=0}^{n_2} \sum_{m=1}^{m_2} D_{nm} \underline{\Phi}_{nm} \tag{2.24}$$

where

$$\underline{\Psi}_{nm} = \left(\frac{\varepsilon_{0n}\varepsilon_{0m}}{a\,b}\right)^{1/2} \sin\left(\frac{n\pi x}{a}\right) \cos\left(\frac{m\pi y}{b}\right) \underline{a}_x \tag{2.25}$$

$$\underline{\Phi}_{nm} = \left(\frac{\varepsilon_{0n}\varepsilon_{0m}}{ab}\right)^{1/2} \sin\left(\frac{m\pi y}{b}\right) \cos\left(\frac{n\pi x}{a}\right) \underline{a}_y$$

These modal functions are orthogonal so that:

$$\iint \psi_{nm}\psi_{n'm'}\, ds = 0 \qquad \text{for } n\neq n' \text{ or } m\neq m'$$

This relation also holds for Φ_{nm} and for any combination of the two sets of functions.

The next step is to set up the integral equations using the magnetic vector potential. $\underline{E}$ and $\underline{H}$ are found using

$$\varepsilon_0 \underline{E} = -\underline{\nabla} \times \underline{A}_m \tag{2.26}$$

$$j\omega\mu_0\varepsilon_0 \underline{H} = (k_0^2 + \underline{\nabla}\underline{\nabla}\cdot)\underline{A}_m$$

The continuity of $\underline{H}$ across the aperture gives:

$$(k_0^2 + \underline{\nabla}\underline{\nabla}\cdot)(\underline{A}_m^{WG} + \underline{A}_m^{INC}) = (k_0^2 + \underline{\nabla}\underline{\nabla}\cdot)\,\underline{A}_m^{HS} \qquad (2.27)$$

where

$\underline{A}_m^{WG}$ = Vector potential due to $\underline{J}_m$ inside guide.

$\underline{A}_m^{HS}$ = Vector potential due to $-\underline{J}_m$ radiating into free space.

$\underline{A}_m^{INC}$ = Vector potential due to the sources under short circuit aperture conditions.

These three vector potentials are the quantities that need to be solved for in terms of the $\underline{J}_m$.

Using the magnetic vector potential integral (Harrington, 1961 Sec. 2.10), duality, and image theory:

$$\underline{A}_m^{HS} = \frac{-\varepsilon_0}{4\pi}\iint 2\underline{J}_m \frac{e^{-jk_0R}}{R}\, dS' \qquad (2.28)$$

where $R = |\underline{r}-\underline{r}'|$ ($\underline{r}$ = field vector and $\underline{r}'$= source vector).
For the vector potential in the waveguide due to the $\underline{J}_m$ it's Green's function needs to be found. Using duality again the form of the equation to be solved is (Collin, 1960 Chap. 2)

$$(\nabla^2 + k_0^2)\underline{A}_m^{WG} = -2\varepsilon_0\underline{J}_m \qquad (2.29)$$

which gives $$\underline{A}_m^{WG} = \int_0^a\int_0^b \underline{\underline{G}}\cdot\underline{J}_m\, dy'dx'$$

Since there are only x and y directed currents the required Green's function should be a dyadic of the form:

$$\underline{\underline{G}} = G_{xx}\, \underline{a}_x \underline{a}_x + G_{yy}\, \underline{a}_y \underline{a}_y \tag{2.30}$$

where $$(\nabla^2 + k_0^2)\, G_{xx} = -2\varepsilon_0\, \delta\,(x-x')\, \delta\,(y-y')\, \delta\,(z) \tag{2.31}$$

$$(\nabla^2 + k_0^2)\, G_{yy} = -2\varepsilon_0\, \delta(x-x')\delta(y-y')\delta(z)$$

For G_{xx} we may assume an expansion of the form

$$G_{xx} = \sum_{n,m} G_{nm}\, \psi_{nm}\, e^{-j\beta_{nm}|z|} \tag{2.32}$$

where the G_{nm} are unknown amplitudes (Collin, 1960, Chapter 2). When we substitute this into (2.31) we obtain

$$\sum_{n,m} G_{nm}\, \psi_{nm} \left[k_0^2 - \left(\frac{n\pi}{a}\right)^2 - \left(\frac{m\pi}{b}\right)^2 + \frac{\partial^2}{\partial z^2}\right] e^{-j\beta_{nm}|z|}$$

$$= -2\varepsilon_0\, \delta\,(x-x')\, \delta\,(y-y')\, \delta\,(z) \tag{2.33}$$

Multiplying this by $\psi_{nm}(x,y)$ and integrating with respect to x and y gives:

$$G_{nm}\left(\beta_{nm}^2 + \frac{\partial^2}{\partial z^2}\right) e^{-j\beta_{nm}|z|} = -2\varepsilon_0\, \psi_{nm}(x',y')\, \delta(z) \tag{2.34}$$

Integrating this equation over z from 0^- to 0^+ gives

$$G_{nm}\, \frac{\partial\, e^{-j\beta nm|z|}}{\partial z} \Bigg|_{0-}^{0+} = -2\varepsilon_0 \psi_{nm}(x',y') = -2j\beta_{nm} G_{nm} \tag{2.35}$$

so finally

$$G_{xx} = \sum_{n,m} \frac{\varepsilon_0}{j\beta_{nm}} \psi_{nm}(x,y)\, \psi_{nm}(x',y')\, e^{-j\beta_{nm}|z|} \qquad (2.36)$$

Similarly G_{yy} is found to be given by:

$$G_{yy} = \sum_{n,m} \frac{\varepsilon_0}{j\beta_{nm}} \Phi_{nm}(x,y)\, \Phi_{nm}(x',y')\, e^{-j\beta_{nm}|z|} \qquad (2.37)$$

Therefore, the $\underline{A}_m^{WG}$ at $z = 0$ is:

$$A_m^{WG} = \sum_{n,m} \int_0^a \int_0^b (G_{xx} C_{nm} \psi_{nm}(x',y')\, \underline{a}_x + G_{yy}\, D_{nm} \Phi_{nm}(x',y')$$

$$\underline{a}_y)\, dy'dx' = \sum_{n,m} \frac{\varepsilon_0 C_{nm}}{j\beta_{nm}} \underline{\psi}_{nm}(x,y) + \sum_{n,m} \frac{\varepsilon_0}{j\beta_{nm}} D_{nm} \underline{\Phi}_{nm}(x,y) \qquad (2.38)$$

Finally, for the $\underline{A}_m^{INC}$ under short circuit conditions we have

$$\underline{A}_m^{INC} = A_{10}\, \underline{\psi}_{10}\, (e^{-j\beta_{10}z} + e^{j\beta_{10}z}) \qquad (2.39)$$

where A_{10} is a known amplitude constant.

This makes $\underline{E}^{INC}$ a TE_{10} mode that is zero at $z = 0$.

The substitution of (2.39), (2.38) and (2.28) into (2.27) gives:

$$(k_0^2 \underline{\underline{I}} + \underline{\nabla}_t \underline{\nabla}_t) \cdot \int_0^a \int_0^b \frac{1}{\varepsilon_0} [\underline{\underline{G}} + \varepsilon_0 \frac{e^{-jk_0 R}}{2\pi R} (\underline{a}_x \underline{a}_x + \underline{a}_y \underline{a}_y)] \cdot$$

$$\underline{J}_m(x',y')\, dy'dx' = (k_0^2\, \underline{\underline{I}} + \underline{\nabla}_t \underline{\nabla}_t) \cdot (-2A_{10}\, \underline{\psi}_{10}) \frac{1}{\varepsilon_0} \qquad (2.40)$$

where the $\underline{\nabla}_t$ is used since only the tangential fields are being analyzed (z has been set to zero), and $\underline{\underline{I}}$ is the unit dyadic.

This is the integral equation that is solved by the method of moments. A finite expansion of $\underline{J}_m$ in terms of $\underline{\psi}_{nm}$ and $\underline{\Phi}_{nm}$ is an appropriate approximation for use in this method. The basis and testing functions are chosen as the same $\underline{\psi}_{nm}$ and $\underline{\Phi}_{nm}$. The following inner product is used:

$$\langle a,b \rangle = \iint_S \underline{a} \cdot \underline{b} \; dS \cdot \qquad (2.41)$$

where the integration is over the aperture opening.

This choice of inner product, basis functions and testing functions yields a set of admittance parameters for the elements of the $[\ell]$ matrix. This can be seen by looking at the integral equation that results for these elements.

$$\langle \underline{J}_m^2, \underline{H}^1 \rangle = \iint_{S_a} \underline{J}_m^2 \cdot \underline{H}^1 \; dS$$

where

$\underline{H}^1$ = H field in aperture #1

$\underline{J}_m^2$ = Current of aperture #2

S_a = Area of aperture # 2

By definition, this is the reaction integral. (Harrington, 1961, Sec. 7-7). It is related to an admittance by (2.4). So after testing (2.40) with the $\underline{\psi}$ and $\underline{\Phi}$ the resulting matrix equation will be of the following form:

$$[Y][V] = [I]$$

with the proper choice of units for C_{nm} and D_{nm} (volts).

The [Y] is, in fact, the sum of two matrices, $[Y^{HS}] + [Y^{WG}]$; each due to the respective magnetic field (H^{HS} and H^{WG}) that is being tested. The [I] is the tested incident magnetic fields, while the [V] is the amplitude matrix that needs to be determined.

In order to make the documentation and further manipulation of the tested eqns. easier, the following admittance parameters are introduced (where ψ_{pq} and ϕ_{pq} are the testing functions):

$Y^{x_1x_1}_{pq,nm}$ = Coefficient of C_{nm} testing $\underline{\psi}_{pq}$ against $\underline{\psi}_{nm}$

$Y^{x_1y_1}_{pq,nm}$ = Coefficient of D_{nm} testing $\underline{\psi}_{pq}$ against $\underline{\phi}_{nm}$

$Y^{y_1x_1}_{pq,nm}$ = Coefficient of C_{nm} testing $\underline{\phi}_{pq}$ against $\underline{\psi}_{nm}$

$Y^{y_1y_1}_{pq,nm}$ = Coefficient of D_{nm} testing $\underline{\phi}_{pq}$ against $\underline{\phi}_{nm}$

Using these admittances in writing the resulting equations we get:

$$\sum_{p,q} \left[\sum_{n,m} \left(Y^{x_1x_1}_{pq,nm} C_{nm} \right) + \sum_{n,m}{}' \left(Y^{x_1y_1}_{pq,nm} D_{nm} \right) = \frac{-2A_{10}}{\varepsilon_0} \left(k_0^2 - \frac{\pi^2}{a^2} \right) \delta_{p1} \delta_{q0} \right]$$

$$\sum_{pq}{}' \left[\sum_{n,m} \left(Y^{y_1x_1}_{pq,nm} C_{nm} \right) + \sum_{n,m}{}' \left(Y^{y_1y_1}_{pq,nm} D_{nm} \right) = 0 \right] \qquad (2.42)$$

where $\sum_{p,q}'$ is over the ϕ_{pq} values and $\sum_{p,q}$ is over the ψ_{pq} values, and likewise for $\sum_{n,m}'$ and $\sum_{n,m}$.

A typical term in the tested equation is of the form:

$$\iint \underline{\psi}_{nm} \cdot \underline{\nabla}_t \underline{\nabla}_t \cdot \underline{A}_m (\underline{J}_m)\, dS \tag{2.43}$$

where $\underline{A}_m$ is given by an integral in certain cases ($\underline{A}_m^{HS}$). To make these integrals easier to carry out, we use the following integration by parts procedure. Consider:

$$\underline{\nabla}_t \cdot (\underline{\psi}_{nm} \underline{\nabla}_t \cdot \underline{A}_m) = (\underline{\nabla}_t \cdot \underline{\psi}_{nm})(\underline{\nabla}_t \cdot \underline{A}_m) + \underline{\psi}_{nm} \cdot \underline{\nabla}_t \underline{\nabla}_t \cdot \underline{A}_m \tag{2.44}$$

which when applied to (2.42) yields

$$\oint_C \underline{n} \cdot \underline{\psi}_{nm} \underline{\nabla}_t \cdot \underline{A}_m\, dl - \iint \underline{\nabla}_t \cdot \underline{\psi}_{nm} \underline{\nabla}_t \cdot \underline{A}_m\, dS =$$

$$- \oint_C (\underline{n} \cdot \underline{A}_m) \underline{\nabla}_t \cdot \underline{\psi}_{nm}\, dl + \iint (\underline{\nabla}_t \underline{\nabla}_t \cdot \underline{\psi}_{nm}) \cdot \underline{A}_m\, dS \tag{2.45}$$

Note that $\underline{n} \cdot \underline{A}_m^{WG} = \underline{n} \cdot \underline{A}_m^{INC} = 0$ on the boundary.

Using (2.42), (2.45) and the orthogonality of the modal functions in solving for the four admittance parameters we get:

$$Y_{pq,nm}^{x_1 x_1} = \frac{-j(k_0^2 - \frac{p^2\pi^2}{a^2})}{\beta_{pq}} \delta_{pn} \delta_{qm} + (k_0^2 - \frac{p^2\pi^2}{a^2}) \int_0^a \int_0^b$$

$$\psi_{pq}(x,y) \left[\int_0^a \int_0^b \frac{e^{-jk_0 R}}{2\pi R} \psi_{nm}(x',y')\, dy'dx' \right] dy\, dx - \oint_C \frac{\partial \psi_{pq}}{\partial x}(x,y)$$

$$\left[\int_0^a \int_0^b \frac{e^{-jk_0 R}}{2\pi R} \; \underline{n} \cdot \underline{\psi}_{nm}(x',y') \; dy'dx' \right] dl \qquad (2.46)$$

$$Y_{pq,nm}^{x_1 y_1} = \frac{jpq\pi^2}{ab\beta_{pq}} \delta_{pn} \delta_{qm} - \frac{pq\pi^2}{ab} \int_0^a \int_0^b \Phi_{pq}(x,y) \left[\int_0^a \int_0^b \frac{e^{-jk_0 R}}{2\pi R} \Phi_{nm}(x',y') \; dy'dx' \right] dy \; dx - \oint_C \frac{\partial \Psi_{pq}}{\partial x}(x,y)$$

$$\left[\int_0^a \int_0^b \frac{e^{-jk_0 R}}{2\pi R} \; \underline{n} \cdot \underline{\Phi}_{nm} \; dy' \; dx' \right] dl \qquad (2.47)$$

$$Y_{pq,nm}^{y_1 x_1} = Y_{pq,nm}^{x_1 y_1} \quad \text{with the } \psi \text{ and } \Phi\text{'s interchanged and the } \frac{\partial}{\partial x} \text{ replaced by } \frac{\partial}{\partial y} \qquad (2.48)$$

$$Y_{pq,nm}^{y_1 y_1} = Y_{pq,nm}^{x_1 x_1} \quad \text{with the } \psi \text{ and } \Phi\text{'s interchanged, the } \frac{\partial}{\partial x} \text{ replaced by } \frac{\partial}{\partial y} \text{ and the two } \left(k_0^2 - \frac{p^2\pi^2}{a^2}\right) \text{'s replaced by } \left(k_0^2 - \frac{q^2\pi^2}{b^2}\right) \text{'s} \qquad (2.49)$$

The next step in the analysis is the multi-aperture problem. The two aperture case is shown in Fig. 2.4. Let C_{nm}^{1} and D_{nm}^{1} be the modal amplitudes of aperture #1 and C_{nm}^{2} and D_{nm}^{2} be the amplitudes of aperture #2. The currents for aperture #2 are then:

$$\underline{J}_m^2 = \sum_{n=1}^{n_1} \sum_{m=0}^{m1} C_{nm}^{2} \; \underline{\Psi}_{nm}(x_2,y_2) + \sum_{n=0}^{n_2} \sum_{m=1}^{m2} D_{nm}^{2} \; \underline{\Phi}_{nm}(x_2,y_2)$$

Also the $\underline{A}_m^{INC}$ of #2 is: $2A_{10}^2 \underline{\psi}_{10}(x_2,y_2)$ at $z = 0$. If we define $Y_{pq,nm}^{x_2x_1}$ as the coefficient of C_{nm}^1 for $\psi_{pq}(x_2,y_2)$ tested against $\psi_{nm}(x_1,y_1)$ and the remaining aperture to aperture admittances in a similar manner the resulting tested equations are:

$$\sum_{p,q} \left[\sum_{n,m} \left(Y_{pq,nm}^{x_1x_1} C_{nm}^1 + Y_{pq,nm}^{x_1x_2} C_{nm}^2 \right) + \sum_{n,m}' \left(Y_{pq,nm}^{x_1y_1} D_{nm}^1 + Y_{pq,nm}^{x_1y_2} D_{nm}^2 \right) = \frac{-2A_{10}^1}{\varepsilon_0} \delta_{p1} \delta_{q0} \left(k_o^2 - \frac{\pi^2}{a^2} \right) \right]$$

$$\sum_{p,q}' \left[\sum_{n,m} \left(Y_{pq,nm}^{y_1x_1} C_{nm}^1 + Y_{pq,nm}^{y_1x_2} C_{nm}^2 \right) + \sum_{n,m}' \left(Y_{pq,nm}^{y_1y_1} D_{nm}^1 + Y_{pq,nm}^{y_1y_2} D_{nm}^2 \right) = 0 \right]$$

$$\sum_{p,q} \left[\sum_{n,m} \left(Y_{pq,nm}^{x_2x_1} C_{nm}^1 + Y_{pq,nm}^{x_2x_2} C_{nm}^2 \right) + \sum_{n,m}' \left(Y_{pq,nm}^{x_2y_1} D_{nm}^1 - Y_{pq,nm}^{x_2y_2} D_{nm}^2 \right) = \frac{-2A_{10}^2}{\varepsilon_0} \delta_{p1} \delta_{q0} \left(k_0^2 - \frac{\pi^2}{a^2} \right) \right]$$

$$\sum_{p,q}' \left[\sum_{n,m} \left(Y_{pq,nm}^{y_2x_1} C_{nm}^1 + Y_{pq,nm}^{y_2x_2} C_{nm}^2 \right) + \sum_{n,m}' \left(Y_{pq,nm}^{y_2y_1} D_{nm}^1 + Y_{pq,nm}^{y_2y_2} D_{nm}^2 \right) = 0 \right] \qquad (2.50)$$

where $Y_{pq,nm}^{x_ix_i}$, $Y_{pq,nm}^{x_iy_i}$, etc. do not depend on whether i = 1 or 2.

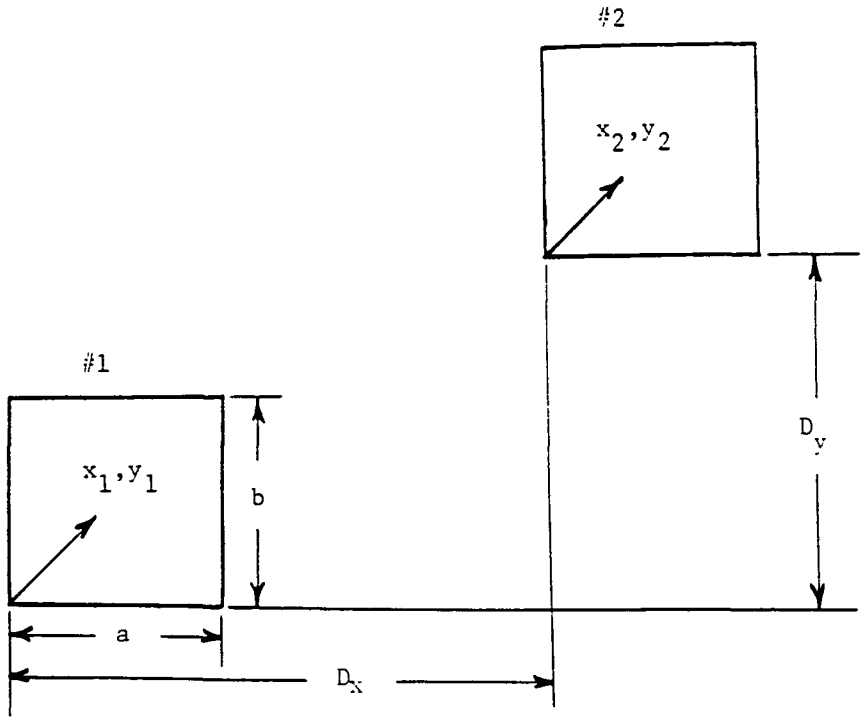

Figure 2.4 Two Aperture Problem.

Using $R = \sqrt{(x_1 - x_2' - D_x)^2 + (y_1 - y_2' - D_y)^2}$ and solving for the new admittance parameters we find that:

$$Y_{pq,nm}^{x_1 x_2} = \int_0^a \int_0^b \left(k_0^2 - \frac{p^2 \tau^2}{a^2}\right) \psi_{pq}(x_1, y_1) \left[\int_0^a \int_0^b \frac{e^{-jk_0 R}}{2\pi R} \psi_{nm}(x_2', y_2')\, dy_2'\, dx_2' \right] dy_1 dx_1 - \oint_C \frac{\partial \psi_{pq}(x_1 y_1)}{\partial x_1} \left[\int_0^a \int_0^b \right.$$

$$\frac{e^{-jk_0R}}{2\pi R}\ \underline{n}\cdot\underline{\Phi}_{nm}(x_2',y_2')\,dy_2'\,dx_2'\Bigg]\,dl_1 \qquad (2.51)$$

$$Y_{pq,nm}^{x_1y_2} = \frac{-pq\pi^2}{ab}\int_0^a\int_0^b \Phi_{pq}(x_1,y_1)\Bigg[\int_0^a\int_0^b \frac{e^{-jk_0R}}{2\pi R}\,\Phi_{nm}(x_2',y_2')\,dy_2'\,dx_2'\Bigg]\,dy_1dx_1 - \oint_C \frac{\partial\psi_{pq}(x_1,y_1)}{\partial x_1}\Bigg[\int_0^a\int_0^b \frac{e^{-jk_0R}}{2\pi R}\,\underline{n}\cdot\underline{\Phi}_{nm}(x_2',y_2')\,dy_2'\,dx_2'\Bigg]\,dl_1 \qquad (2.52)$$

$$Y_{pq,nm}^{y_1x_2} = Y_{pq,nm}^{x_1y_2} \quad \text{with the } \psi\text{'s and } \Phi\text{'s interchanged and the } \frac{\partial}{\partial x_1} \text{ replaced by } \frac{\partial}{\partial y_1} \qquad (2.53)$$

$$Y_{pq,nm}^{y_1y_2} = Y_{pq,nm}^{x_1x_2} \quad \text{with the } \psi\text{'s and } \Phi\text{'s interchanged, the } \frac{\partial}{\partial x_1} \text{ replaced by } \frac{\partial}{\partial y_1} \text{ and the } \left(k_0^2 - \frac{p^2\pi^2}{a^2}\right) \text{ replaced by } \left(k_0^2 - \frac{q^2\pi^2}{b^2}\right) \qquad (2.54)$$

For the other 4 terms reciprocity shows that:

$$Y_{pq,nm}^{x_iy_j} = Y_{nm,pq}^{y_jx_i}$$

$$Y_{pq,nm}^{y_ix_j} = Y_{nm,pq}^{x_jy_i}$$

$$Y_{pq,nm}^{x_i x_j} = Y_{nm,pq}^{x_j x_i}$$

$$Y_{pq,nm}^{y_i y_j} = Y_{nm,pq}^{y_j y_i} \qquad (2.55)$$

By using (2.45) - (2.55) it would be a straight forward task to extend this analysis to the cases of three or more apertures. So those situations will not be presented here.

These equations completely describe the system of several apertures in a ground plane and can be solved directly for the C_{nm}'s and D_{nm}'s There is still one remaining problem with them and that is the three and four-fold integrations that need to be carried out numerically. If Simpson's rule is used and n or m were allowed to be as large as 3 then the minimum number of intervals for an acceptable approximation would be 6 (4 points per period of sinusoid being integrated). So, if 8 were used, for somewhat better accuracy, then each four-fold integration needs $8^4 \simeq 4000$ operations, where each operation involves both exponentiation and trigonometric computations. Considering that each guide can have several modes and there are several guides and the number of terms to be integrated before symmetry is considered is the square of the product of the number of modes times the number of apertures, this rapidly leads to an enormous amount of cpu time. So the integrals need to be reduced as far as possible. A double integral using 20 points would only use 1/10 the computing time, so by reducing these integrals to double integrals

fairly accurate results can be had at a fraction of the cpu time. The reduction of these terms analytically will be outlined in the next section.

At this point some of the advantages of using the vector potential method and an expansion of it can be readily appreciated. First of all there is a single set of amplitude coefficients along with the x and y components of the vector potential. In contrast an expansion of the aperture field in terms of TE and TM modes results in two sets of amplitudes associated with each component of the electric field. This results in a splitting of the admittance parameters into sets representing coupling between TE-TE modes, TM-TM modes, and TE-TM modes. As a result the notational complexity is increased substantially. In the vector potential approach no distinction between TE and TM modes needs to be made. Luzwick and Harrington use both the vector and scalar potentials and do one integration by parts (Luzwick and Harrington, 1982). In the approach given above, two integrations by parts is carried out which leads to simpler final integrals to evaluate.

2.5 Reduction of the Three and Four-Fold Integrals

By making a change of variables it is possible to reduce the three and four-fold integrals encountered at the end of the last section to double integrals. This greatly eases the computational costs by reducing run times and reducing the needed programming tasks. The first step will be to analyze the coupling terms between modes within a single guide. The steps used to solve this case can then be

applied to the coupling terms between different guides.

Consider the following integral:

$$\int_C^a \int_0^b \int_0^a \int_0^b \psi_{pq}(x,y) \quad g(x,x',y,y') \; \psi_{nm}(x',y') \; dy\,dx\,dy'\,dx' \qquad (2.56)$$

where:

$$g(x,x',y,y') = \frac{e^{-jk_0R}}{2\pi R}$$

$$R = [(x-x')^2 + (y-y')^2]^{1/2}$$

Let $u = x-x'$ and $v = x+x'$. This gives $x = \frac{v+u}{2}$ and $x' = \frac{v-u}{2}$

and

$$dxdx' = \begin{vmatrix} \frac{\partial x}{\partial u} & \frac{\partial x}{\partial v} \\ \frac{\partial x'}{\partial u} & \frac{\partial x'}{\partial v} \end{vmatrix} \quad dudv = \begin{vmatrix} 1/2 & 1/2 \\ -1/2 & 1/2 \end{vmatrix} \quad du\,dv = \frac{1}{2}\,dudv$$

The new limits of integration are:

$x = 0$ corresponds to $v = -u$

$x = a$ corresponds to $v = 2a-u$

$x' = 0$ corresponds to $v = u$

$x' = a$ corresponds to $v = u + 2a$

Thus the mapping into u-v space is a parallelogram as shown in Fig. 2.5

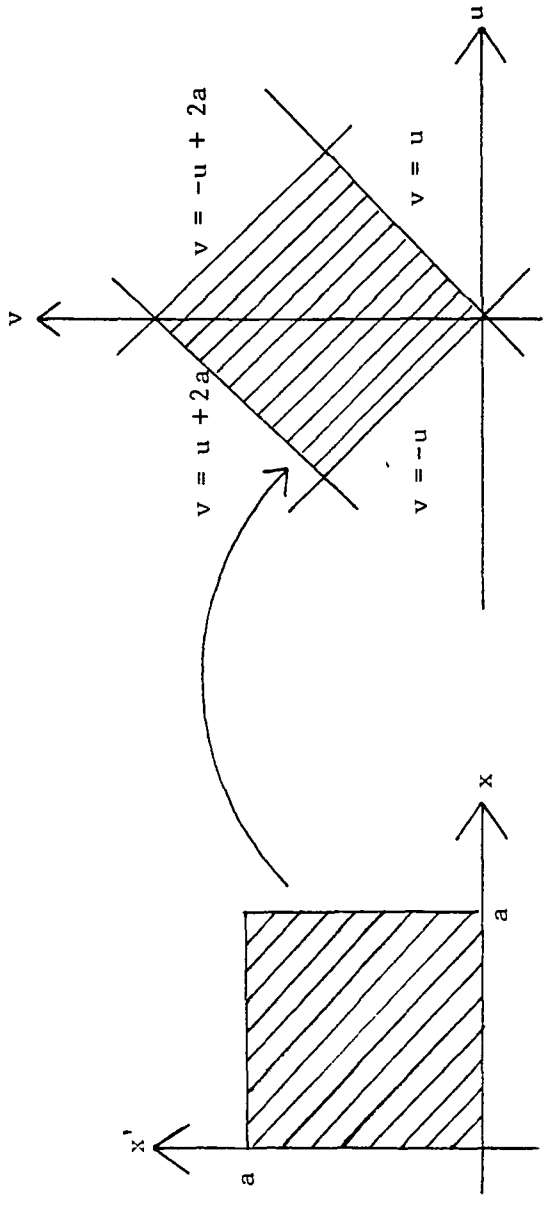

Figure 2.5 New Mapping

Now let $y-y' = w$ and $y+y' = z$, so that $y = \frac{w+z}{2}$ and $y' = \frac{z-w}{2}$. A similar mapping takes place here. These two changes, when made to (2.56) yield

$$\frac{1}{4}\iiiint \psi_{pq}\left(\frac{v+u}{2}, \frac{w+z}{2}\right) \cdot g(u,w)\, \psi_{nm}\left(\frac{v-u}{2}, \frac{z-w}{2}\right) du\,dv\,dw\,dz \qquad (2.57)$$

Equation (2.57) can now be integrated analytically over v and z.

The $g(u,w)$ is an even function of u and w since $R = (u^2 + w^2)^{1/2}$ while the other term in (2.54) is:

$$\left(\frac{\varepsilon_{0n}\varepsilon_{0m}\varepsilon_{0p}\varepsilon_{0q}}{a^2 b^2}\right)^{1/2} \sin\left(\frac{p\pi}{2a}(u+v)\right) \sin\left(\frac{n\pi}{2a}(v-u)\right) \cos\left(\frac{q\pi}{2b}(w+z)\right)$$

$$\cos\left(\frac{m\pi}{2b}(z-w)\right) \qquad (2.58)$$

To integrate out the v term, start by looking at:

$$\sin\left(\frac{p\pi}{2a}(u+v)\right) \sin\left(\frac{n\pi}{2a}(v-u)\right) = \sin\left(\frac{p\pi u}{2a}\right) \cos\left(\frac{n\pi u}{2a}\right) \sin\left(\frac{n\pi v}{2a}\right)$$

$$\cos\left(\frac{p\pi v}{2a}\right) - \sin\left(\frac{p\pi u}{2a}\right) \sin\left(\frac{n\pi u}{2a}\right) \cos\left(\frac{p\pi v}{2a}\right) \cos\left(\frac{n\pi v}{2a}\right) + \cos\left(\frac{p\pi u}{2a}\right)$$

$$\cos\left(\frac{n\pi u}{2a}\right) \sin\left(\frac{p\pi v}{2a}\right) \sin\left(\frac{n\pi v}{2a}\right) - \sin\left(\frac{n\pi u}{2a}\right) \cos\left(\frac{p\pi u}{2a}\right) \cos\left(\frac{n\pi v}{2a}\right)$$

$$\sin\left(\frac{p\pi v}{2a}\right) \qquad (2.59)$$

This is multiplied by $g(u,w)$ and integrated. Since $g(u,w)$ is even in u, only the terms that are also even in u will contribute. Expanding these terms gives:

$$\frac{1}{4}\left\{\left[\cos\left(\frac{p+n}{2a}\pi u\right) - \cos\left(\frac{p-n}{2a}\pi u\right)\right] \left[\cos\left(\frac{p+n}{2a}\pi v\right) + \cos\left(\frac{p-n}{2a}\pi v\right)\right]\right.$$

$$+ \left[\cos \left(\frac{p+n}{2a}\right) \pi u) + \cos \left(\frac{p-n}{2a} \pi u\right)\right] \quad \left[-\cos \left(\frac{p+n}{2a} \pi v\right) + \cos \left(\frac{p-n}{2a} \pi v\right)\right]\Bigg\} \tag{2.60}$$

The integral over v is then over the strip shown in Fig. 2.6

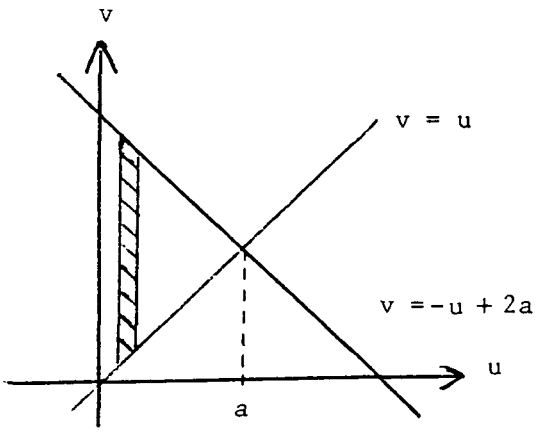

Figure 2.6 Integration Limits

Since it is an even function in u let $\int_{-a}^{a} \{\ \}\, du = 2\int_{0}^{a} \{\ \}\, du$.

The only terms left to be integrated are cosines, where a typical term yields:

$$\int_{u}^{2a-u} \cos (sv)dv = - \sin (su)\left[\frac{1 + \cos (2as)}{s}\right] \tag{2.61}$$

where $s = \frac{(p+n)}{2a}\pi$ or $\frac{(p-n)}{2a}\pi$. Using (2.61) in integrating (2.60) over v leaves:

$$\frac{1}{2} \left\{ \frac{\cos \left[\frac{(p-n)}{2a} \pi u\right] \sin \left[\frac{(p+n)}{2a} \pi u\right][1 + \cos ((p+n)\pi)]}{\frac{(p+n)}{2a}\pi} \right.$$

$$\left.\frac{-\cos\left[\frac{(p+n)\pi u}{2a}\right]\sin\left[\frac{(p-n)\pi u}{2a}\right]\left[1+\cos((p-n)\pi)\right]}{\frac{(p-n)\pi}{2a}}\right\} = \frac{T_1(u)\ a}{\sqrt{\varepsilon_{0n}\varepsilon_{0p}}} \qquad (2.62)$$

Note that integrating over the LHP strip in the u-v space ($\int_{-u}^{2a+u} \{\}\, du$) would give $T_1(-u)$ for $u < 0$ So the result in (2.62) should be $\frac{a}{\sqrt{\varepsilon_{0n}\varepsilon_{0p}}}$ $T_1(|u|)$.

For the $\cos\left(\frac{q\pi}{2b}(w+z)\right)\cos\left(\frac{m\pi}{2b}(z-w)\right)$ term the even functions in w are:

$$\frac{1}{2}\left\{\cos\left(\frac{(q+m)}{2b}\pi w\right)\cos\left(\frac{(q-m)}{2b}\pi z\right)+\cos\left(\frac{(q-m)}{2b}\pi w\right)\cos\left(\frac{(q+m)}{2b}\pi z\right)\right\} \qquad (2.63)$$

Integrating (2.63) over z using (2.61) yields:

$$\frac{1}{2}\left\{-\frac{\cos\left(\frac{(q-m)}{2b}\pi w\right)\sin\left(\frac{(q+m)}{2b}\pi|w|\right)\left[1+\cos((q+m)\pi)\right]}{\frac{(q+m)\pi}{2b}}\right.$$

$$\left.-\frac{\cos\left(\frac{(q+m)}{2b}\pi w\right)\sin\left(\frac{(q-m)}{2b}\pi|w|\right)\left[1+\cos((q-m)\pi)\right]}{\frac{(q-m)\pi}{2b}}\right\} = \frac{T_2(|w|)b}{\sqrt{\varepsilon_{0m}\varepsilon_{0q}}} \qquad (2.64)$$

For the integral $\frac{1}{2\pi}\iiint \Phi_{pq}\left(\frac{v+u}{2},\ \frac{w+z}{2}\right)\cdot g(u,w)\ \Phi_{nm}\left(\frac{v+u}{2},\ \frac{z-w}{2}\right)$ dudv dwdz the two equations that we get after integrating over v and z are:

$$T_3(|u|) = T_2(|u|) \text{ with } b \text{ replaced by } a.$$

$$T_4(|w|) = T_1(|w|) \text{ with } a \text{ replaced by } b. \qquad (2.65)$$

Let

$$T_{pn}^{\pm}(t/h) = \frac{\sqrt{\varepsilon_{0p}\varepsilon_{0n}}}{2h}\left\{\frac{\pm\cos[\frac{(p-n)\pi t}{2h}][1+\cos((p+n)\pi)]\sin[\frac{(p+n)\pi|t|}{2h}]}{\frac{(p+n)\pi}{2h}}\right.$$

$$\left. - \frac{\cos[\frac{(p+n)\pi t}{2h}]\sin[\frac{(p-n)\pi|t|}{2h}][1+\cos((p-n)\pi)]}{\frac{(p-n)\pi}{2h}}\right\} \qquad (2.66)$$

Then

$$T_1(|u|) = T_{pn}^{+}(u/a)$$

$$T_2(|w|) = T_{qm}^{-}(w/b)$$

$$T_3(|u|) = T_{pn}^{-}(u/a)$$

$$T_4(|w|) = T_{qm}^{+}(w/b) \qquad (2.67)$$

Using the same techniques and variable changes the triple integrals can be reduced also. This then gives:

$$Y_{pq,nm}^{x_1x_1} = \frac{-j(k_0^2 - \frac{n^2\pi^2}{a^2})}{\beta_{nm}}\delta_{pn}\delta_{qm} + (k_0^2 - \frac{p^2\pi^2}{a^2})\frac{1}{2\pi}\int_0^a\int_0^b$$

$$T_{pn}^{+}(u/a)\,T_{qm}^{-}(w/b)\,\frac{e^{-jk_0(w^2+u^2)^{1/2}}}{(w^2+u^2)^{1/2}}\,dwdu + \int_0^a\int_0^b(\varepsilon_{0n}\varepsilon_{0p})^{1/2}$$

$$\frac{p}{2a^2}\left[\frac{e^{-jk_0(x_1'^2+w^2)^{1/2}}}{(x_1'^2+w^2)^{1/2}} - \cos(p\pi)\frac{e^{-jk_0((a-x_1')^2+w^2)^{1/2}}}{[(a-x_1')+w^2]^{1/2}}\right]$$

$$\sin\left(\frac{n\pi x_1'}{a}\right) \cdot T_{qm}^{-}(w/b)\, dw dx_1' \qquad (2.68)$$

$$Y_{pq,nm}^{x_1 y_1} = \frac{j\pi^2}{\beta_{nm}} \frac{nm}{ab} \delta_{pn}\delta_{qm} - \frac{pq\pi}{2ab} \int_0^a \int_0^b T_{pn}^{-}(u/a)\, T_{qm}^{+}(w/b)$$

$$\frac{e^{-jk_0(w^2+u^2)^{1/2}}}{(w^2+u^2)^{1/2}}\, dwdu + \int_0^a \int_0^b \frac{(\varepsilon_{0q}\varepsilon_{0m})^{1/2}\, p}{2ab} \left[\frac{e^{-jk_0(u^2+y_1'^2)^{1/2}}}{(u^2+y_1'^2)^{1/2}} \right.$$

$$\left. - \cos(q\pi)\, \frac{e^{-jk_0(u^2+(b-y_1')^2)^{1/2}}}{(u^2+(b-y_1')^2)^{1/2}} \right] \sin\left(\frac{m\pi y_1'}{b}\right) T_{pn}^{-}(u/a)\, dy_1' du \qquad (2.69)$$

$$Y_{pq,nm}^{y_1 x_1} = \frac{j}{\beta_{nm}} \frac{nm\pi^2}{ab}\, \delta_{pn}\, \delta_{qm} - \frac{pq\pi}{2ab} \int_0^a \int_0^b T_{pn}^{+}(u/a)\, T_{qm}^{-}(w/b)$$

$$\frac{e^{-jk_0(u^2+w^2)^{1/2}}}{(u^2+w^2)^{1/2}}\, dwdu + \int_0^a \int_0^b \frac{(\varepsilon_{0n}\varepsilon_{0p})^{1/2}\, q}{2ab} \left[\frac{e^{-jk_0(x_1'^2+w^2)^{1/2}}}{(x_1'^2+w^2)^{1/2}} \right.$$

$$\left. - \frac{\cos(p\pi)\, e^{-jk_0((a-x_1')^2+w^2)^{1/2}}}{((a-x_1')^2+w^2)^{1/2}} \right] \sin\left(\frac{n\pi x_1'}{a}\right) \cdot T_{qm}^{-}(w/b)\, dw dx_1' \qquad (2.70)$$

$$Y_{pq,nm}^{y_1 y_1} = \frac{-j}{\beta_{nm}} \left(k_0^2 - \frac{m^2\pi^2}{b^2}\right) \delta_{pn}\delta_{qm} + \left(k_0^2 - \frac{q^2\pi^2}{b^2}\right) \int_0^a \int_0^b \frac{1}{2\pi} T_{pn}^{-}(u/a)$$

$$T_{qm}^{+}(w/b)\, \frac{e^{-jk_0(u^2+w^2)^{1/2}}}{(u^2+(w)^2)^{1/2}}\, dwdu + \int_0^a \int_0^b \frac{(\varepsilon_{0m}\varepsilon_{0q})^{1/2}\, q}{2b^2}$$

$$\left[\frac{e^{-jk_0(u^2+y_1'^2)^{1/2}}}{(u^2+y_1'^2)^{1/2}} - \frac{\cos(q\pi)\, e^{-jk_0(u^2+(b-y_1')^2)^{1/2}}}{(u^2+(b-y')^2)^{1/2}} \right] \sin\left(\frac{m\pi y_1'}{b}\right)$$

$$T_{pn}^{-}(u/a)\, dy_1' du \tag{2.71}$$

These are the integral equations that are to be solved numerically.

It should be noted that these four integral equations must be further manipulated before applying any of the standard numerical integration techniques. First, if p=n in (2.66) then there exists a singularity in one of the terms where $1/(p-n) = {}^1/_0$. The $T_{pn}^{\pm}(t/h)$ is incorrect at that point. The reason being that $\int_0^a \cos(0\,u)\, du$ should be $\int_0^a 1\, du = a$ not $\left.\frac{\sin(0u)}{0}\right|_0^a$. So for these special cases the p+n or p-n equal to zero should be substituted in first before integrating over the v or z. This gives:

$$T_{00}^{-}(t/h) = 2/h(h-|t|) \tag{2.72}$$

$$T_{00}^{+}(t/h) = 0$$

$$T_{pp}^{+}(t/h) = \frac{1}{h}\left\{ \frac{[\cos(2p\pi)+1]\sin(p\pi|t|/h)}{p\pi/h} - 2\cos(p\pi t/h)(|t|-h) \right\}$$

$$T_{pp}^{-}(t/h) = \frac{1}{h}\left\{ \cos\left(\frac{p\pi t}{h}\right)(2h-2|t|) - \frac{\sin\left(\frac{p\pi|t|}{h}\right)[1+\cos(2p\pi)]}{p\pi/h} \right\}$$

With this change in (2.6o) a new problem arises. That of what to do about the singularities that now occur in the integral equations at u = w = 0 for the three non-zero cases listed above. The term is:

$$\iint \frac{T_{pn}^{\pm}(u)\, T_{qm}^{\pm}(w)\, e^{-jk_0(u^2+w^2)^{1/2}}}{(u^2+w^2)^{1/2}}\, dudw \qquad (2.73)$$

and when integrated numerically the u = w = 0 point is a singular point since $T_{pn}^{\pm}$ and $T_{qm}^{\pm}$ are no longer equal to zero in these cases. To get around this difficulty, the singularity must be subtracted out. This is accomplished by adding and subtracting

$$\iint \frac{T_{pn}^{\pm}(0)\, T_{qm}^{\pm}(0)\, dudw}{\sqrt{u^2+w^2}} \quad \text{from (2.73) leaving:}$$

$$\iint \frac{T_{pn}^{\pm}(u)\, T_{qm}^{\pm}(w) - T_{pn}^{\pm}(0)\, T_{qm}^{\pm}(0)}{(u^2+w^2)^{1/2}}\, dudw + \iint \frac{T_{pn}^{\pm}(0)\, T_{qm}^{\pm}(0)}{(u^2+w^2)^{1/2}}\, dudw$$

The first term then equals zero at u = w = 0 and the second term's denominator can be integrated analytically to yield:

$$b \ln (a + (a^2+b^2)^{1/2}) + a \ln (b + (a^2+b^2)^{1/2}) - b \ln (b) - a \ln (a)$$

Note that for $p \neq n$ in (2.66) that the numerator is zero in the integrals given in (2.73), so no singularity exists.

The last step then is to reduce the equations for coupling between different guides. First, it should be noted that (2.66) is no longer sufficient to cover these 4 cases since g(u, w) is no longer symmetric in u and w, since a typical R here is $((u-D_x)^2 + (w-D_y)^2)^{1/2}$. So a second term needs to be added to the $T_{pn}^{\pm}(t/h)$ to include the non-symmetric terms dropped earlier. The (2.59) non-

symmetric terms are:

$$-\frac{1}{2}\sin\left[\frac{(p+n)}{2a}\pi u\right]\sin\left[\frac{(p-n)}{2a}\pi v\right]+\frac{1}{2}\sin\left[\frac{(p-n)}{2a}\pi u\right]\sin\left[\frac{(p+n)}{2a}\pi v\right]$$

and for (2.63) we have: (2.74)

$$\frac{1}{2}\sin\left[\left(\frac{m+q}{2b}\right)\pi z\right]\sin\left[\left(\frac{m-q}{2b}\right)\pi w\right]+\frac{1}{2}\sin\left[\left(\frac{m-q}{2b}\right)\pi z\right]\sin\left[\left(\frac{m+q}{2b}\right)\pi w\right] \quad (2.75)$$

Solving (2.71) and (2.72) using:

$$\int_u^{2a-u}\sin(sv)\,dv=\frac{\cos(su)\,(1-\cos(2as))}{s} \quad (2.76)$$

with $s=(p\pm n)\pi/2a$ results in the following:

$$R_{pn}^{\pm}(t/h)=\left\{\pm\frac{h}{2}\left[\sin\left(\frac{p\pi t}{h}\right)-\sin\left(\frac{n\pi t}{h}\right)\right]\left[\frac{1-\cos((p+n)\pi)}{(p+n)\pi}\right.\right.$$

$$\left.\left.-\frac{h}{2}\left[\sin\left(\frac{p\pi t}{h}\right)+\sin\left(\frac{n\pi t}{h}\right)\right]\left[\frac{1-\cos((p-n)\pi)}{(p-n)\pi}\right]\right\}\sqrt{\frac{\varepsilon_{0n}\varepsilon_{0p}}{h}} \quad (2.77)$$

The admittance parameters representing coupling between different apertures are found to be:

$$Y_{pq,nm}^{x_1x_2}=\left(k_0^2-\frac{p^2\pi^2}{a^2}\right)\frac{1}{4}\int_{-a}^{a}\int_{-b}^{b}\left[T_{pn}^{+}(u/a)+R_{pn}^{+}(u/a)\right]\left[T_{qm}^{-}(w/b)+\right.$$

$$\left.R_{qm}^{-}(w/b)\right]G(u-D_x,\,w-D_y)\,dwdu+\frac{p\pi}{2a^2}(\varepsilon_{0n}\varepsilon_{0p})^{1/2}\int_{-b}^{b}\int_{0}^{a}\sin\left(\frac{n\pi x_2'}{a}\right)$$

$$\left[G(0-x_2'-D_x,w-Dy)-\cos(p\pi)\,G(a-x_2'-D_x,w-D_y)\right]\left[T_{qm}^{-}(w/b)+R_{qm}^{-}(w/b)\right]\,dx_2'dw$$

(2.78)

$$Y^{x_1y_2}_{pq,nm} = \frac{-p\pi^2 q}{4ab}\int_{-a}^{a}\int_{-b}^{b}[T^-_{pn}(u/a) + R^-_{pn}(u/a)]\,[T^+_{qm}(w/b) +$$

$$R^+_{qm}(w/b)]\;G(u-D_x, w-D_y)\;dwdu + \frac{p\pi}{2ab}(\varepsilon_{0n}\varepsilon_{0q})^{1/2}\int_{-a}^{a}\int_{0}^{b}$$

$$\sin\left(\frac{m\pi y_2'}{b}\right)\,[G(u-D_x, 0-y_2'-D_y) - \cos(q\pi)\;G(u-D_x, b-y_2'-D_y)]$$

$$[T^-_{pn}(u/a) + R^-_{pn}(u/a)]\,dy_2'\,du \qquad (2.79)$$

$$Y^{y_1x_2}_{pq,nm} = \frac{-pq\pi^2}{4ab}\int_{-a}^{a}\int_{-b}^{b}[T^+_{pn}(u/a) + R^+_{pn}(u/a)]\,[T^-_{qm}(w/b) + R^-_{qm}(w/b)]$$

$$G(u-D_x, w-D_y)\,dwdu + \frac{q\pi}{2ab}(\varepsilon_{0n}\varepsilon_{0p})^{1/2}\int_{-b}^{b}\int_{0}^{a}\sin\left(\frac{n\pi x_2'}{a}\right)$$

$$(G(0-x_2'-D_x, w-D_y) - \cos(p\pi)\;G(a-x_2'-D_x, w-D_y))\,[T^-_{qm}(w/b) + R^-_{qm}(w/b)]$$

$$dx_2'\,dw \qquad (2.80)$$

$$Y^{y_1y_2}_{pq,nm} = (k_0^2 - \frac{q^2\pi^2}{b^2})\frac{1}{4}\int_{-a}^{a}\int_{-b}^{b}[T^-_{pn}(u/a) + R^-_{pn}(u/a)]\,[T^+_{qm}(w/b) +$$

$$R^+_{qm}(w/b)]\;G(u-D_x, w-D_y)\,dwdu + \frac{q\pi}{2b^2}(\varepsilon_{0m}\varepsilon_{0q})^{1/2}\int_{-a}^{a}\int_{0}^{b}\sin\left(\frac{m\pi y_2'}{b}\right)$$

$$[G(u-D_x, 0-y_2'-D_y) - \cos(q\pi)\;G(u-D_x, b-y_2'-D_y)]\,[T^-_{pn}(u/a) +$$

$$R^-_{pn}(u/a)]\,dy_2'\,du \qquad (2.81)$$

where $$G(u,w) = \frac{e^{-jk_0(u^2+w^2)^{1/2}}}{2\pi(u^2+w^2)^{1/2}}$$

It should also be noted that in looking at the equations, it can be

seen that

$$Y^{x_2y_1}_{pq,nm} = Y^{y_1x_2}_{nm,pq} \qquad (2.82)$$

For aperture to aperture coupling there is no need to worry about singularities since R will never equal zero. The only way it can happen is if the distance between the apertures exactly equals the size of the apertures with zero wall thickness, but then there wouldn't be two apertures only one larger one.

This concludes the mathematical manipulations needed to reduce the integral equations. The terms are now all double integrals that can be easily evaluated by Simpson's rule.

2.6 Scattering Parameters and Radiation Patterns

By using any of the techniques described in the earlier sections the amplitudes of the equivalent magnetic currents (or of the $\underline{E}_a$ in the case of the Fourier transform approaches) can be found. Once these are known the information must be put into a form usable by the antenna designer. The parameters that can be solved for using these quantities are the scattering parameters and the radiation patterns (which provide the side lobe levels, cross-polarization, etc.). By using the C_{nm} and D_{nm} solved for in the vector potential approach the equations for the S parameters and the ϕ = 0, 45° and 90° co- and cross-polarization patterns will be derived in this section. The C_{nm} and D_{nm} are chosen since the vector potential approach is the one used in this report.

First we consider 2 guides each driven by the TE_{10} mode. Let

V_1^+ and V_1^- be the incident and reflected voltages in guide 1 and V_2^+ and V_2^- in guide 2. These are related as follows:

$$V_1^- = S_{11}V_1^+ + S_{12}V_2^+$$

$$V_2^- = S_{21}V_1^+ + S_{22}V_2^+$$

Where the S_{ij} are the scattering matrix elements.

The equivalent voltages are proportional to the amplitude of the incident and reflected 10 vector potential modes so $V_1^+ \propto A_{10}^1$ and $V_2^+ \propto A_{10}^2$. The reflected vector potential mode is proportional to A_{10}^1 plus that contributed by the aperture currents using the Greens dyadic derived in Sec. 2.3. The latter contributes $\frac{\varepsilon_0}{j\beta_{10}} C_{10}^1$. Thus $V_1^- \propto -(A_{10}^1 + \frac{\varepsilon_0}{j\beta_{10}} C_{10}^1)$ where the negative sign is due to electric field's dependence on the derivative with respect to z of the $\underline{A}_m^{wg}$. Knowing this, then:

$$-(A_{10}^1 + \frac{\varepsilon_0}{j\beta_{10}} C_{10}^1) = S_{11}A_{10}^1 + S_{12}A_{10}^2 \qquad (2.83)$$

$$-(A_{10}^2 + \frac{\varepsilon_0}{j\beta_{10}} C_{10}^2) = S_{21}A_{10}^1 + S_{22}A_{10}^2$$

If only the 1st guide is driven the following holds:

$$S_{21} = \frac{jC_{10}^2\varepsilon_0}{\beta_{10}A_{10}} \quad \text{and} \quad S_{11} = \frac{jC_{10}^1\varepsilon_0}{A_{10}\beta_{10}} - 1 \qquad (2.84)$$

Using this the coupled power from 1 to 2 is $20\log(|S_{21}|)$ and the reflection coefficient in guide #1 is S_{11}.

In practice the only scattering matrix parameters that are useful are those that relate the amplitudes of the dominant propagating modes in each waveguide. Therefore the scattering matrix parameters for the other modes that may exist in the aperture aren't included. For the cases where there are more than two apertures the scattering parameters (S_{21}, S_{31}, S_{41}, . . .) are found by exciting one guide and computing the amplitude of the propagating modes excited in the other guides and then solving for the S_{ij} one at a time. The procedure is a straightforward extension of that described above for obtaining S_{21}.

The next topic in this discussion is the derivation of the far zone radiation patterns of the array. We use the fact that the far zone radiated magnetic field $\underline{H}_F$ is given by the θ and ϕ components of $-j\omega \underline{A}_m^{HS}$ and that $\underline{E}_F = -Z_0 \underline{a}_r \times \underline{H}_F$ (Stutzman and Theile, 1981). The equation for the $\underline{A}_m^{HS}$ has already been presented in (2.28) and it's far zone form is:

$$\underline{A}_m^{HS} = \frac{e^{-jk_0 r}}{2\pi r} \underline{n} \times \int\int \varepsilon_0 \underline{E}_a \, e^{jk_0 \underline{a}_r \cdot \underline{r}'} \, dS' \qquad (2.85)$$

which is a two dimensional Fourier transform where

$$\underline{a}_r \cdot \underline{r}' = (\underline{a}_x \sin\theta \cos\phi + \underline{a}_y \cdot \sin\theta \sin\phi) \cdot (x' \underline{a}_x + y' \underline{a}_y)$$

$$= x' \sin\theta \cos\phi + y' \sin\theta \sin\phi$$

In this situation then the two $\underline{A}_m^{HS}$ terms for a single radiating element ($A_{m,x}^{HS} \underline{a}_x$ and $A_{m,y}^{HS} \underline{a}_y$) are proportional to the following two terms

$$J_{m,x} = \int_0^a \int_0^b \sum_{n,m} C_{nm}^{1} \psi_{nm}(x', y') e^{(jk_x x' + jk_y y')} dy' dx' \tag{2.86}$$

$$J_{m,y} = \int_0^a \int_0^b \sum_{n,m}' D_{nm}^{1} \phi_{nm}(x', y') e^{(jk_x x' + jk_y y')} dy' dx' \tag{2.87}$$

where $k_x = k_o \sin\theta \cos\phi$ and $k_y = k_0 \sin\theta \sin\phi$

Once these two have been solved they can be substituted into the following two equations to find E_ϕ and E_θ in the far zone region. (Stutzman and Thiele, 1981, Sec. 8.1):

$$\underline{E}_\theta = \frac{jk_0}{2\pi r} e^{-jk_0 r} (J_{m,y} \cos\phi - J_{m,x} \sin\phi) \underline{a}_\theta \tag{2.88}$$

$$\underline{E}_\phi = \frac{-jk_0}{2\pi r} e^{-jk_0 r} (J_{m,x} \cos\phi + J_{m,y} \sin\phi) \underline{a}_\varphi \cos\theta \tag{2.89}$$

For the multi aperture problem the $J_{m,x}$ and $J_{m,y}$ terms need to be changed to account for the added current terms.

Terms due to the other aperture currents, shifted in phase due to their physical spacing must be included. This gives for (2.86) and (2.87):

$$J_{m,x} = \sum_{n.m} \int_0^a \int_0^b e^{j(k_x x' + k_y y')} [C_{nm}^{1} \psi_{nm}(x', y') + C_{nm}^{2} \psi_{nm}(x', y') e^{j(k_x D_x + k_y D_y)} + \ldots] dy' dx' \tag{2.90}$$

$$J_{m,y} = \sum_{n,m}{}' \int_0^a \int_0^b e^{j(k_x x' + k_y y')} \left[D_{nm}^{1} \Phi_{nm}(x',y') + D_{nm}^{2} \Phi_{nm}(x',y') e^{j(k_x D_x + k_y D_y)} + \ldots \right] dy' dx' \qquad (2.91)$$

where the spacings are all referenced to guide #1. These, when added to (2.85) and (2.86) give the far zone field patterns for the given array.

The co-and cross-polarization fields as defined by Ludwig are the fields measured by a horn polarized in the same direction as the radiating antenna for the former and as the fields measured by a horn polarized at right angles to the source for the latter (Ludwig, 1973). The co- and cross-polarized patterns provide an important set of patterns for use in analyzing the cross polarization interference between adjacent scanning areas. The definitions of the two are:

$$R(\theta,\phi) = \underline{E}(\theta,\phi) \cdot (\sin\phi\, \underline{a}_\theta + \cos\phi\, \underline{a}_\phi) \qquad (2.92)$$

$$C(\theta,\phi) = \underline{E}(\theta,\phi) \cdot (\cos\phi\, \underline{a}_\theta - \sin\phi\, \underline{a}_\phi)$$

where $R(\theta,\phi)$ is the reference or co-polarization field and $C(\theta,\phi)$ the cross-polarization pattern (Ludwig, 1973). Using this the resulting pattern equations are:

$$R(\theta,\phi)\big|_{\phi=0} = -J_{m,x} \cos\theta \qquad (2.93)$$

$$C(\theta,\phi)\big|_{\phi=0} = J_{m,y}$$

$$R(\theta,\phi)\Big|_{\phi = 45°} = \frac{J_{m,y}}{2}(1-\cos\theta) - \frac{J_{m,x}}{2}(1+\cos\theta) \qquad (2.94)$$

$$C(\theta,\phi)\Big|_{\phi = 45°} = \frac{J_{m,y}}{2}(1+\cos\theta) + \frac{J_{m,x}}{2}(\cos\theta - 1)$$

$$R(\theta,\phi)\Big|_{\phi = 90°} = -J_{m,x} \qquad (2.95)$$

$$C(\theta,\phi)\Big|_{\phi = 90°} = J_{m,y}\cos\theta$$

where the common $\frac{jk_0\, e^{-jk_0 r}}{2\pi r}$ factor was not included in the equations.

With the equations now defined, the only problem remaining is the solution for the $J_{m,x}$ and $J_{m,y}$ terms.

Using the following:

$$\int \sin(bx)\, e^{ax} dx = \frac{e^{ax}(a\sin bx - b\cos bx)}{a^2 + b^2}$$

$$\int \cos(bx)\, e^{ax} dx = \frac{e^{ax}(a\cos bx + b\sin bx)}{a^2 + b^2}$$

(2.86) and (2.87) can be solved to yield:

$$J_{m,x} = \sum_{n,m} C_{nm} \left(\frac{\varepsilon_{on}\varepsilon_{om}}{ab}\right)^{1/2} \left\{ \frac{n\pi}{a} \frac{[1-\cos(n\pi)\, e^{jk_x a}]}{\left[\left(\frac{n\pi}{a}\right)^2 - k_x^2\right]} jk_y \right.$$

$$\left. \frac{[e^{jk_y b}\cos(m\pi) - 1]}{\left[\left(\frac{m\pi}{b}\right)^2 - k_y^2\right]} \right\} \qquad (2.96)$$

$$J_{m,y} = \sum_{n,m}{}' C_{nm} \left(\frac{\varepsilon_{on}\varepsilon_{om}}{ab}\right)^{1/2} \left\{ \frac{m\pi}{b} \frac{[1-\cos(m\pi)\, e^{jk_y b}]}{\left[\left(\frac{m\pi}{b}\right)^2 - k_y^2\right]} jk_x \right.$$

$$\left. \frac{[e^{jk_x a}\cos(n\pi) - 1]}{\left[\left(\frac{n\pi}{a}\right)^2 - k_x^2\right]} \right\} \qquad (2.97)$$

The only problem with the use of these equations ((2.96) and (2.97)) is the case where $k_y = k_x = 0$ ($\theta = 0°$). At that point $J_{m,x} = 0$ except when $m = 0$ also, then $J_{m,x} = \frac{0}{0}$. So this situation must be tested for and when it arises, the result, found by using l'Hospital's rule substituted in it's place.

That concludes the pattern analysis. Since the 2 sets of terms are the same for each current (different modes in different guides) except for the D_x, D_y phase terms the patterns can easily be calculated as a sum of these quantities.

These two sets of parameters then conclude the analysis of an antenna array with mutual coupling. The S parameters yield coupled power and reflection coefficients while the patterns calculations yield the side lobe levels, cross-polarization and scan affects.

2.7 First Order Coupling

Since the computer time needed to solve large arrays can be considerable, future work in ways to approximate the problem is needed. One possible technique is the idea of first order coupling.

First order coupling solves for the coupling from a driven guide to it's surrounding undriven guides and ignores any fields that might be coupled back due to the undriven guides re-radiating the fields. The possible use of this technique could reduce computational costs significantly, but needs further study before it can be considered complete.

The main idea behind this technique is that the magnitude of a field that is coupled to a neighboring guide from a driven guide

and then re-radiated back again should be small enough to be ignored. Figure 2.7 may help explain it better. For the two aperture case (guides 1 and 2) only the Y_{21} is considered. The Y_{12} is ignored.

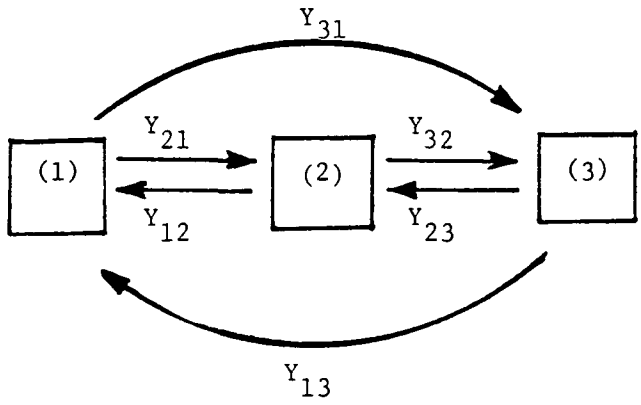

Figure 2.7 Coupling in a Three Aperture Array.

For the case where only one aperture is driven the results taken using the computer model for 2 and 3 apertures seem to support this theory (see Chapter 3). It was also found that for the 3 aperture case with the first one driven, that the coupling from the second to the third aperture must also be included to accurately predict the field in the third. Looking at Figure 2.7 this means that the Y_{21}, Y_{31} and Y_{32} must be accounted for. The reason for including Y_{32} is that (3) is closer to (2) than (1). So the re-radiated field from (2) is large enough compared to the field from (1) that it cannot be ignored in the case presented here where all three apertures are in a straight line.

The incorporation of this idea into the computer model is very

easy. Basically all the terms for coupling from (2) to (1), (3) to (1) and (3) to (2) are set to zero.

This is shown below:

$$\begin{bmatrix} Y_{11} & Y_{12} & Y_{13} \\ Y_{12} & Y_{22} & Y_{23} \\ Y_{13} & Y_{23} & Y_{33} \end{bmatrix} \qquad \begin{bmatrix} Y_{11} & 0 & 0 \\ Y_{12} & Y_{22} & 0 \\ Y_{13} & Y_{23} & Y_{33} \end{bmatrix}$$

Full Coupling First Order Coupling

(reciprocity is used in these matrices). This is for the case of a single driven element.

The advantage of this approach is that for large arrays with only ψ_{10} modes in the current approximation, the resulting matrix is a lower triangular matrix, like the one shown above. These types of matrices are very easy to solve using back substitution (Cheney and Kincaid, 1980), which does not require a matrix inversion. Also, the number of needed storage locations is cut almost in half. So a given computer could handle larger arrays. Using these results then, the S parameters and the radiation pattern of a single radiating element in a large array could be found quite rapidly, even if more than a single mode is used the computation time is still reduced in large arrays because the number of admittance terms to solve for is smaller.

To use this idea in a large array with several guides driven is not as easy to do. This is a part that needs further study.

A possible technique may be to solve for the currents in a few representative cases (guides on the edge, on a corner and in the middle) using this approximation in smaller arrays. Then applying superposition, the entire array solution could be found. A second and maybe more promising idea would start by breaking the large array up into a smaller one. The coupling terms from this smaller array could then be substituted into the complete larger matrix which would then be inverted. This says that if first order coupling is all that's needed then coupling from far away guides (several rows away) and from re-radiated fields can be ignored. This idea would considerably reduce the time needed to calculate the admittance matrix.

Further tests on this subject need to be run before it can be considered a valid approach. Some tests for 2 and 3 aperture arrays are presented in the next chapter.

2.8 Conclusion

In this chapter four techniques for solving for the mutual coupling between open ended waveguide elements in an array were presented. They were (1) Fourier transform method, which solves directly for field amplitudes in the transform domain, (2) the TE and TM mode and (3) sinusoidal-piecewise aperture field expansion methods which use the method of moments to solve for the amplitude of equivalent magnetic currents, and (4) the vector potential approach which is similar to (2) except in the choice of basis functions and the manner in which the integral equations are derived.

In looking at the various approaches many similarities between them appear. The Fourier transform method used by Bailey (1972) is very similar to the TE and TM modal function approach. They both solve for the admittance matrix that relates the inputs (the source modes of the driven guides) to the resulting fields which are approximated by TE and TM modal functions. The latter uses the method of moments to derive the admittance equations and the former solves the reaction integral for admittance directly, using Fourier transforms.

The three method of moments approaches set up the same problem, but differ in choice of basis functions. Harrington and Luzwick and the vector potential approach use modal functions to reduce the size of the resulting matrix. The sinusoidal-piecewise basis functions used by Fenn et al, on the other hand, are used because the resulting integral equations are easier to evaluate. Another advantage of this approach is that for large numbers of basis functions per aperture the guide edge singularities can be analyzed (see Fenn et al, 1982). The main drawback with it though is that for square guides large numbers of patches are needed (24 was found to be necessary) per aperture. This results in very large matrices that must be solved for and inverted, preventing the solution of large arrays.

The vector potential approach was the one chosen for use in the computer model presented in this report and was derived in greater detail. The reason for it's choice was that by using the

vector potential modal functions the integral equations were more straight-forward to work with and solve. It is also easier to include several, including orthogonal modes, in the solution, and finally, the resulting equivalent magnetic corrents are easy to work with in solving for the radiation patterns.

The rest of the chapter (the last three sections) present mathematical techniques and parameter derivations that were used in designing the computer model along with a possible method for approximating large arrays.

CHAPTER 3

COUPLING EFFECTS

3.1 Introduction

A computer program was written to solve the equations derived in the last chapter using Simpson's Rule (see Appendices A and B for listing and user instructions). It is a very flexible program that can accept any reasonable number of modes and array elements. It can also be configured to output first order coupling results. In this chapter samples of data run on this program will be presented. Some of it will be compared against published data to test the validity of the model, while the rest will be used to provide more insight into the mutual coupling problem.

3.2 Single Aperture

The analysis of a single aperture in a ground plane provides much needed information for use in computer runs involving larger arrays. The results provide a means for determining the best magnetic current approximation to use (which modes). The data also provides insight into the problem of a waveguide to free space interface by showing the types and magnitude of the fields excited there and the size of the reflected wave.

The determination of the number of modes needed for a good approximation is the first topic to be considered. The symmetry of the incident TE_{10} E field is even about the midplane of the y axis and even about the midplane of the x axis. The only fields excited in the aperture then should be ones of like symmetry (Borgiotti, Nov.

1968). It follows then that the testing and basis functions should be ψ_{nm} with n = 1, 3, 5, . . . and m = 0, 2, 4, . . . and Φ_{nm} with n = 1, 3, 5, . . . and m = 2, 4, 6, . . Table I shows the results of computer runs made using various combinations of these modes. The aperture is square and 0.6λ in width. Shown are the normalized aperture E field modal amplitudes. (see Appendix C for normalization used). Table II shows the results for a like set of modes for a rectangular aperture where $a = 0.8\lambda$ and $b = 0.4\lambda$ using the same normalization. It can be seen from these two tables that ψ_{10}, ψ_{12}, ψ_{30} and Φ_{12} appears to be the best choice. It has the fewest number of modes that shows no change in C_{10} when additional modes are included. Also any added modes are of magnitudes that are 3% or less of C_{10}.

It should be noted when looking at these tables that there appears to be a strong interaction between orthogonal modes of identical n and m. In Table I C_{12} changed by almost 50% when Φ_{12} was added. This happened for all such cases listed in both tables. This interdependence is expected due to the fact that for a given nm waveguide mode where $m \neq 0$ there is both an x and y component to the E field. It is because of this phenomenon that Φ_{12} should be included in rectangular waveguide solutions (Table II). The magnitude of D_{12} is less than 2% of C_{10} but it's addition means a large change in C_{12}. So when using a ψ_{nm} with $m \neq 0$ it's corresponding Φ_{nm} should be included to insure proper results.

After the number of modes was determined a comparison of reflection coefficients, found using the vector potential approach, against ones, found by Fenn et al. using the piecewise sinusoidal functions.

TABLE I

Normalized Aperture Electric Field Modal Amplitudes, Square Aperture.

NUMBER OF MODES	MODE AMPLITUDES (Magnitude, Phase) C_{10}	C_{12}	C_{30}	C_{32}	D_{12}	D_{32}
1	.894, -1.4°	-	-	-	-	-
2	.924, -2.3°	.28, -57°	-	-	-	-
3	.916, -2.2°	.283, -57°	.044, -53°	-	-	-
4	.916, -2.2°	.283, -57°	.044, -53°	.003, 203°	-	-
4	.911, -1.5°	.145,-39.5°	.045, -54°	-	.0474,-79°	-
5	.911, -1.5°	.145,-39.6°	.045, -54°	.008, 124°	.0474,-79°	-
6	.911, -1.5°	.145,-39.6°	.045, -54°	.014, -92°	.047, -79°	.027, -79°

TABLE II

Normalized Aperture Electric Field Modal Amplitudes, Rect. Aperture.

NUMBER OF MODES	MODE AMPLITUDES (Magnitude, Phase)					
	C_{10}	C_{12}	C_{30}	C_{32}	D_{12}	D_{32}
1	1.03, -12°	-	-	-	-	-
2	1.05, -12°	.246, -43°	-	-	-	-
3	1.05, -11°	.246, -44°	.056, -77°	-	-	-
4	1.05, -11°	.247, -44°	.056, -78°	.0095, 150°	-	-
4	1.044, -11°	.21, -38°	.057, -78°	-	.018, -76°	-
5	1.044, -11°	.21, -38°	.056, -78°	.011, 151°	.019, -75°	-
6	1.044, -11°	.21, -38°	.056, -78°	.019, 264°	.018, -75°	.014, -75°

was run. The first set of points is for a rectangular aperture varying the width (measured in number of λ) but not the width to length ratio. Plots of the results are shown in Fig. 3.1. The comparison data is read off a graph included in the article (Fenn et al, 1982) for 7 sinusoidal patches all x directed. The next case was a square aperture, again varying the width. It is shown in Fig. 3.2, Fenn et al's data were also read off a plot included in their article. These two sets of plots show the excellent agreement that exists between the two models.

Finally the plots of the radiation patterns for a single square aperture are presented in Figures 3.3, 3.4, and 3.5, Each plot is for a given phi angle (0°, 45° or 90°) with the theta varying from -90 to 90°. The coordinate system is shown in Fig. 2.1. The phi = 0° is equivalent to an H-plane pattern and phi = 90° to an E-plane pattern. The phi = 45° plot shows both the co- and cross-polarized patterns. For ϕ = 90° and 0° there is no cross-pol. pattern due to the symmetry of the single aperture antenna. These plots are included here for comparison against results presented in later sections.

3.3 Two Aperture Analysis

In this section further comparisons of computer derived results against published data will be presented. These will be followed by a look as some tests of the first order coupling hypothesis for two aperture arrays.

The first comparison presented is one between results from this model and some of the results presented by Luzwick and Harrington

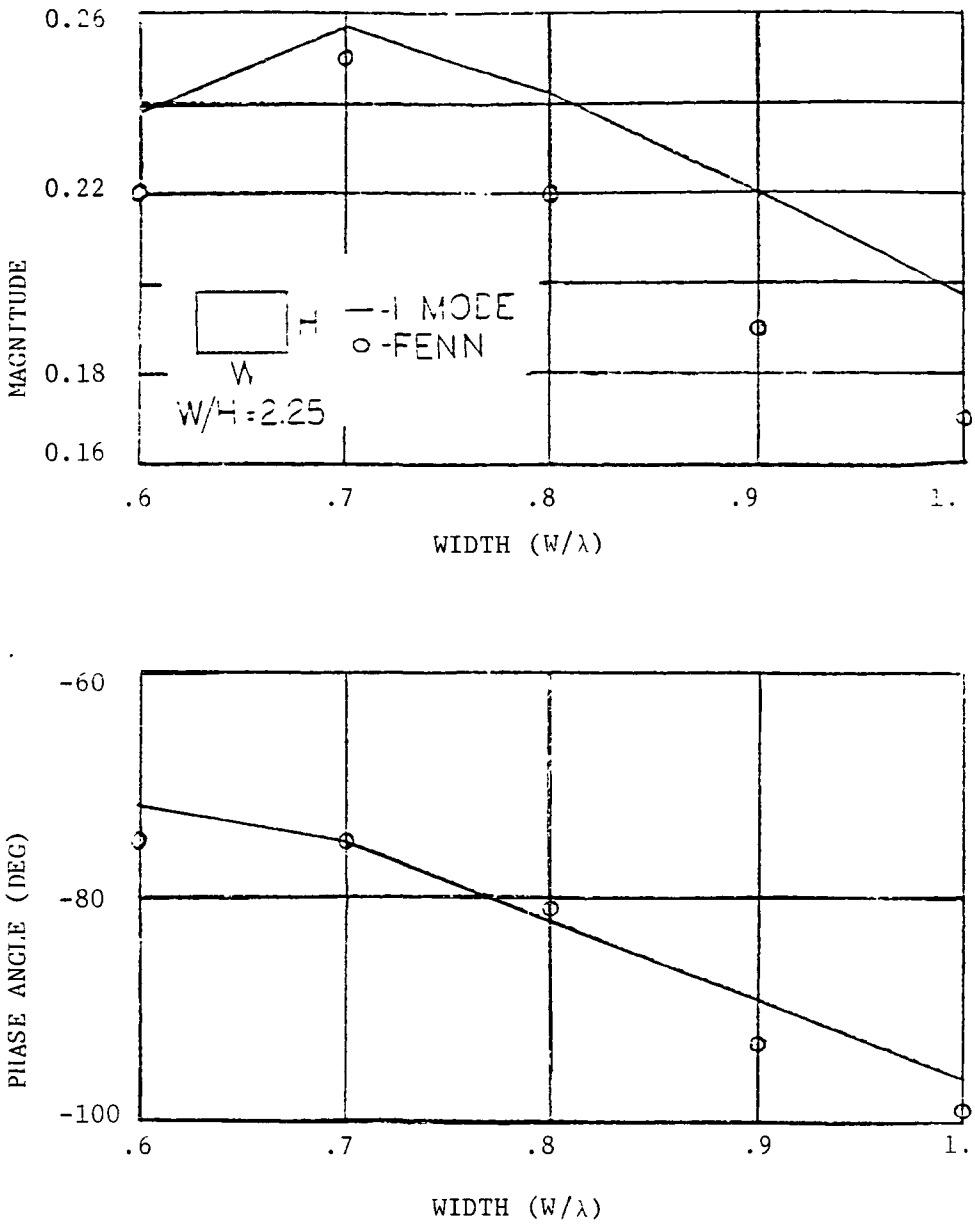

Figure 3.1 Reflection Coefficient of a Rectangular Aperture.

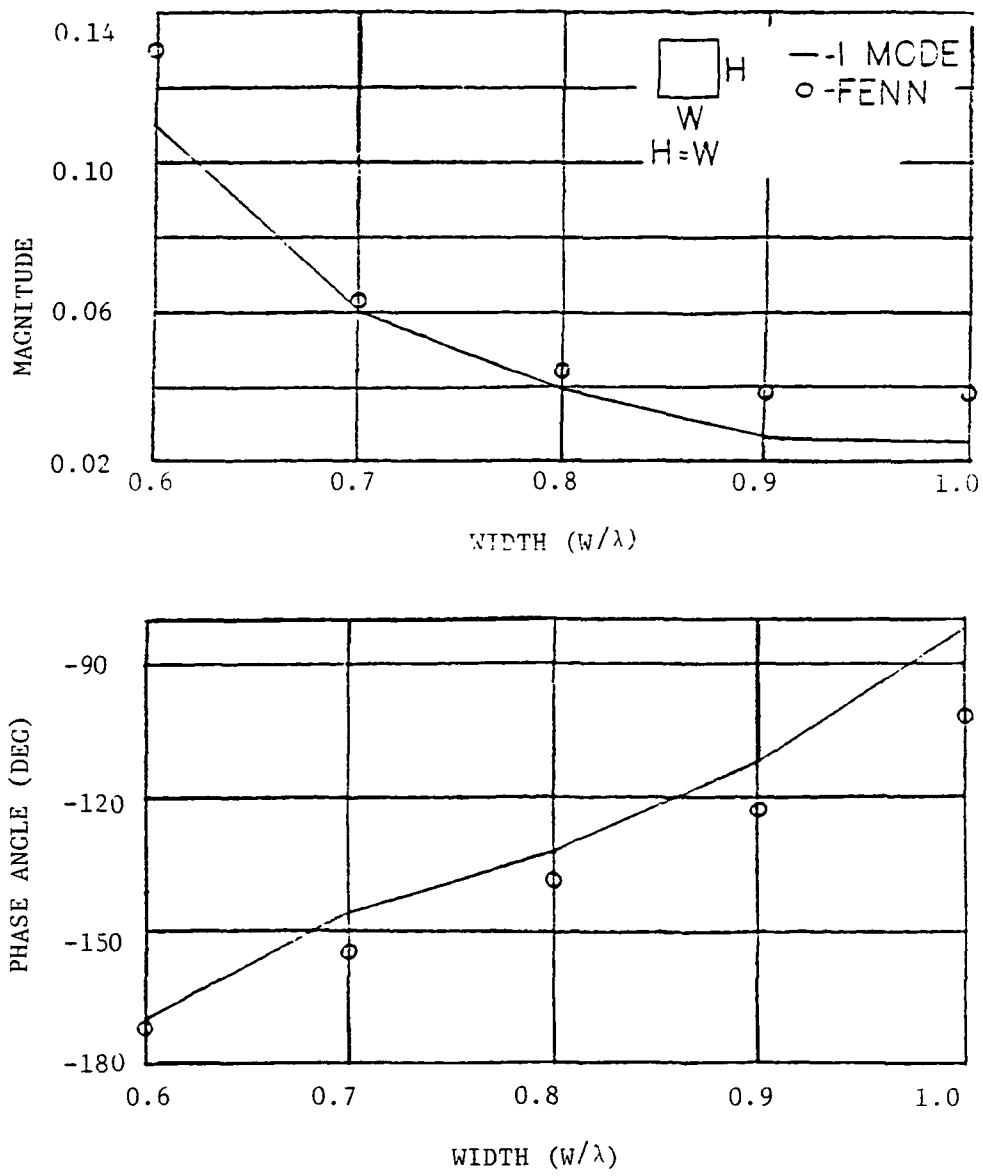

Figure 3.2 Reflection Coefficient of a Square Aperture.

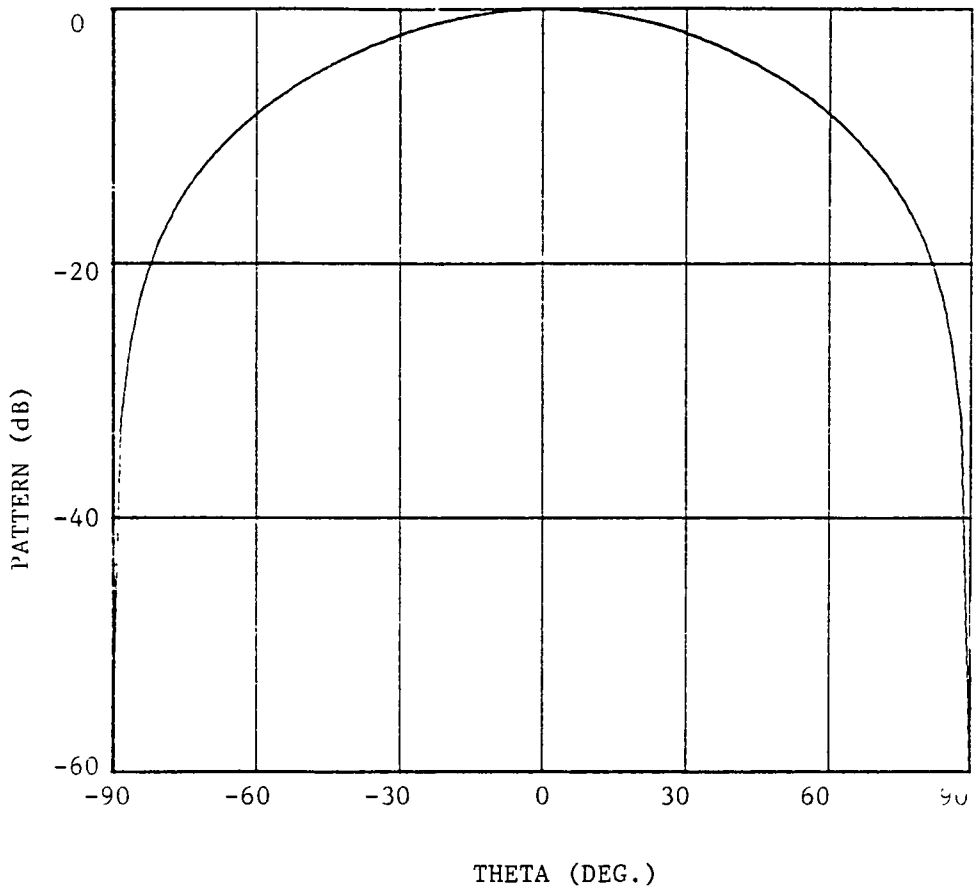

Figure 3.3 Co-Polarized Radiation Pattern, $\phi = 0°$
For a Single Square Aperture (.6λx.6λ)

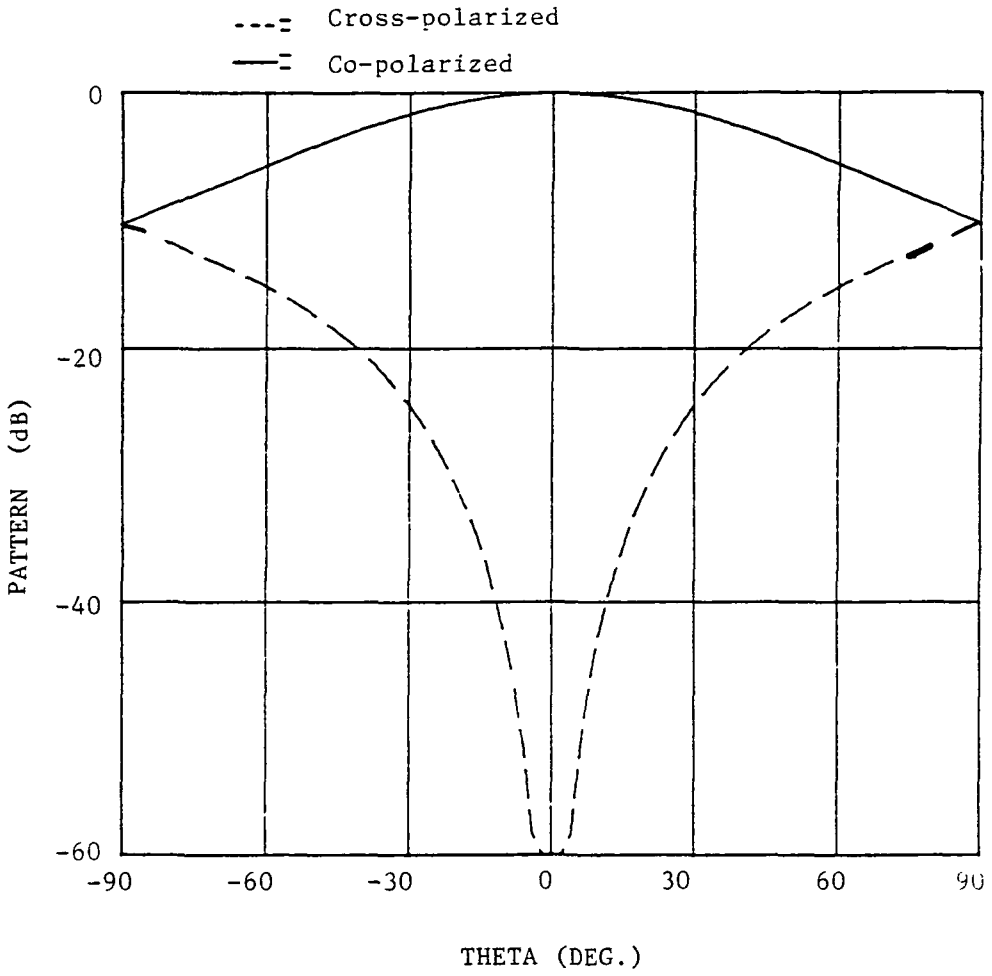

Figure 3.4 Radiation Patterns, $\phi = 45°$

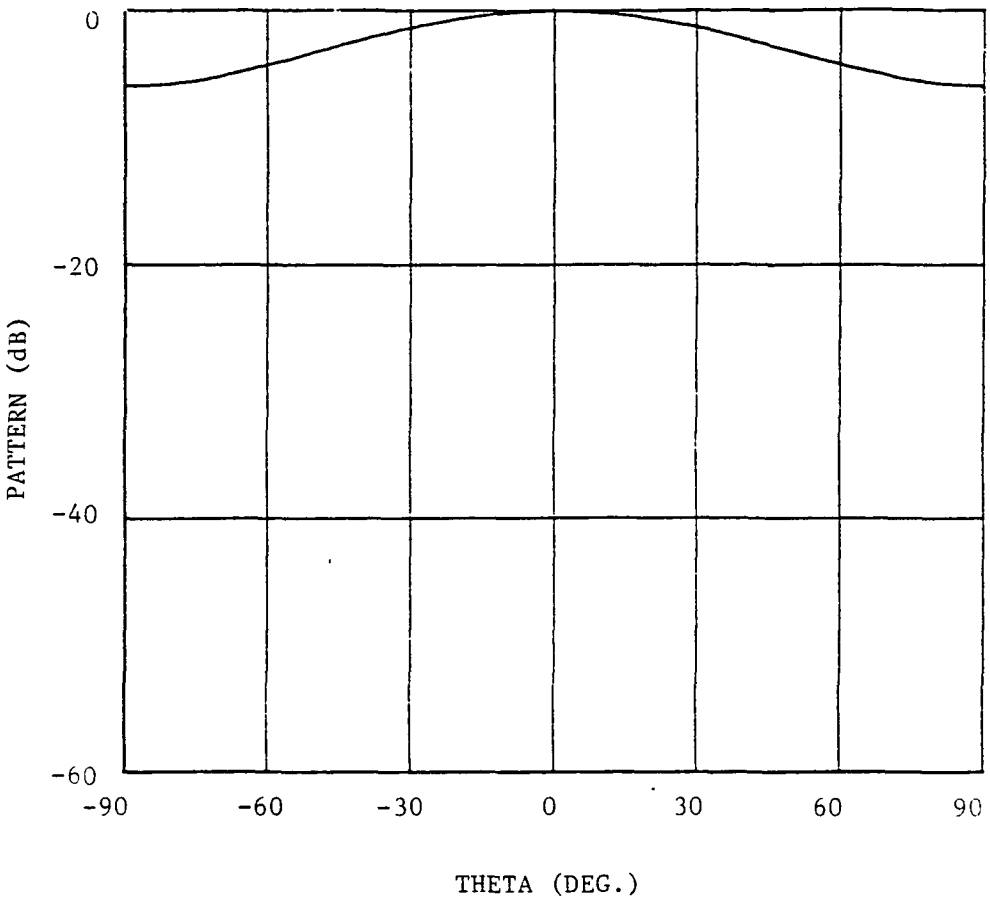

Figure 3.5 Co-Polarized Radiation Pattern, $\phi = 90°$

(Luzwick and Harrington, 1982). They presented plots of the Y^{HS} admittance term (see Section 2.4) for coupling between two apertures at a constant distance but at varying angles referenced to each other. The comparisons are shown in Fig. 3.6, where dimensions are given in terms of λ. The computer data used a single mode approximation (ψ_{10}), similar to what was used by Harrington and Luzwick. The agreement here is very good.

The next comparison is against data published by Mailloux (Mailloux, Nov. 1969). In his article, results are presented for coupling between two apertures that each support two orthogonal modes (TE_{10} and TE_{01}). The S parameters for coupling from the dominant TE_{10} mode in the driven guide to the TE_{10} and TE_{01} modes in the undriven neighboring guide are plotted. The results are for two apertures at constant distance, but with varying angles again. Comparisons of $S_{TE_{10}^1, TE_{10}^2}$ and $S_{TE_{10}^1, TE_{01}^2}$ are shown in Fig's 3.7, 3.8, 3.9, and 3.10, for two different spacings. Dimensions are in terms of λ. Here again good agreement can be seen. ψ_{10} and ϕ_{01} modes were used in the computer approximation.

It should be noted that the agreement with Harrington and Luzwick's results appears to be better than the agreement with Mailloux's results. Harrington's plots were larger and easier to read data off of and that is the reason for the better fit on those plots.

Now that the validity of the computer model has been established a few tests of the first order coupling hypothesis, whose validity needs to be checked, will be presented. As a reminder, the idea

behind this approximation technique is to assume that the fields re-radiated by neighboring undriven elements are small enough to be left out of the calculation, for a more detailed discussion see Sec. 2.8.

To test the first order coupling idea, computer runs were made for two co-linear apertures mounted horizontally using the four mode approximation determined in the last section. Figures 3.11, 3.12, 3.13 and 3.14 show comparisons of the mode amplitudes found using first order coupling against the mode amplitudes found using the complete matrix. It can be seen that the effects seem to be larger on the driven element than on the neighboring undriven one. This is because the effect on the undriven element due to the removal of the re-radiated fields is a second order effect so, it's change will be small. Since it is so small the next set of plots will look only at the driven aperture amplitudes.

Figures 3.15, 3.16, 3.17 and 3.18 show the comparison of first order mode amplitudes verses the complete matrix amplitudes for two different aperture arrangements. Figures 3.19 and 3.20 show the same set of amplitudes but for a pair of rectangular apertures.

Finally to test the effect on the patterns, Fig. 3.21, 3.22, and 3.23 show a comparison of the patterns for the three configurations with square guides and 0.8λ spacings. All are for only one element driven. The dashed curves which are the first order coupled plots are almost indistinguishable from the solid curves which are the complete plots. Therefore these patterns can be considered virtually identical.

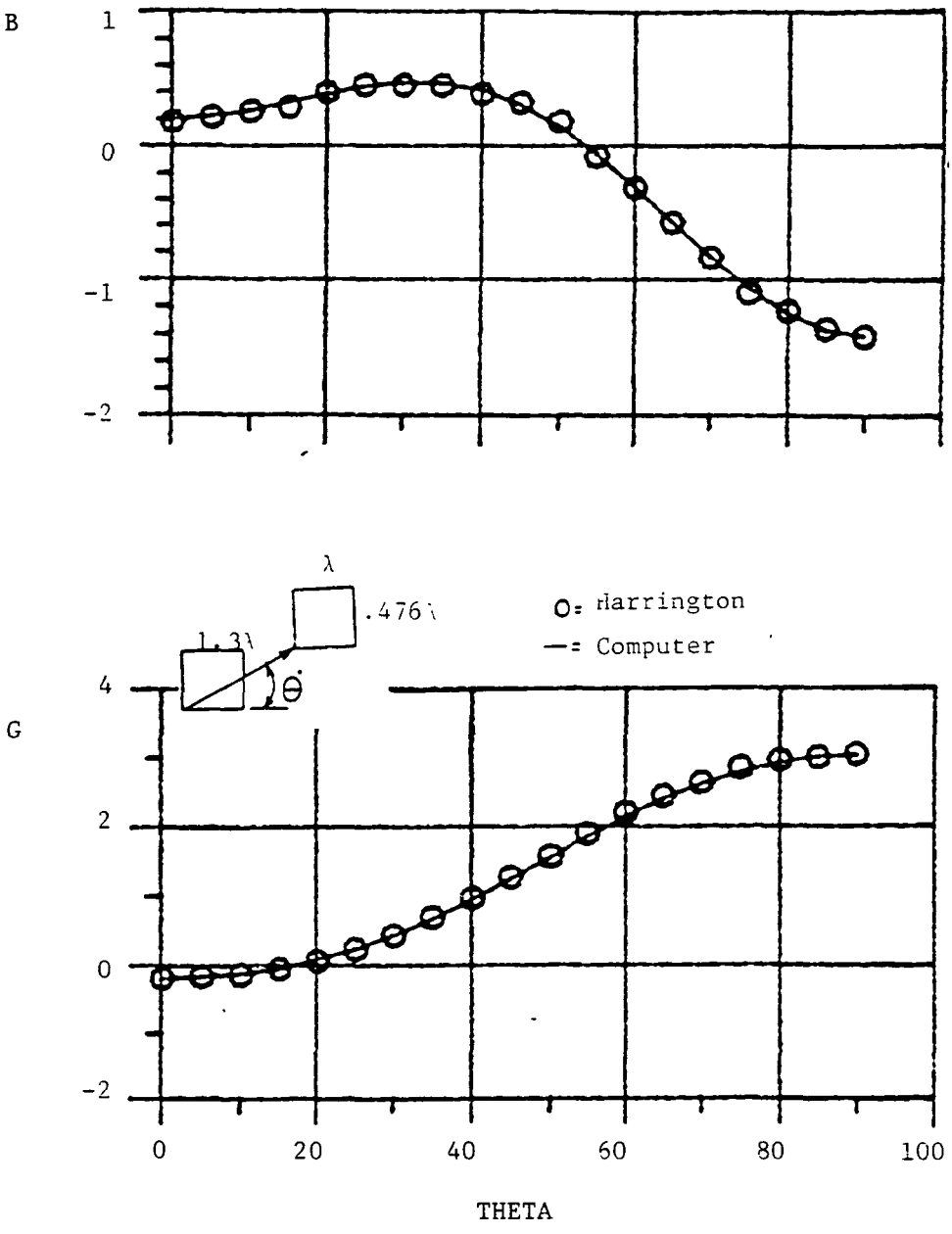

Figure 3.6 Comparison of $Y^{HS} = G + jB$ (in .0001 mhos)

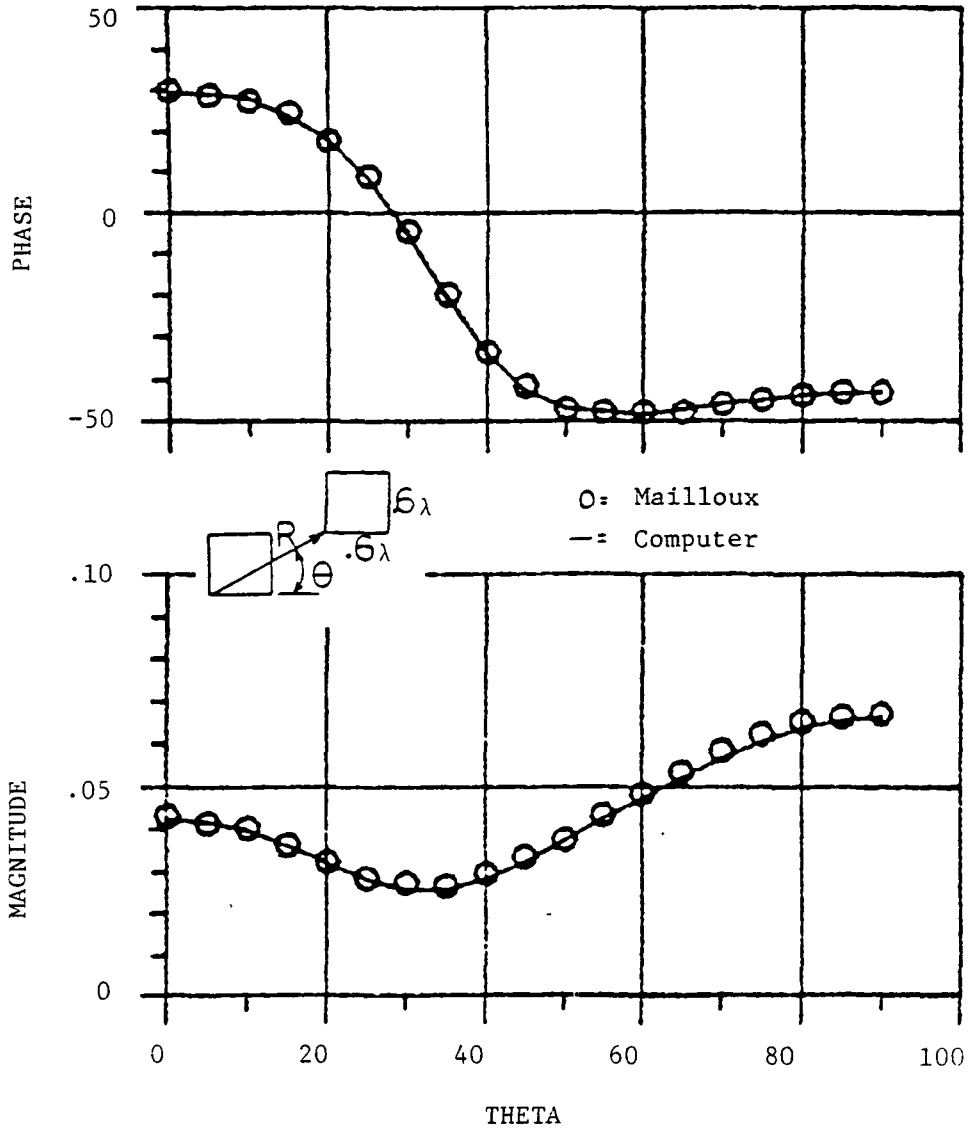

Figure 3.7 Comparisons of $S_{TE_{10}1}$, $TE_{10}2$, R = .9λ

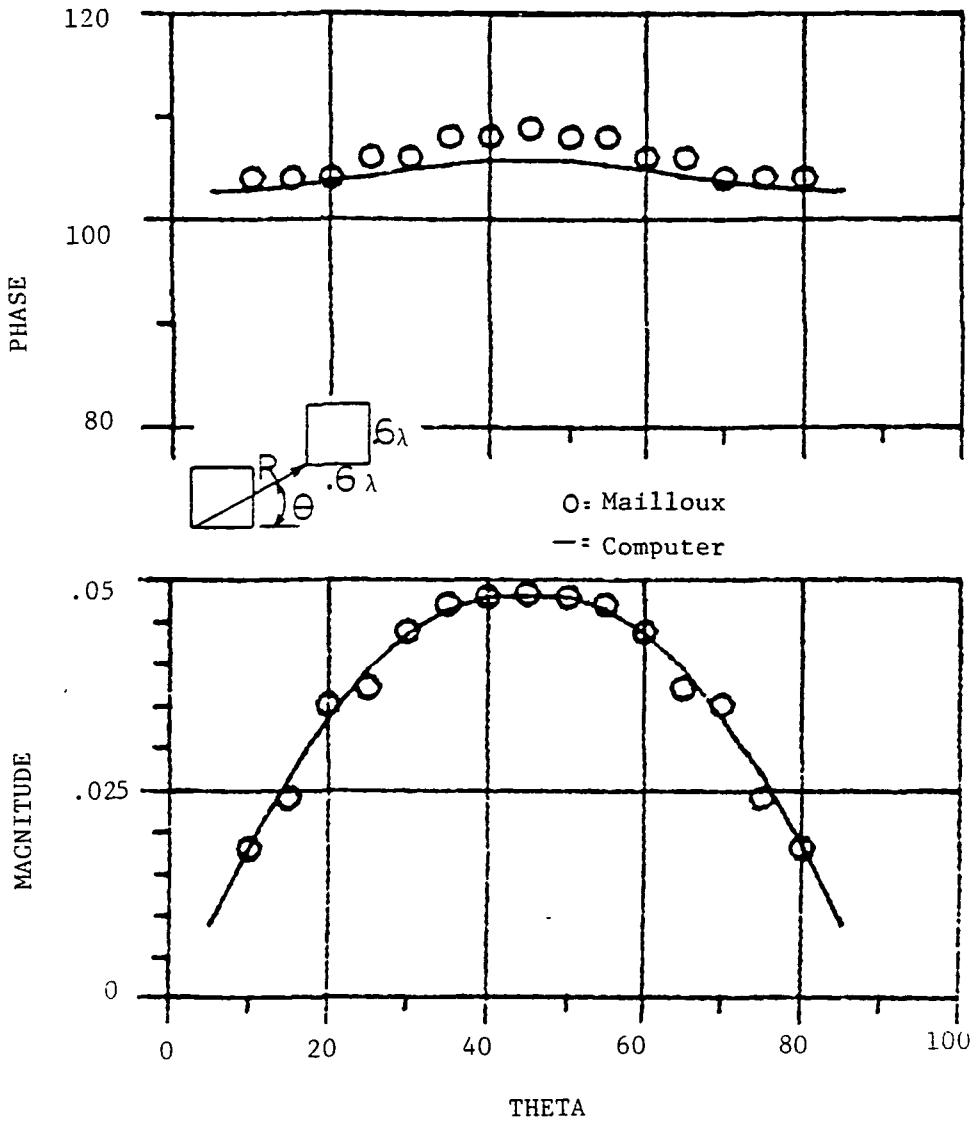

Figure 3.8 Comparison of $S_{TE_{10}1}$, $TE_{01}2$, $R = .9\lambda$

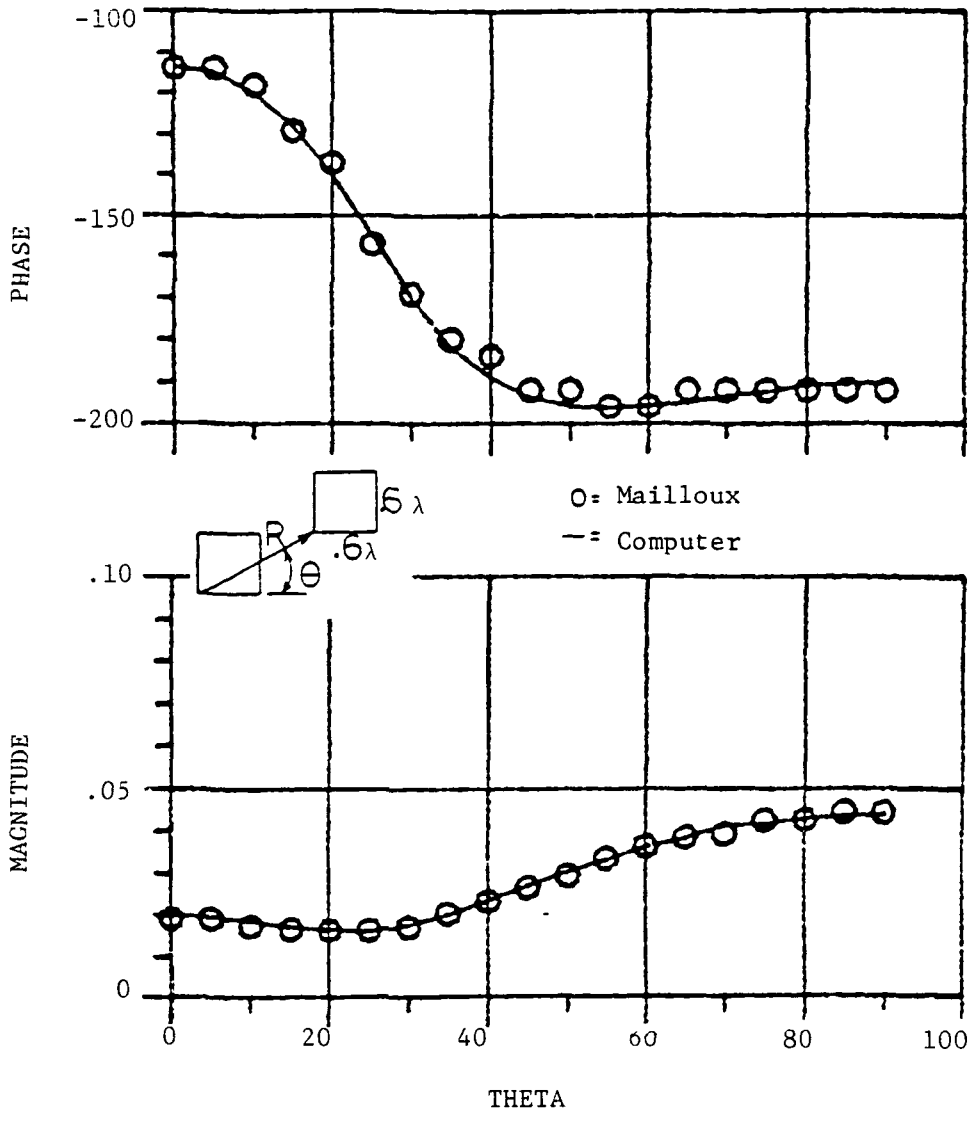

Figure 3.9 Comparison of $S_{TE_{10}1}$, $TE_{10}2$, R = 1.3λ

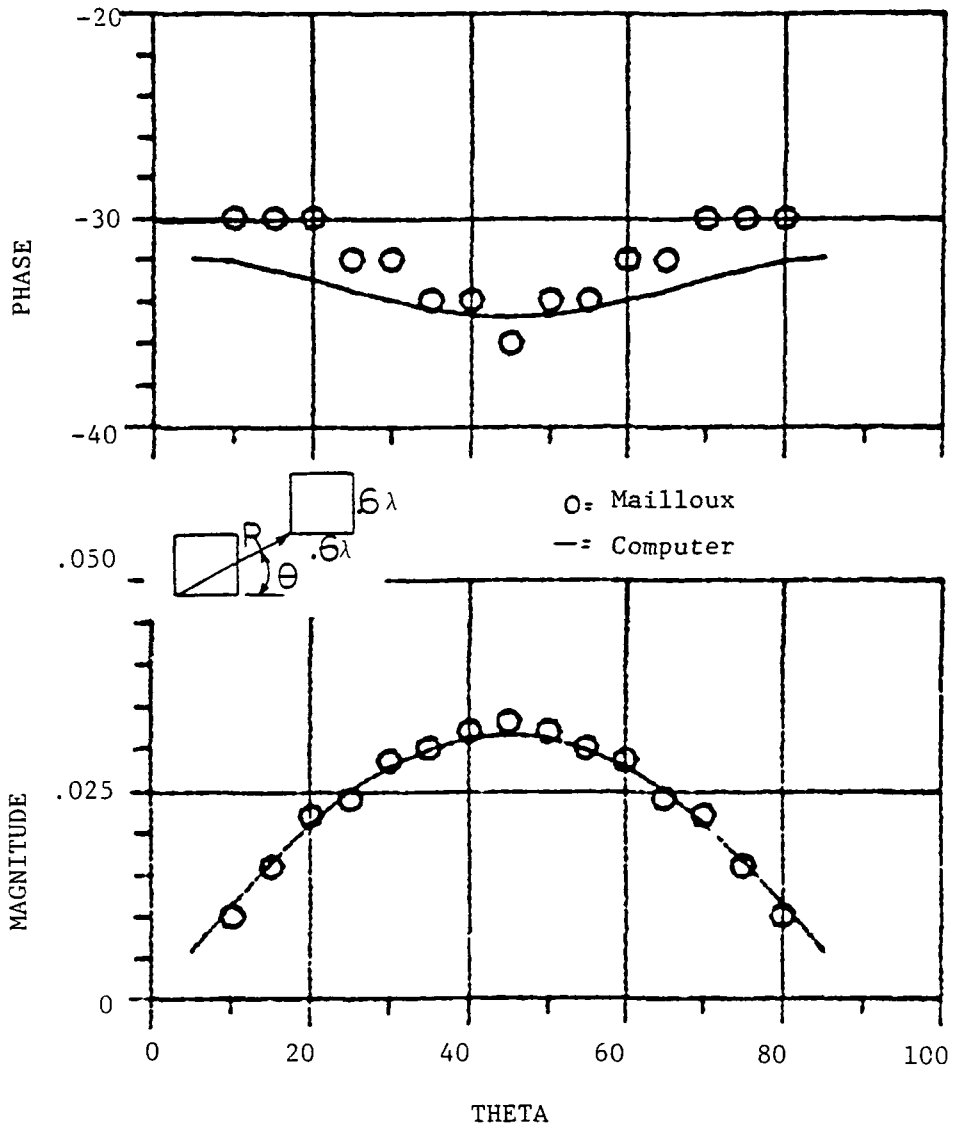

Figure 3.10 Comparison of $S_{TE_{10}1}$, $TE_{01}2$, R = 1.3λ.

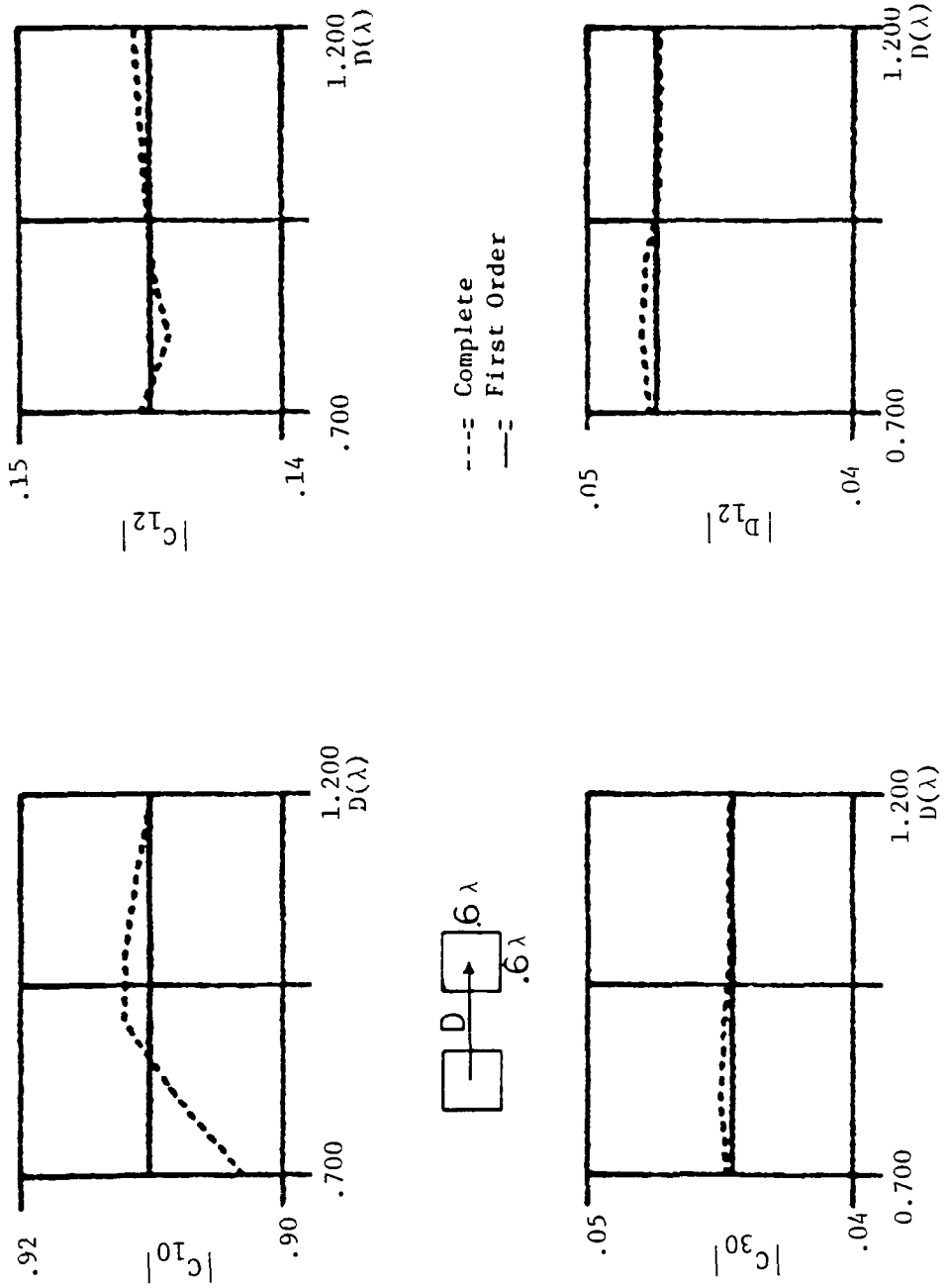

Figure 3.11 Comparison of Normalized Mode Magnitudes in the Driven Guide.

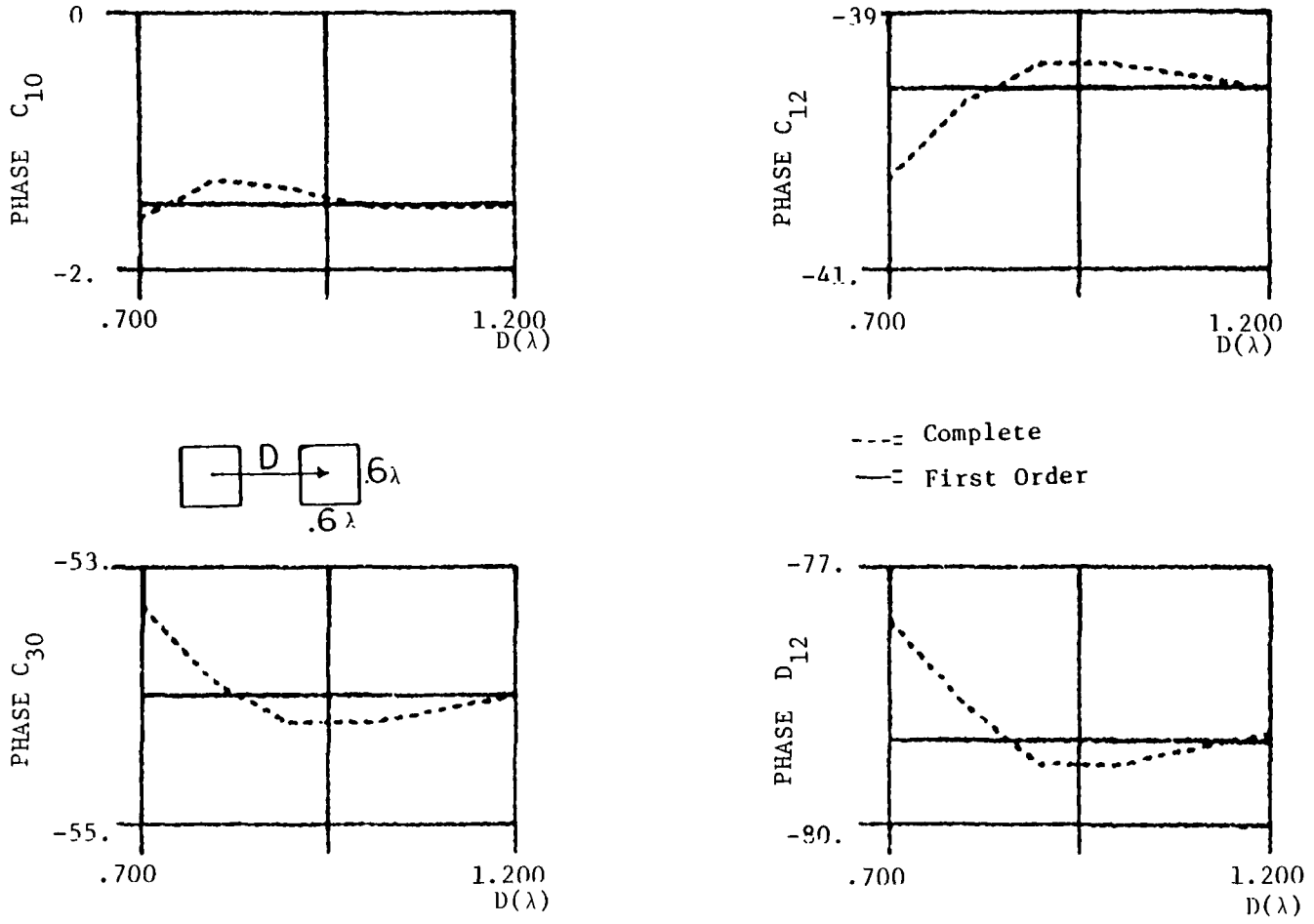

Figure 3.12 Comparison of Normalized Mode Phase Angles of the Driven Guide (Deg).

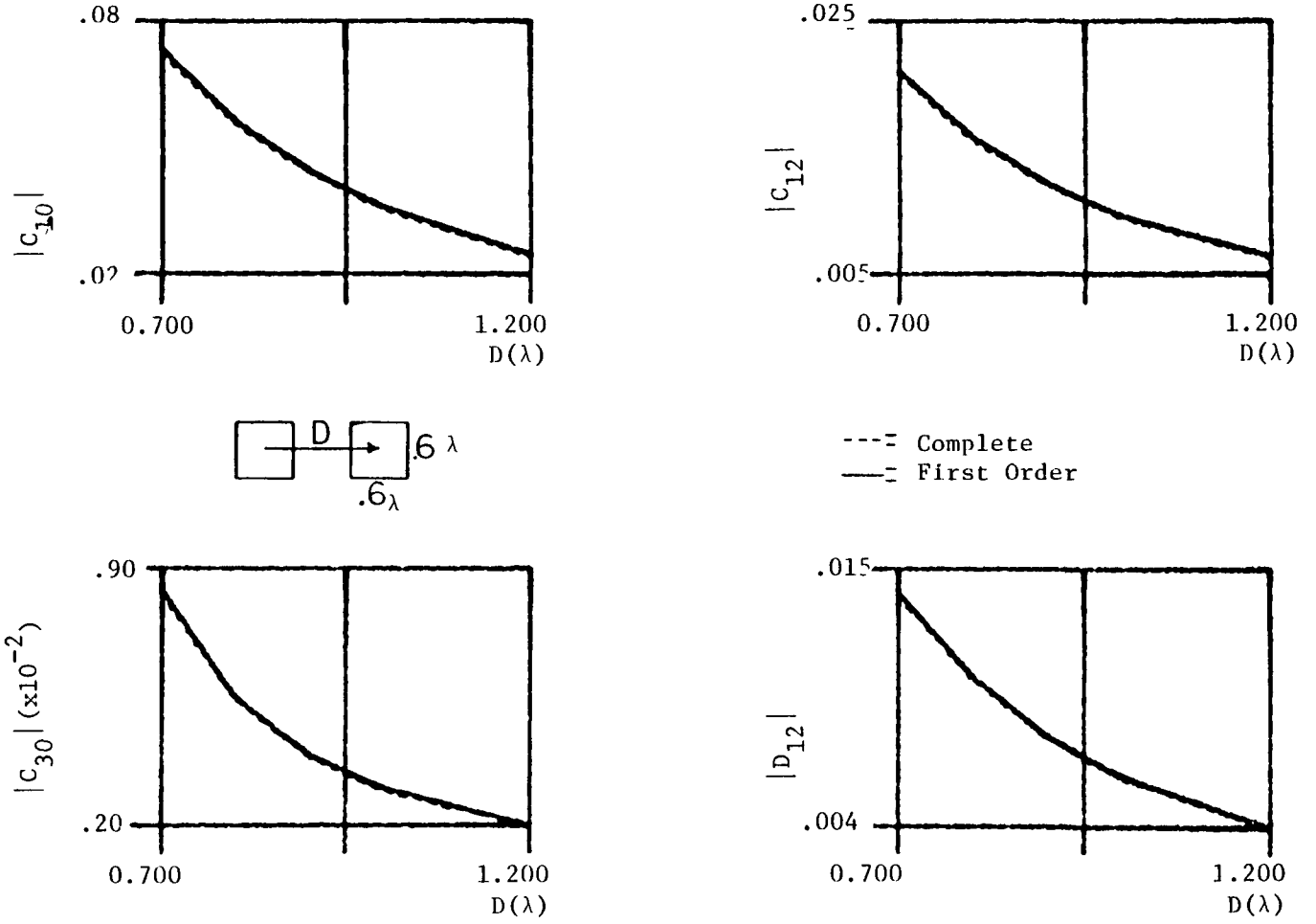

Figure 3.13 Comparison of Normalized Mode Magnitude in the Undriven Guide.

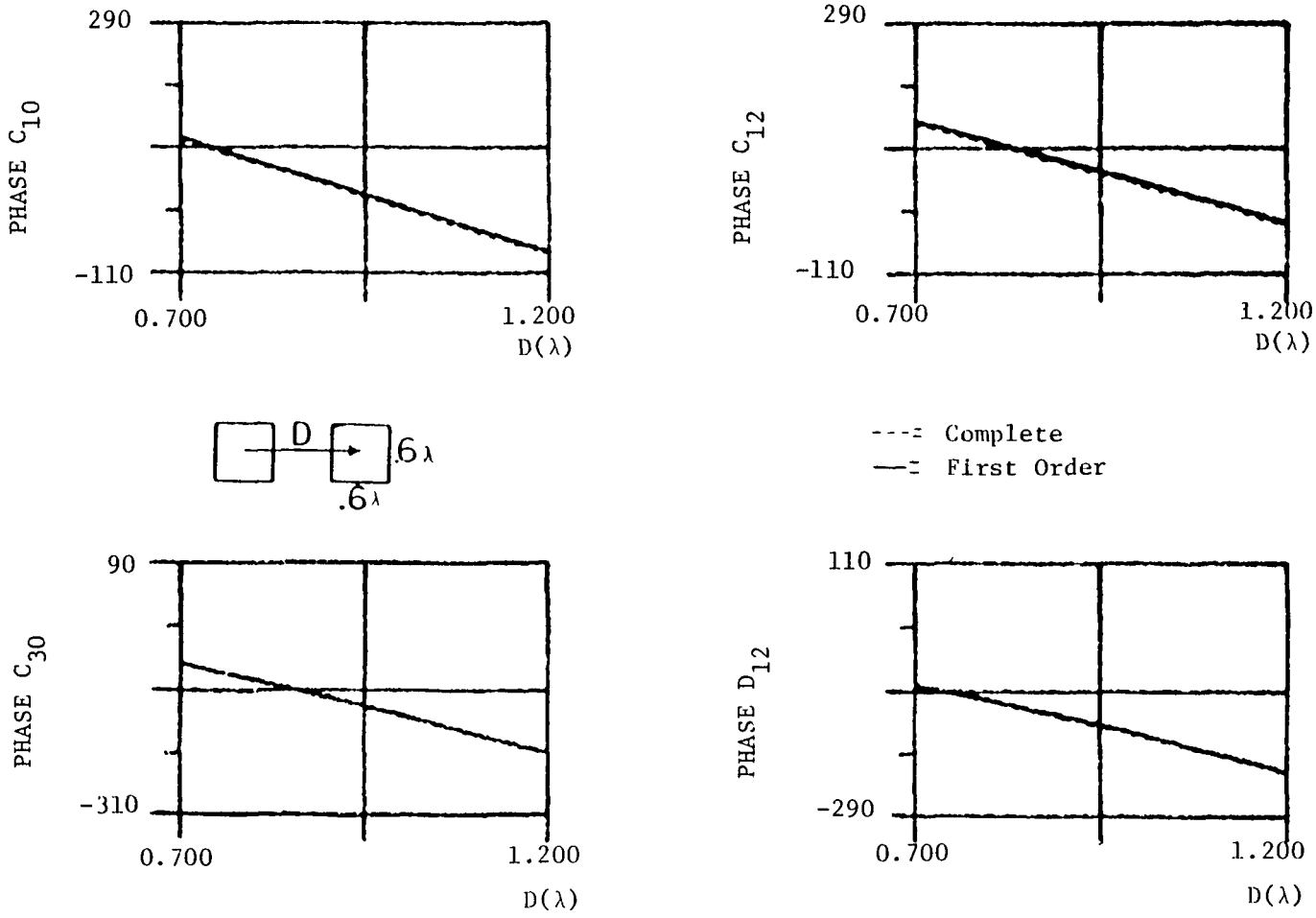

Figure 3.14 Comparison of Normalized Mode Phase Angles in the Undriven Guide (Deg.)

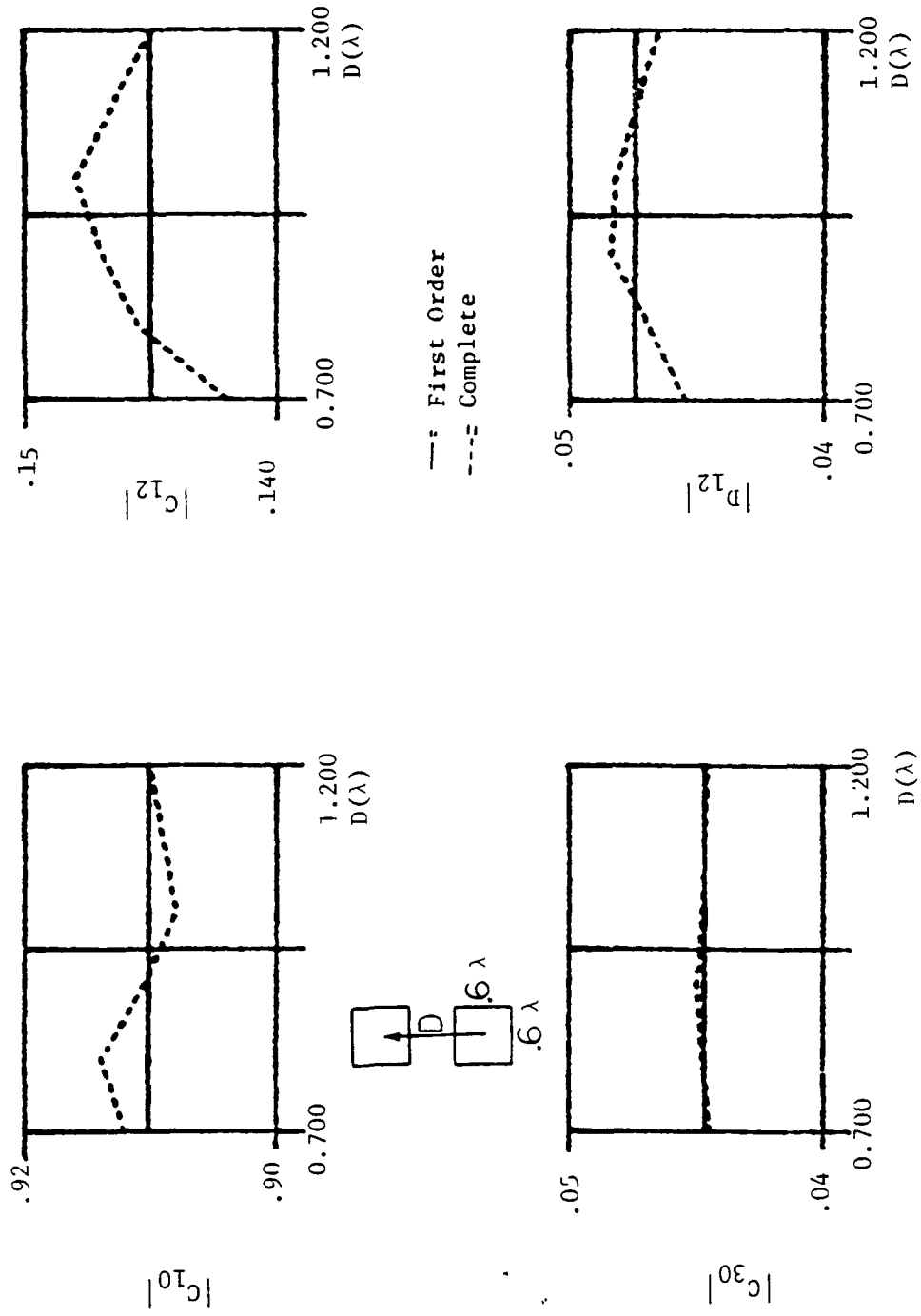

Figure 3.15 Comparison of Normalized Mode Magnitudes in the Driven Guide.

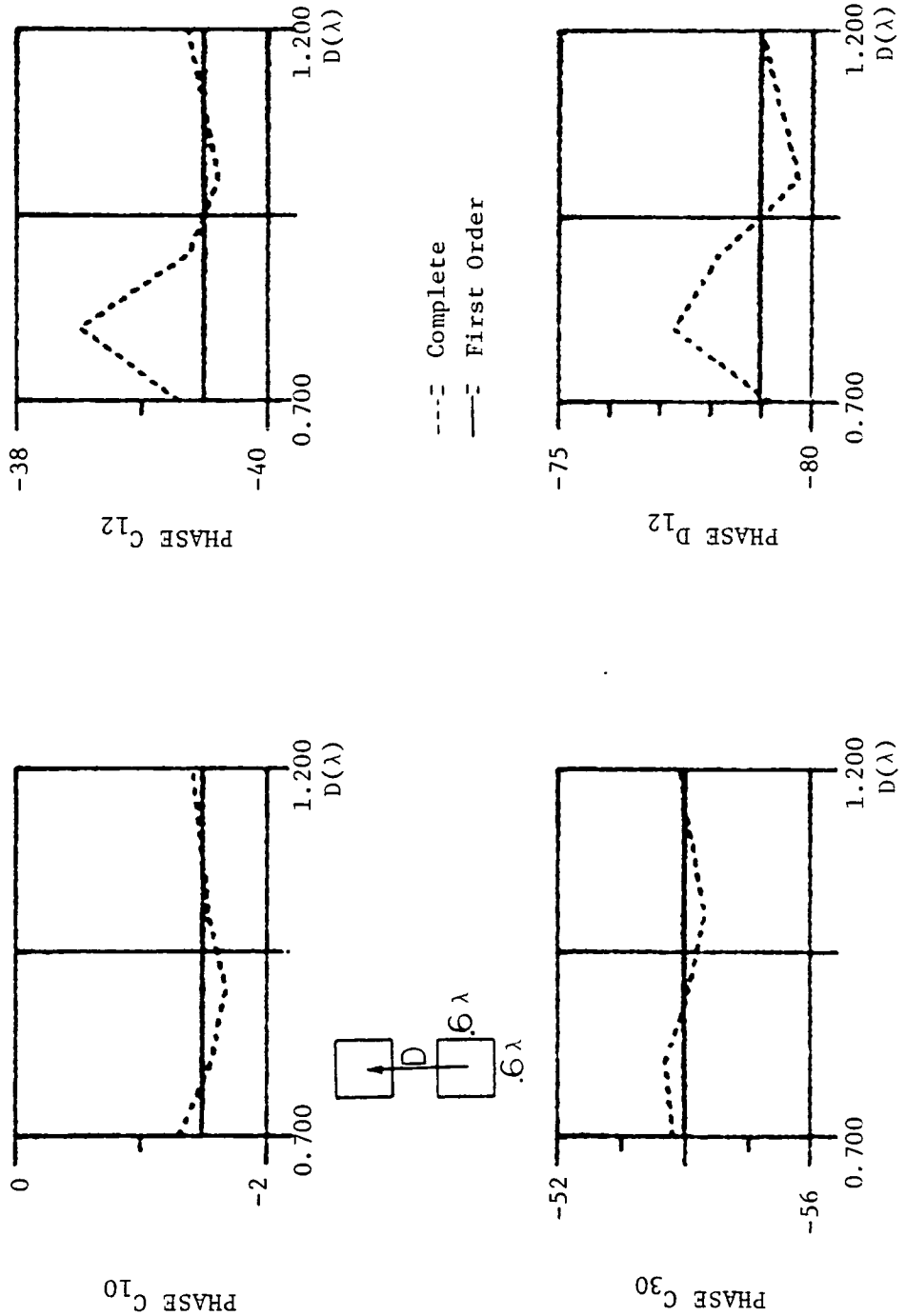

Figure 3.16 Comparison of Normalized Mode Phase Angles of the Driven Guide (Deg.)

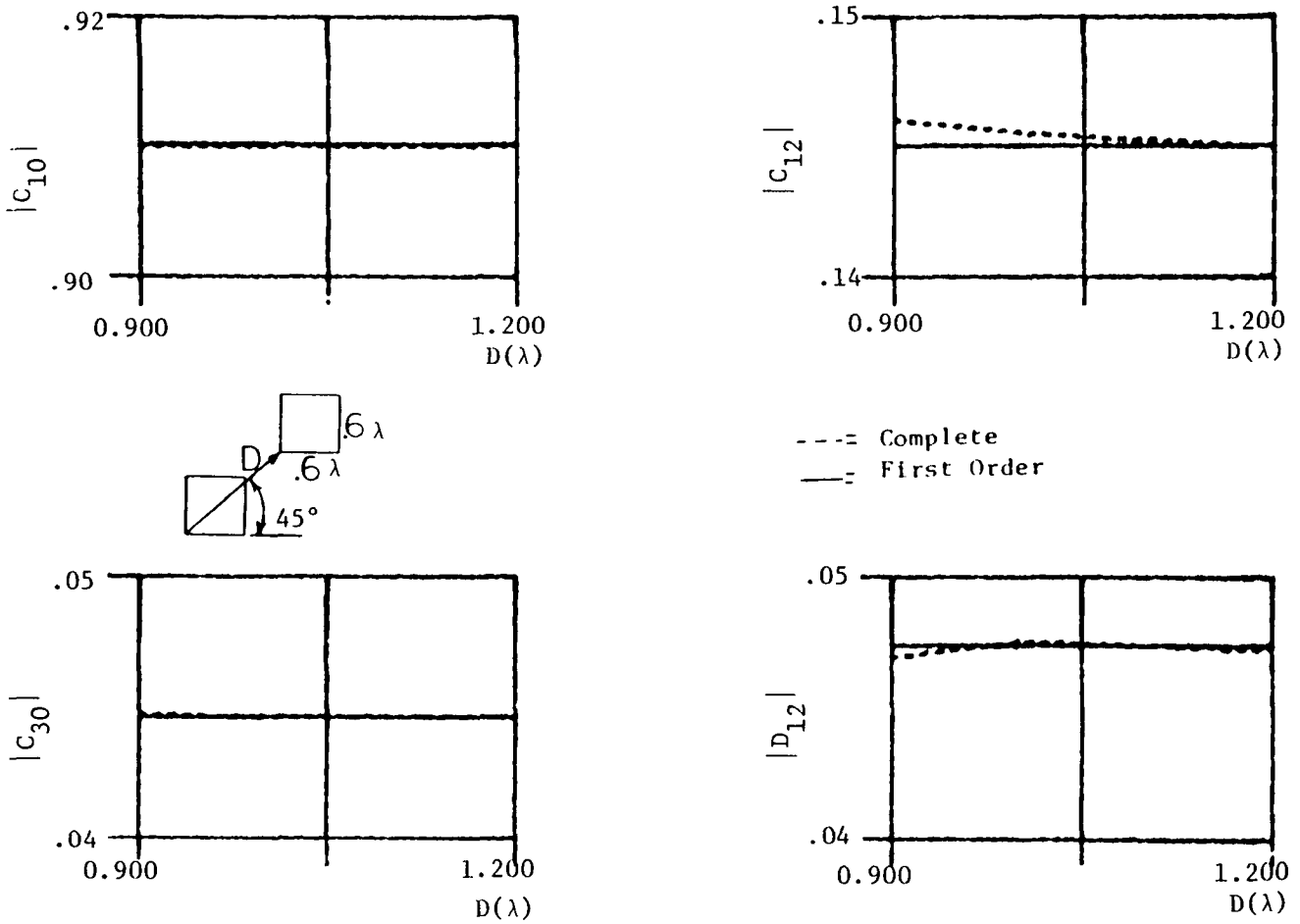

Figure 3.17 Comparison of Normalized Mode Magnitudes in Driven Guide.

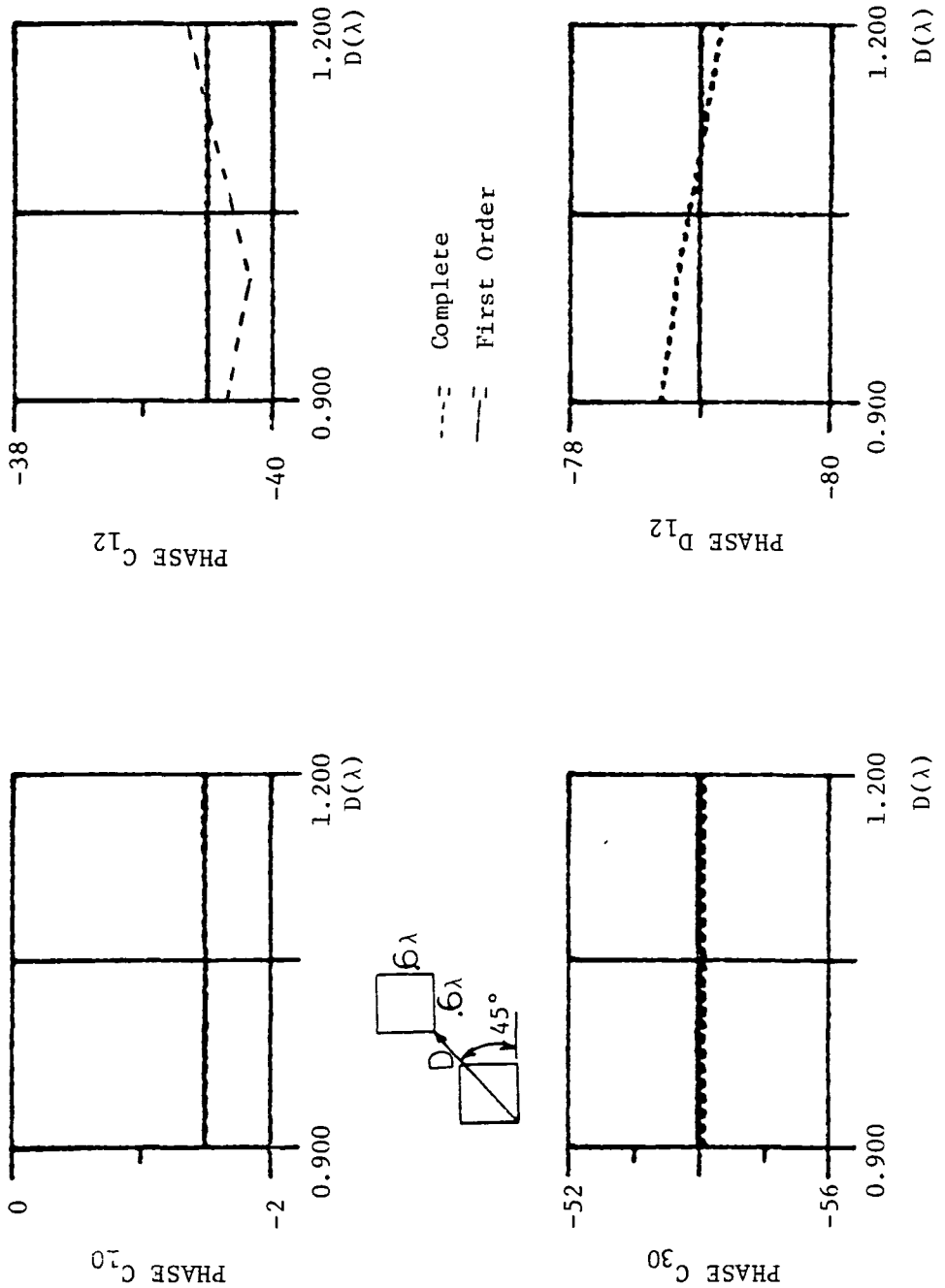

Figure 3.18 Comparison of Normalized Mode Phase Angles of the Driven Guide (Deg.)

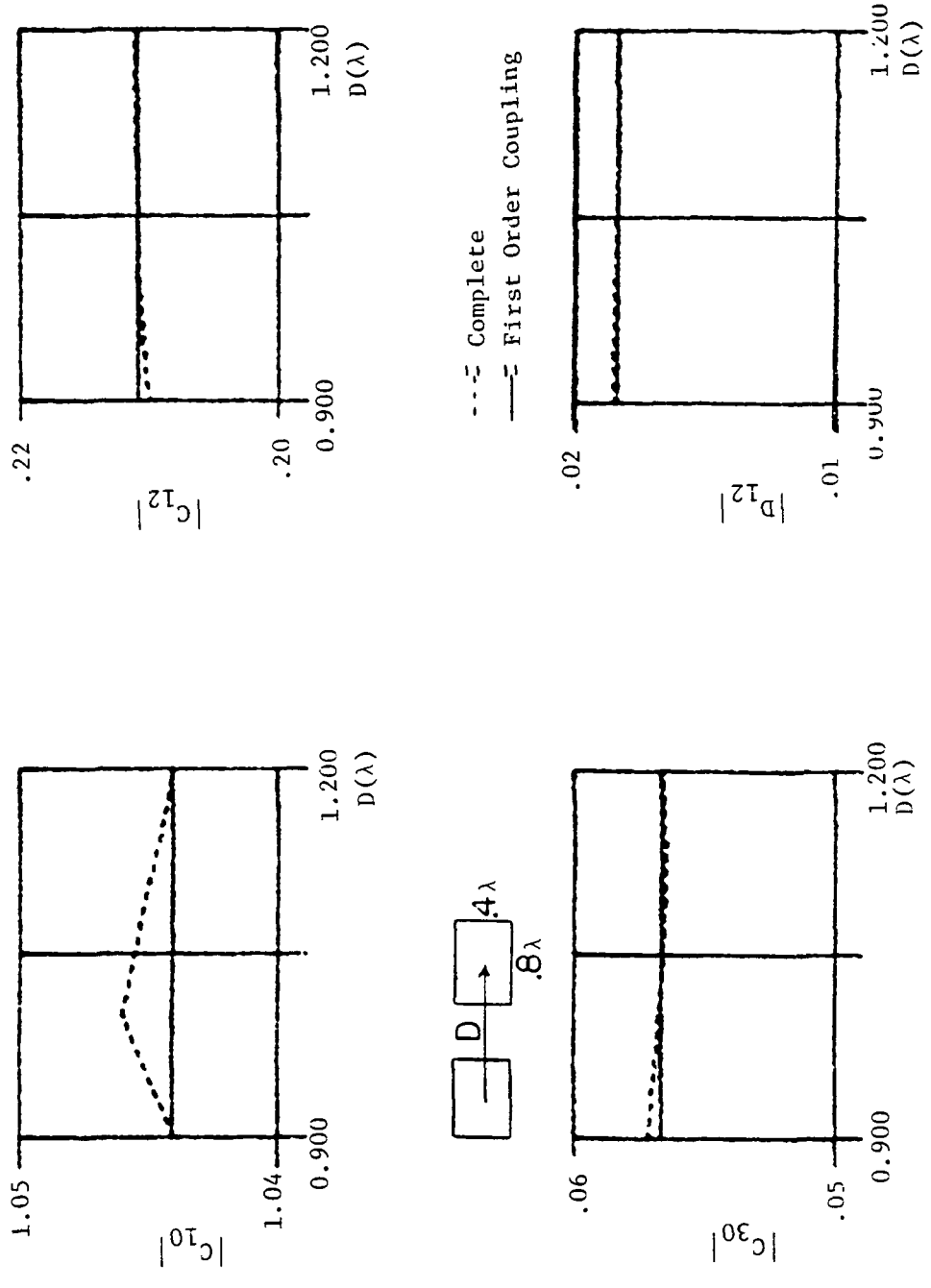

Figure 3.19 Comparison of Normalized Mode Magnitude of Driven Guide.

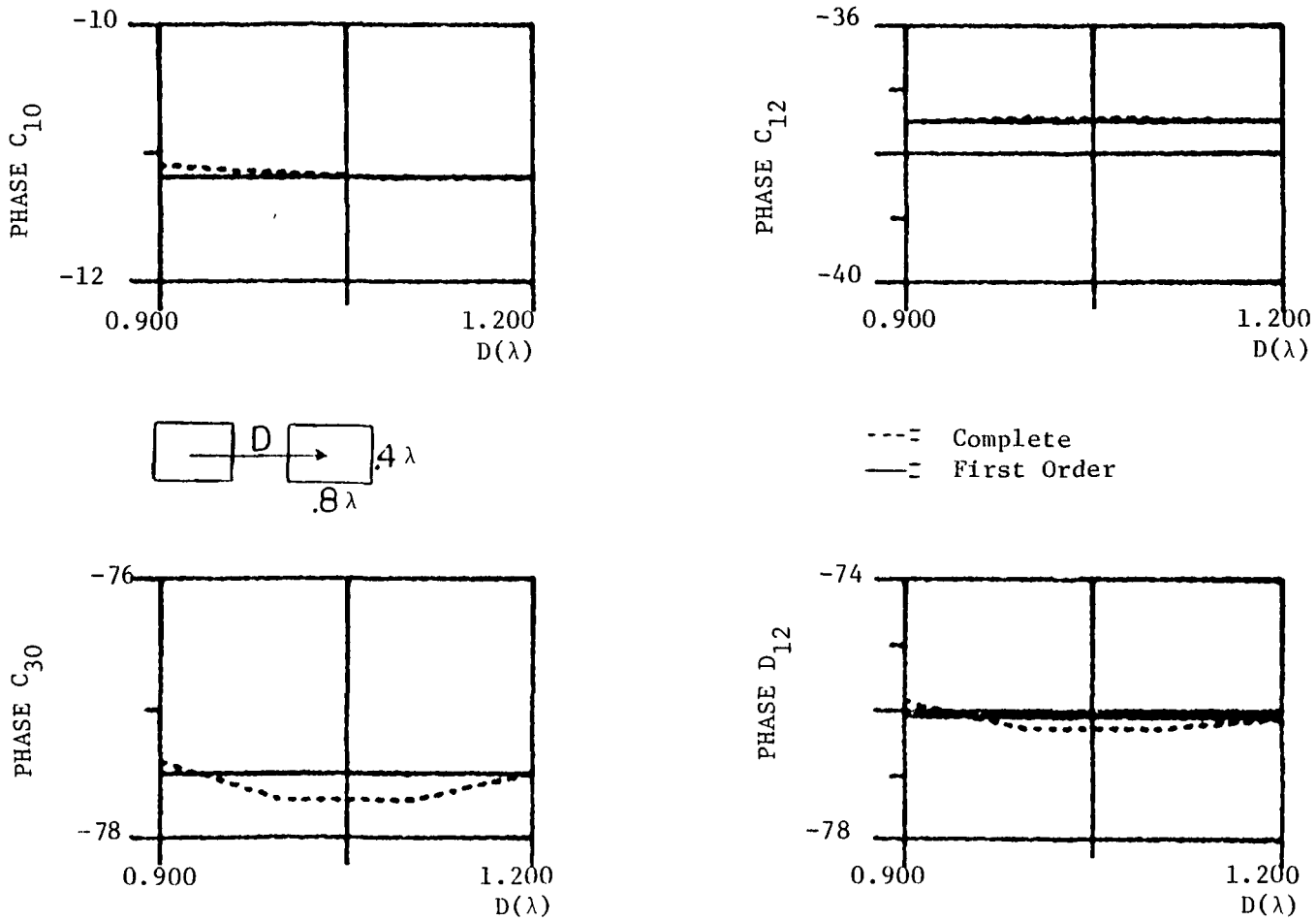

Figure 3.20 Comparison of Normalized Mode Phase Angles of the Driven Guides (Deg.).

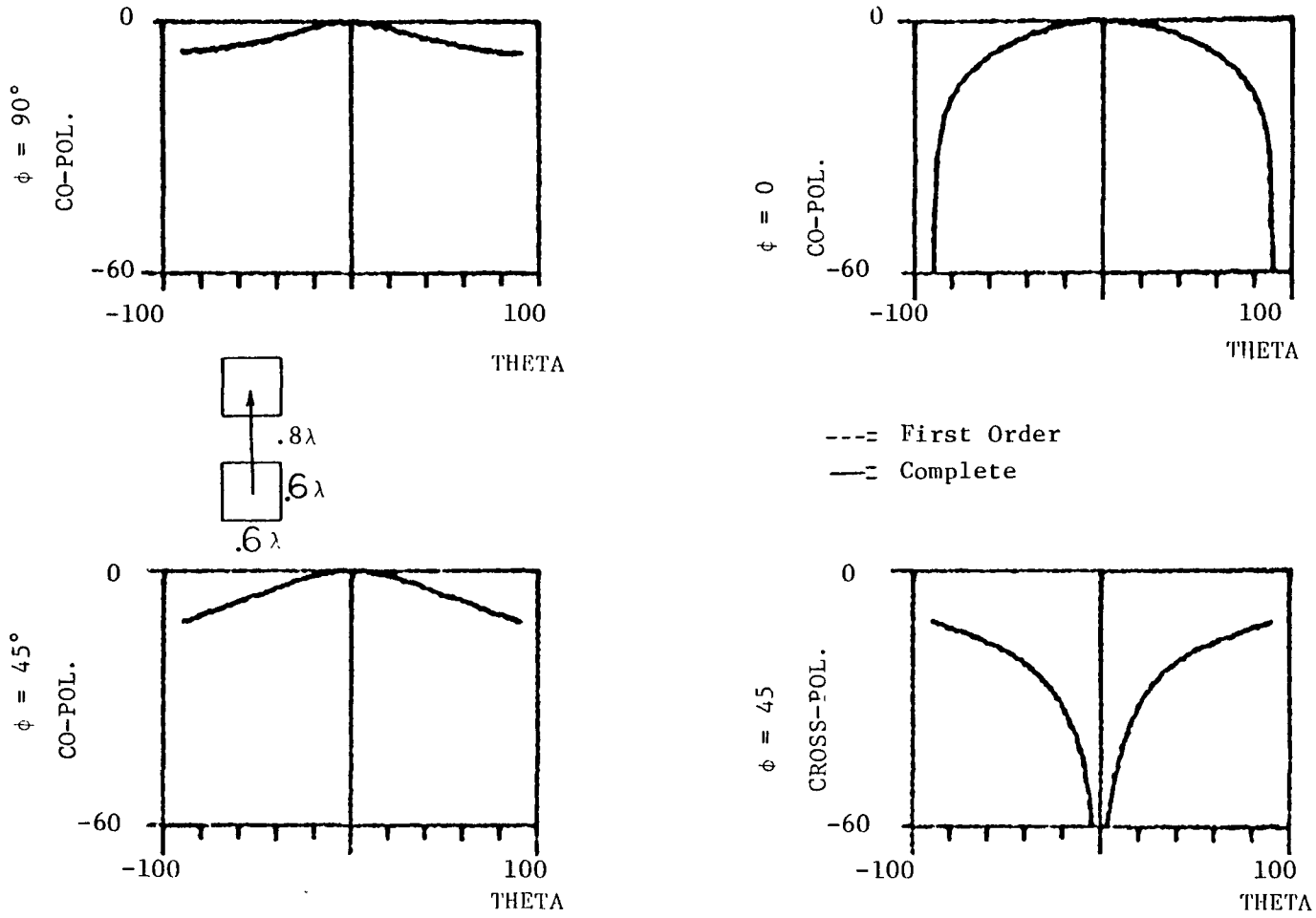

Figure 3.21 Comparisons of Patterns with Single Driven Guide (dB).

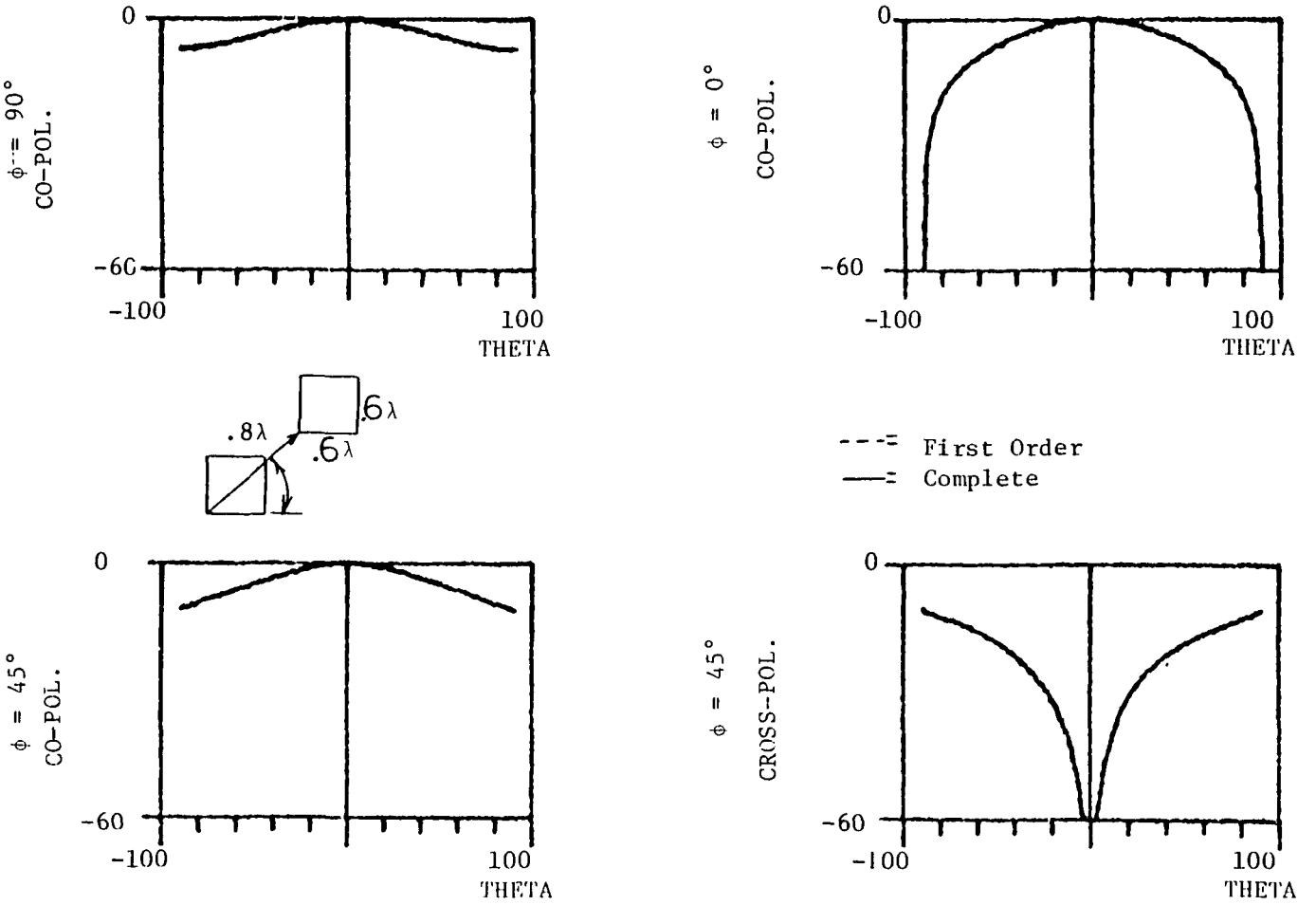

Figure 3.22 Comparison of Patterns with Single Driven Guide (dB).

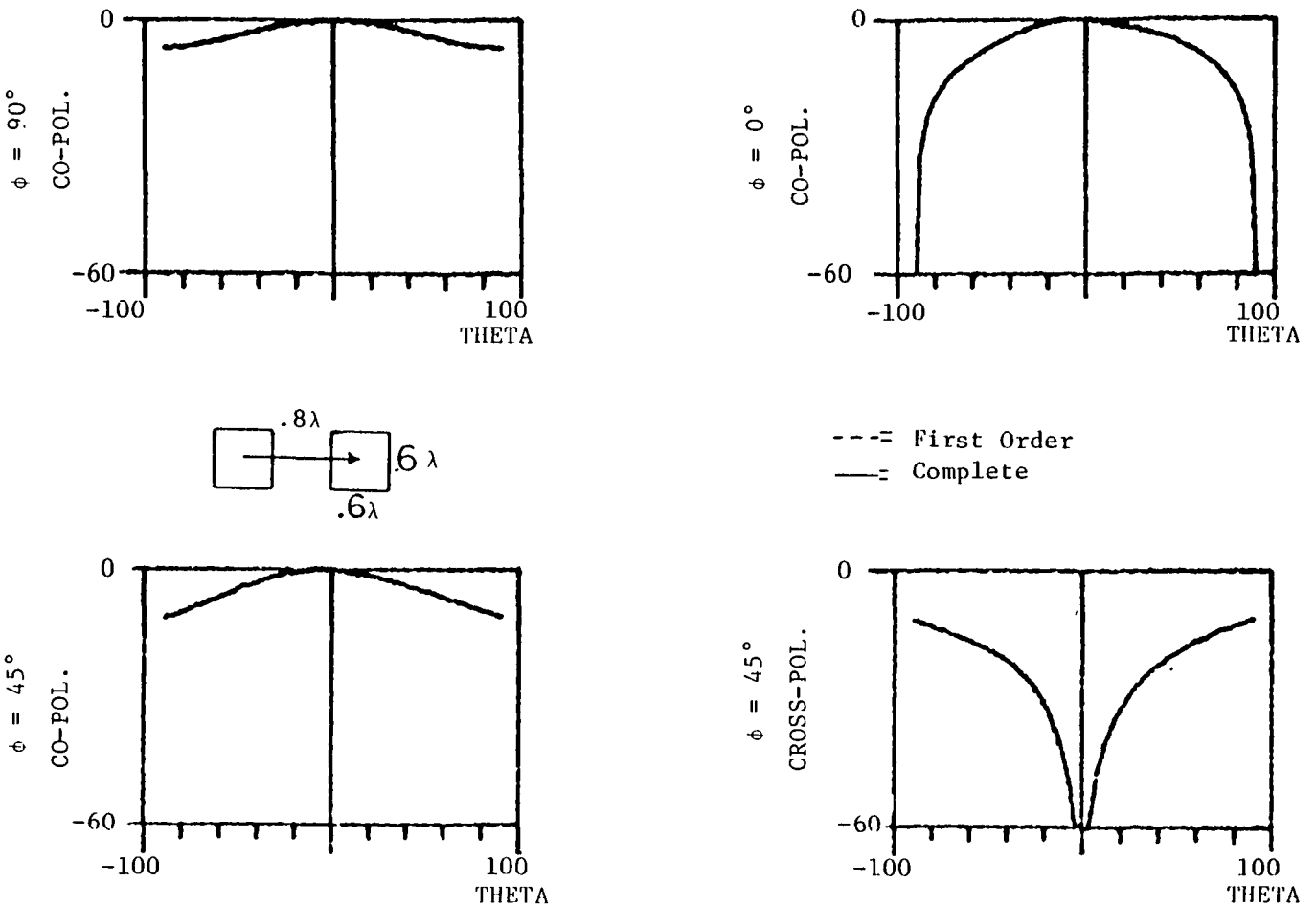

Figure 3.23 Comparison of Patterns with Single Driven Guide (dB).

This concludes the two aperture analysis which helped to provide some validity to the computer model derived using the vector potential approach. Further testing of first order coupling will be presented in the next section on three aperture arrays, and any comment on it will be with-held till that time.

3.4 Three Aperture Arrays

The results shown in this section will help to further test the first order coupling hypothesis. Computer data for three co-linear, horizontally mounted apertures were collected. These data show that the first order coupling approximation does give valid results. Also included in this section will be a few plots of the patterns of three different arrays where the beam is being scanned. These patterns illustrate the beam forming capability of the computer model.

The first order coupling tests performed were similar to the ones presented in the previous section but with three apertures. In this case the co-linear apertures were mounted horizontally at various spacings. The first set of plots is for the left most aperture driven. The 4 mode approximation discussed in Sec. 3.1 (ψ_{10}, ψ_{12}, ψ_{30} and Φ_{12}) is used here for all the data in this section. Figures 3.24-3.29 show the mode amplitude results for all three apertures of this test. Figures 3.24 and 3.25 show the mode amplitudes of the driven guide while Fig's. 3.26-3.29 show the same for the middle and right most guides. In this situation only, coupling between the second and third apertures was included. Preliminary tests showed that without it large errors in the third aperture's field resulted.

C-2

The reason for this is that the coupling from the driven to the third is small enough that the re-radiated fields from the second aperture could have a sizable affect on it.

The next set of data is for the same aperture arrangement, but with the middle guide driven. Shown in Fig's. 3.30-3.31 are the mode amplitudes of the driven guide. With no coupling between the end elements their amplitudes should be similar to the two aperture case of Fig's. 3.13 and 3.14 and will not be repeated here.

Finally, Fig's. 3.32 and 3.33 shows the comparisons of the radiation patterns for the two cases described above. Each shows the full coupling patterns and the first order coupling patterns for three aperture arrays with 0.7λ spacings. There appears to be little difference between the first order and the full coupling plots. This is an expected result due to the near identical patterns found in the two aperture case, Fig's. 3.22 and 3.23.

This concludes the computer tests for the first order coupling idea. Some experimental tests were performed and are presented in the next chapter. These experimental results agree with the computer data presented so far. The preliminary conclusion to be made from this testing is that the theory gives a fairly accurate solution to the mutual coupling problem, at least in the cases presented here. The largest difference found was less than 5% for the magnitudes and a few degrees for the phase. It was also found to have very little affect on the dominant TE_{10} mode, which is the largest mode present. These encouraging results warrent further testing of the theory and

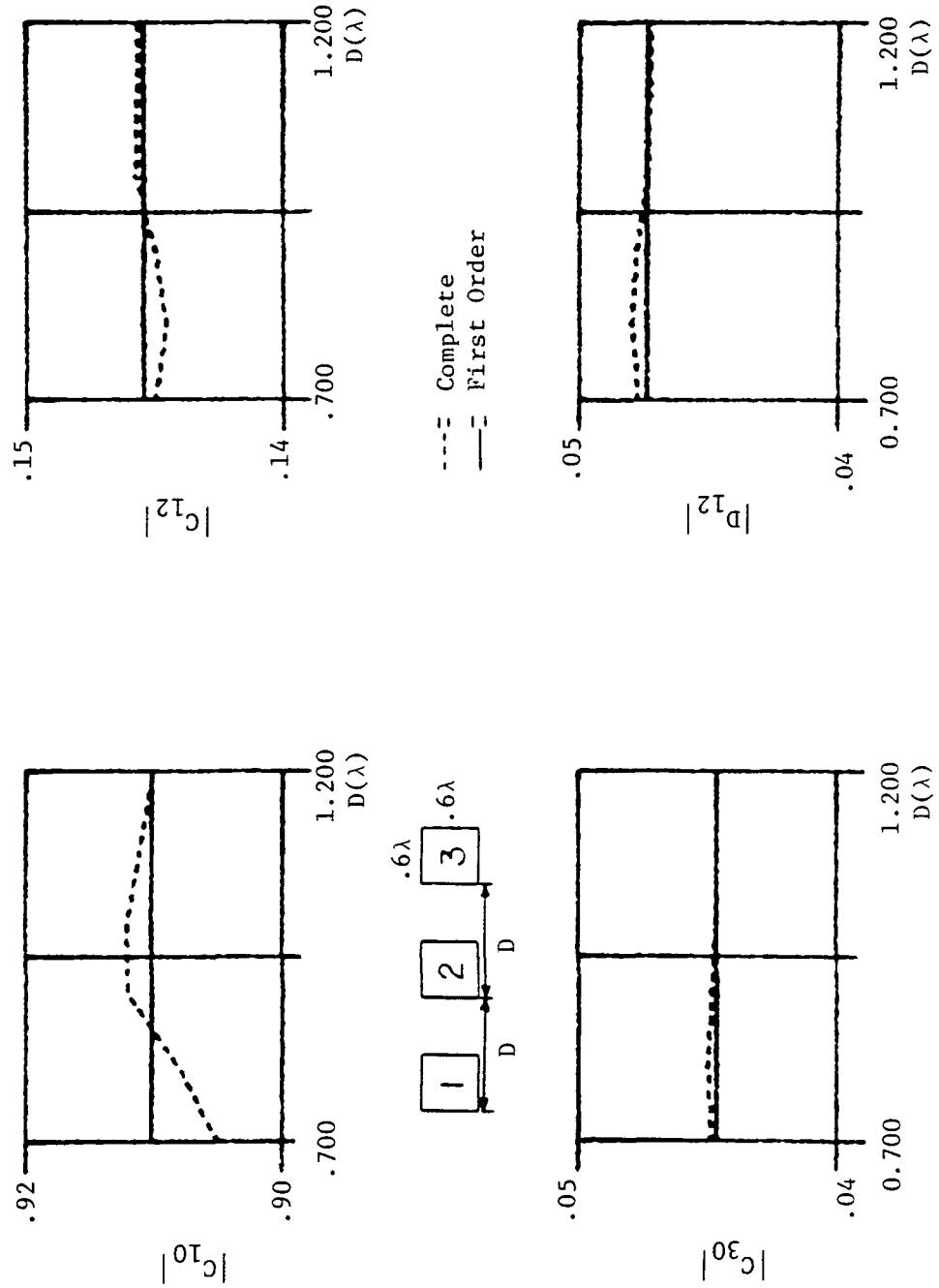

Figure 3.24 Comparison of Normalized Mode Magnitudes in #1 with #1 Driven.

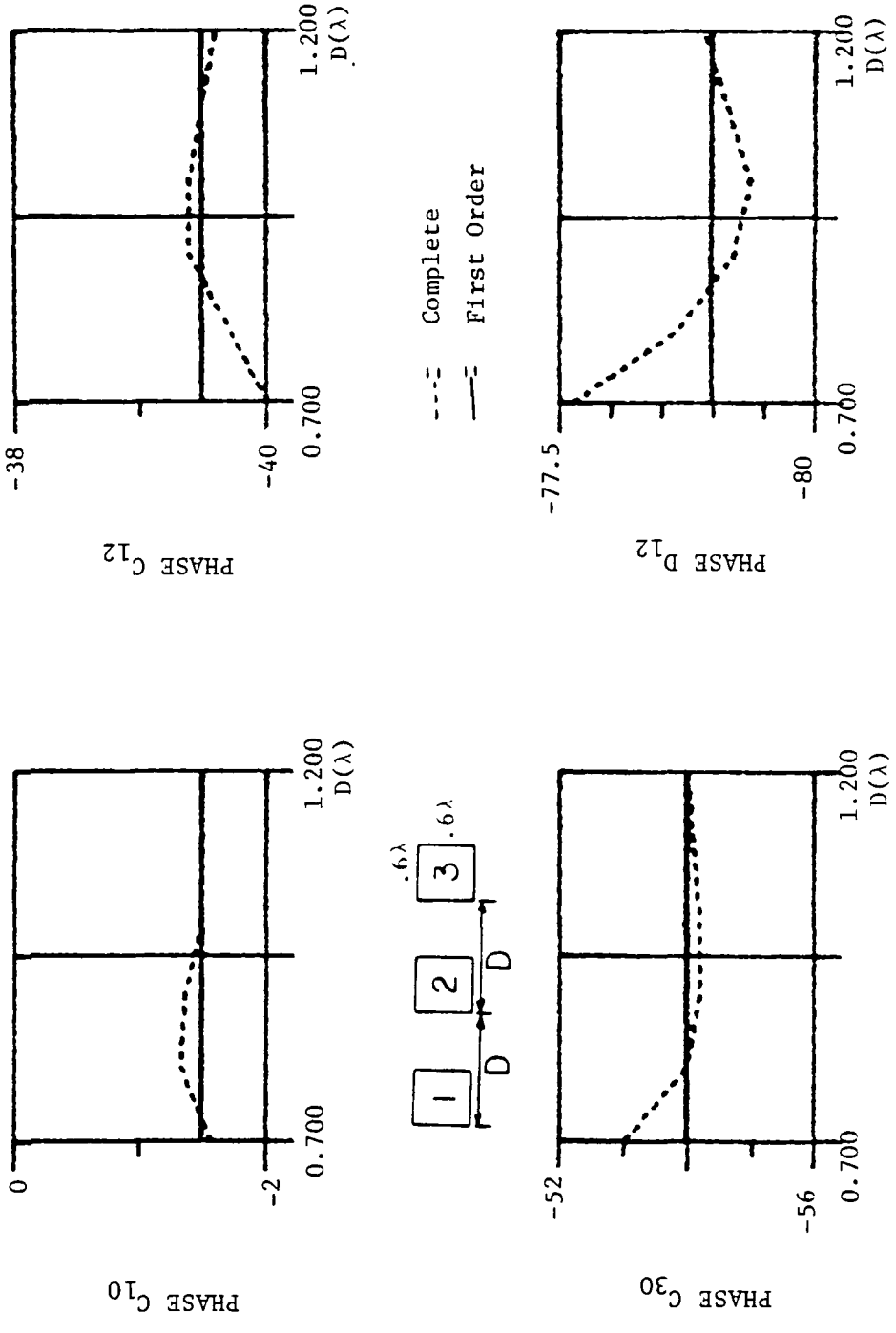

Figure 3.25 Comparison of Normalized Mode Phase Angles in #1 with #1 Driven (Deg.).

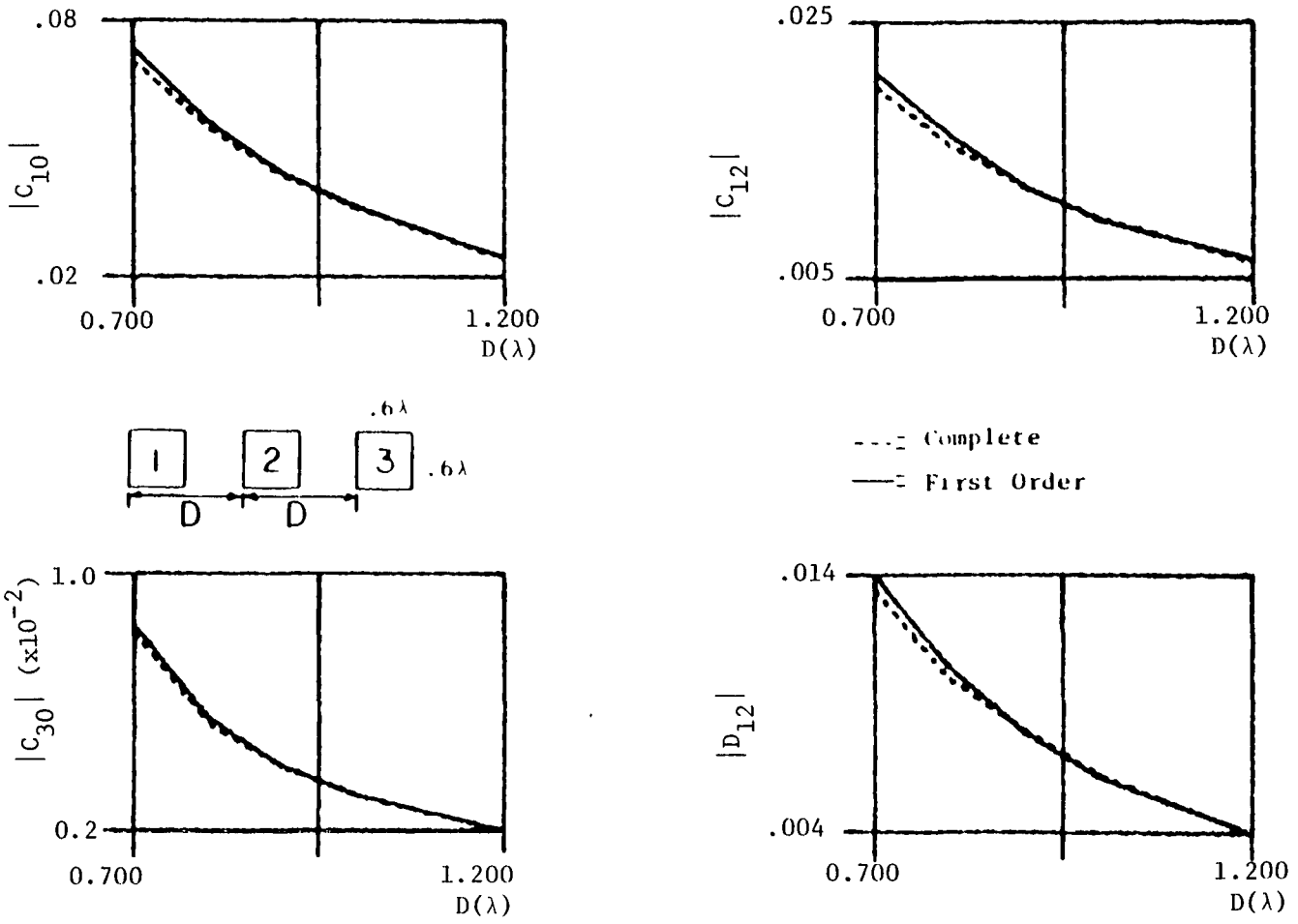

Figure 3.26 Comparison of Normalized Mode Magnitudes in #2 with #1 Driven.

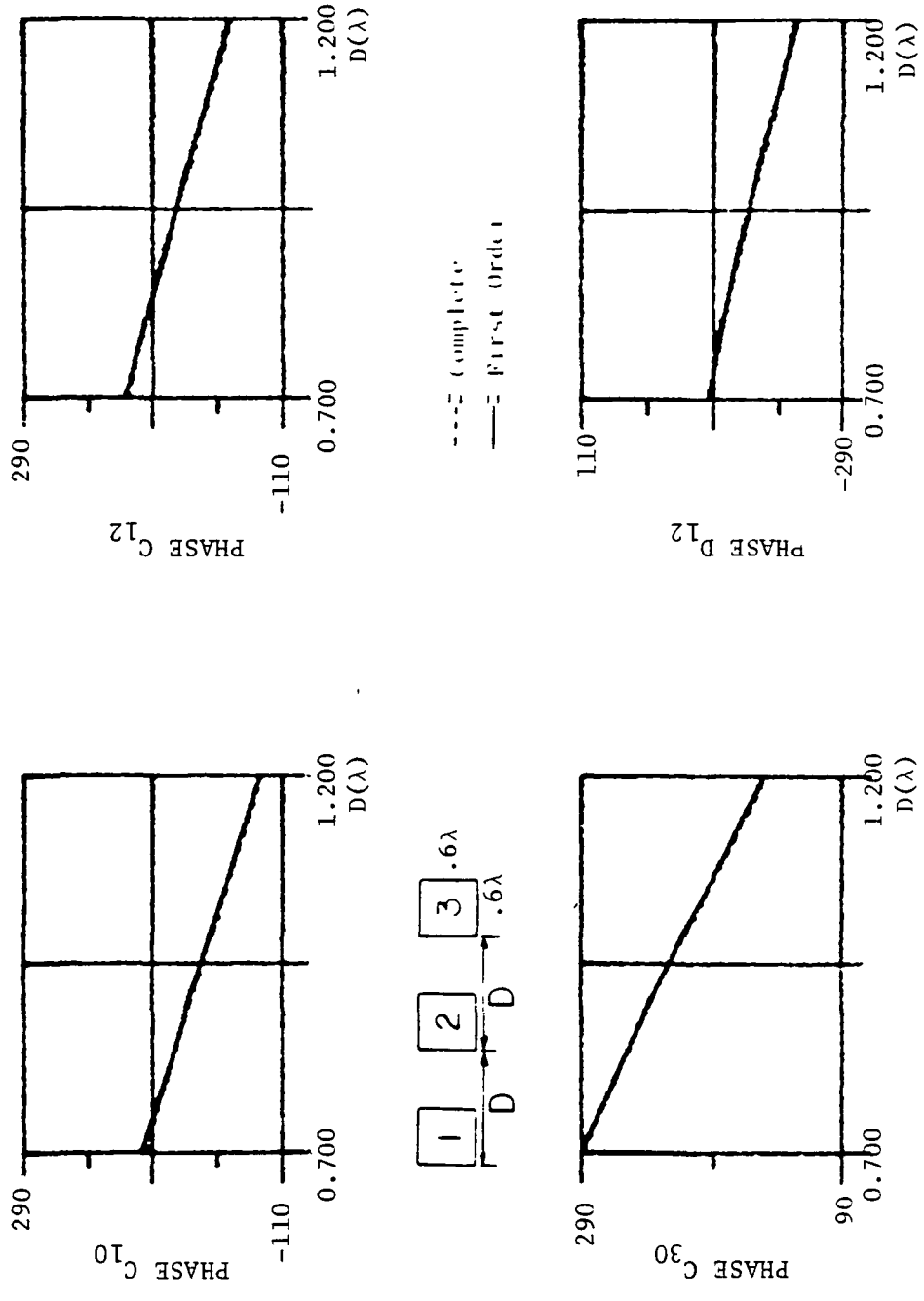

Figure 3.27 Comparison of Normalized Mode Phase Angles in #2 with #1 Driven (Deg.).

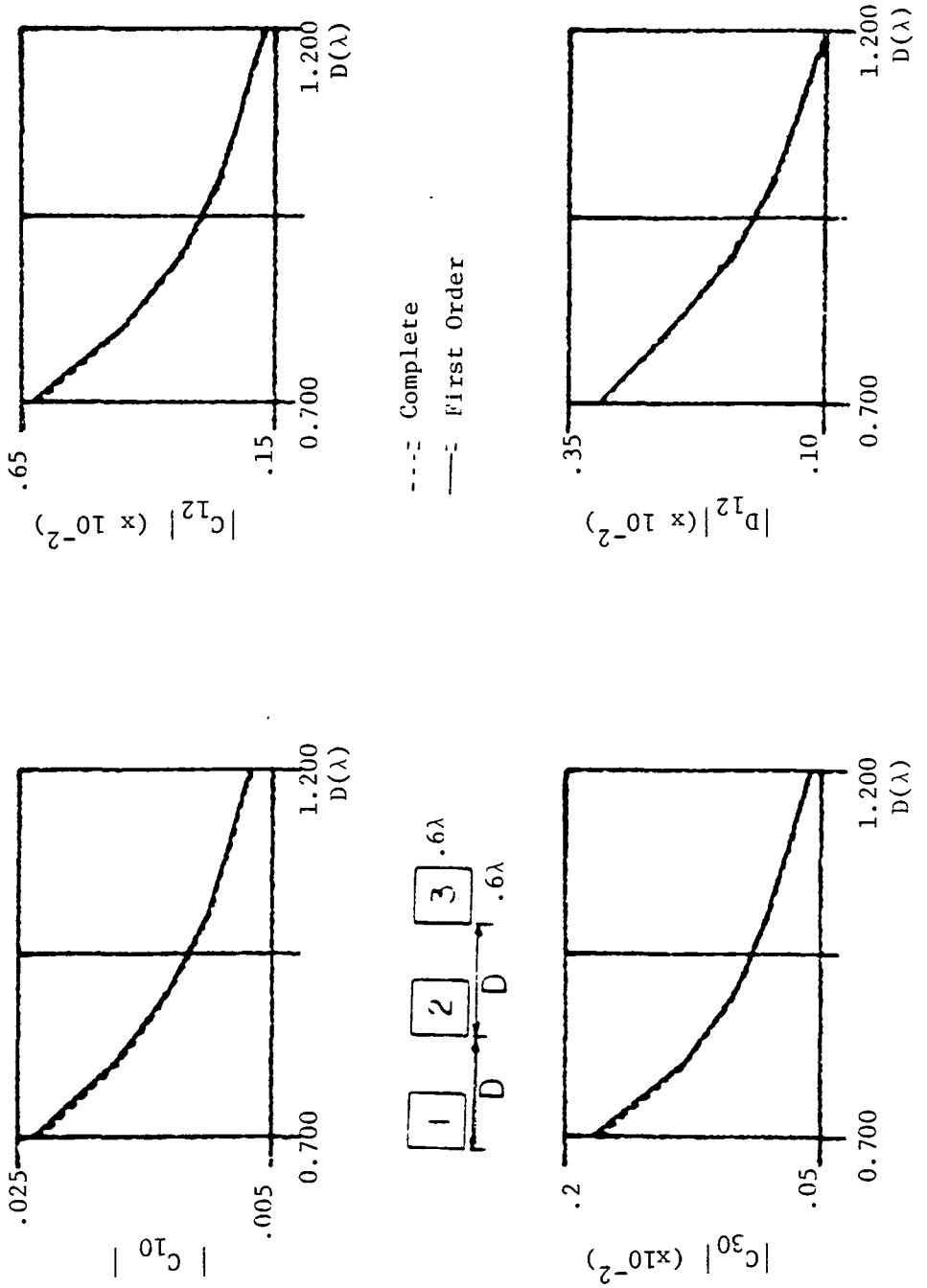

Figure 3.28 Comparison of Normalized Mode Magnitudes in #3 with #1 Driven.

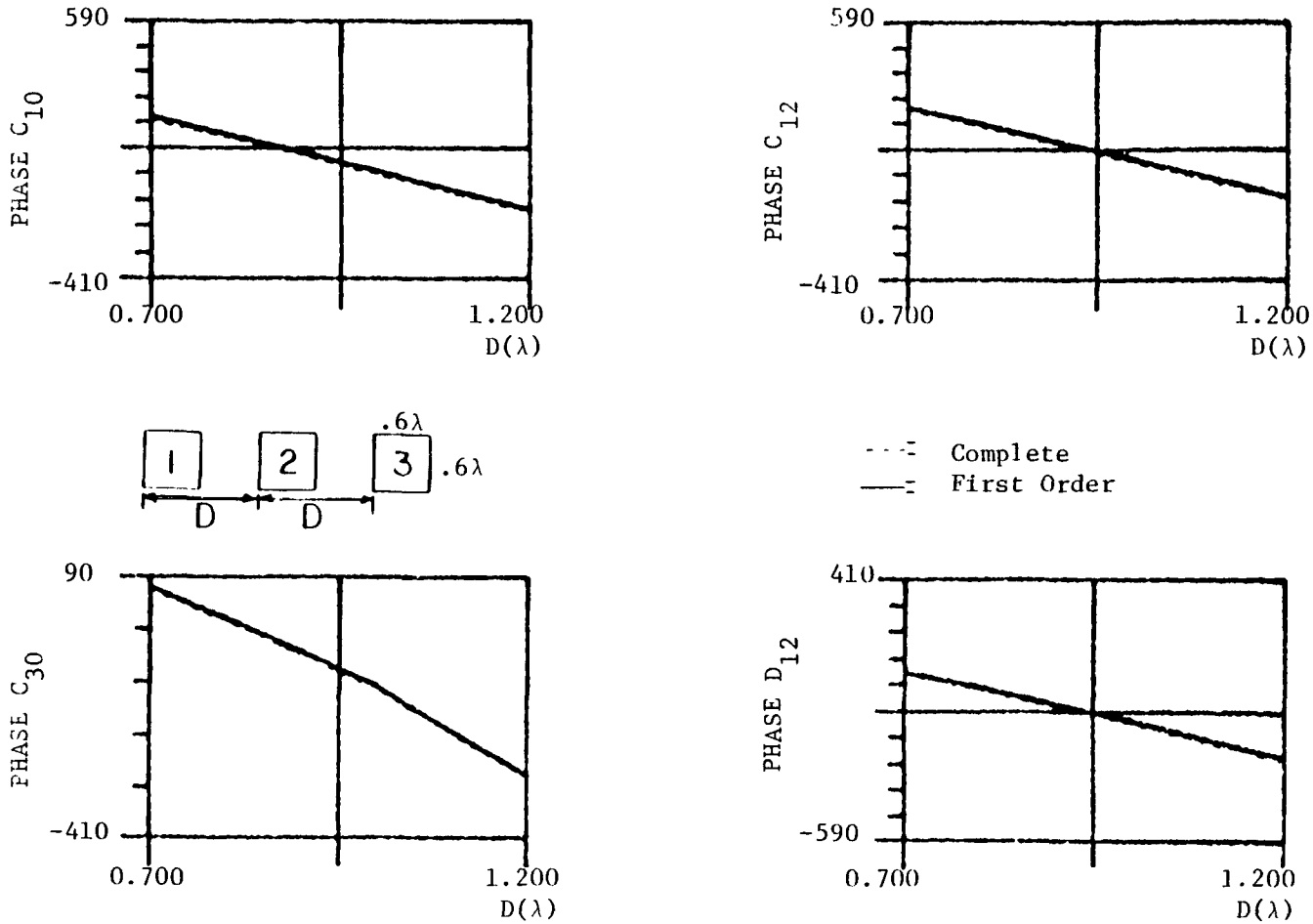

Figure 3.29 Comparison of Normalized Mode Phase Angles in #3 with #1 Driven (Deg.).

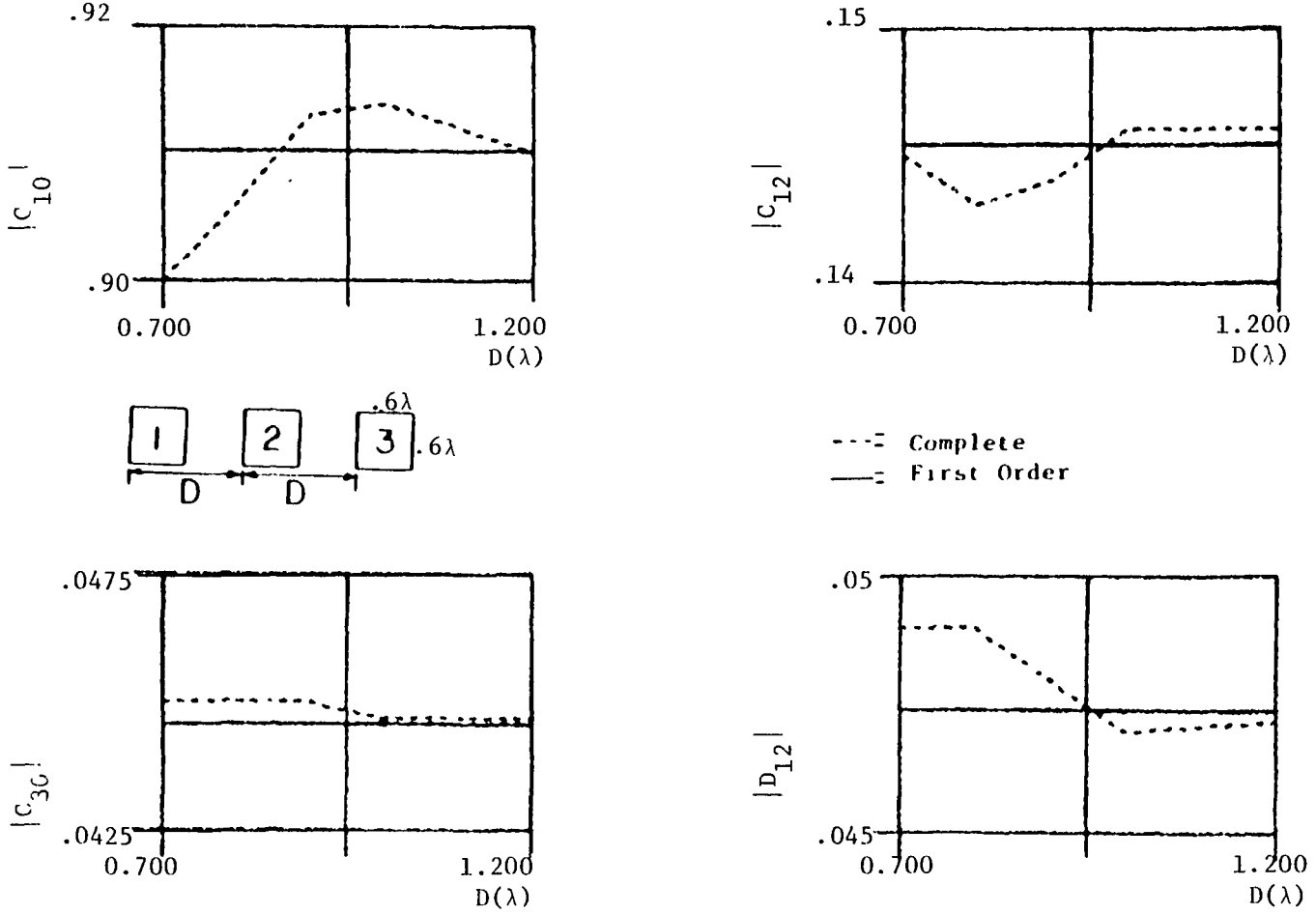

Figure 3.30 Comparison of Normalized Mode Magnitudes in #2 with #2 Driven.

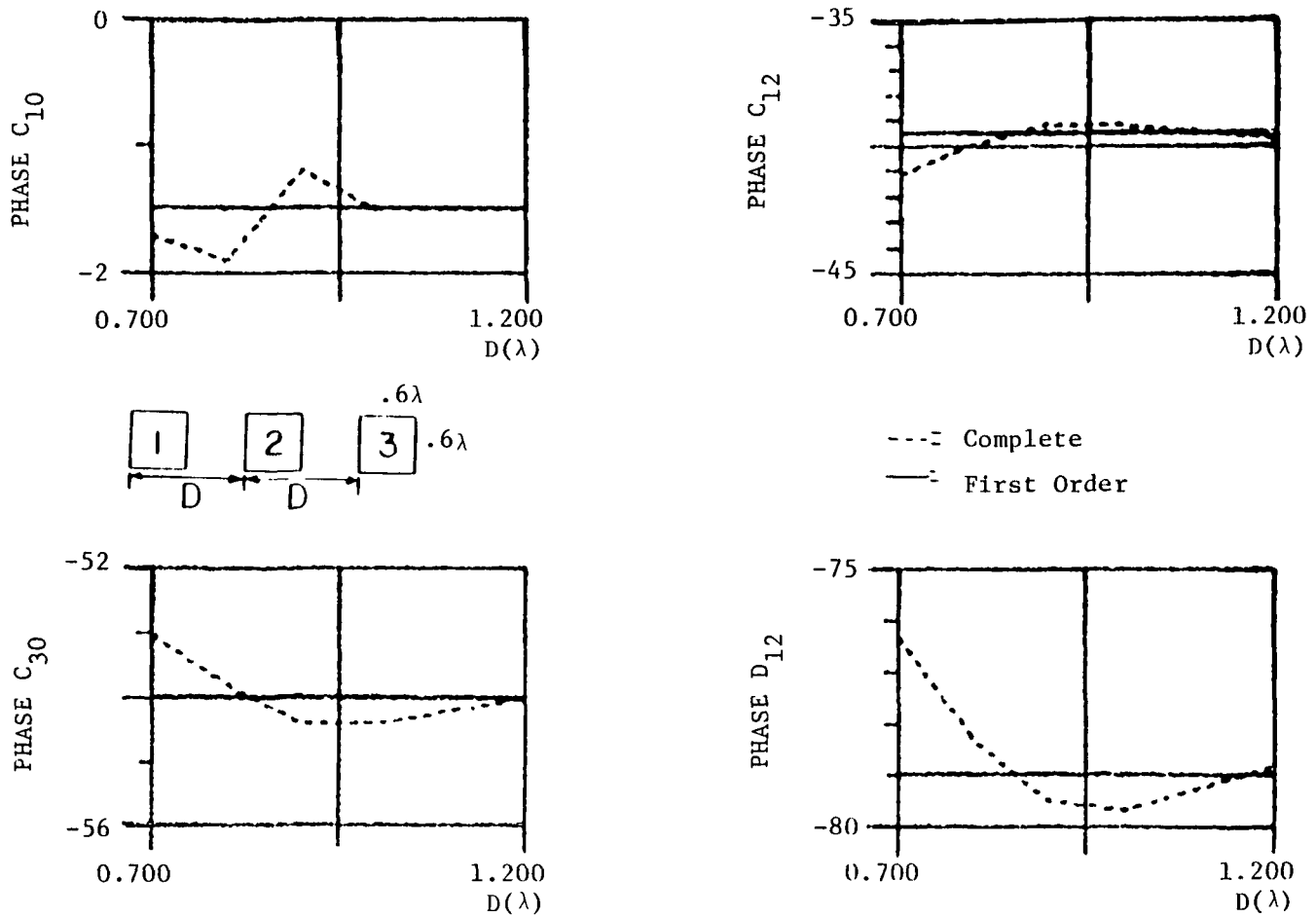

Figure 3.31 Comparison of Normalized Mode Phase Angles in #2 with #2 Driven (Deg.).

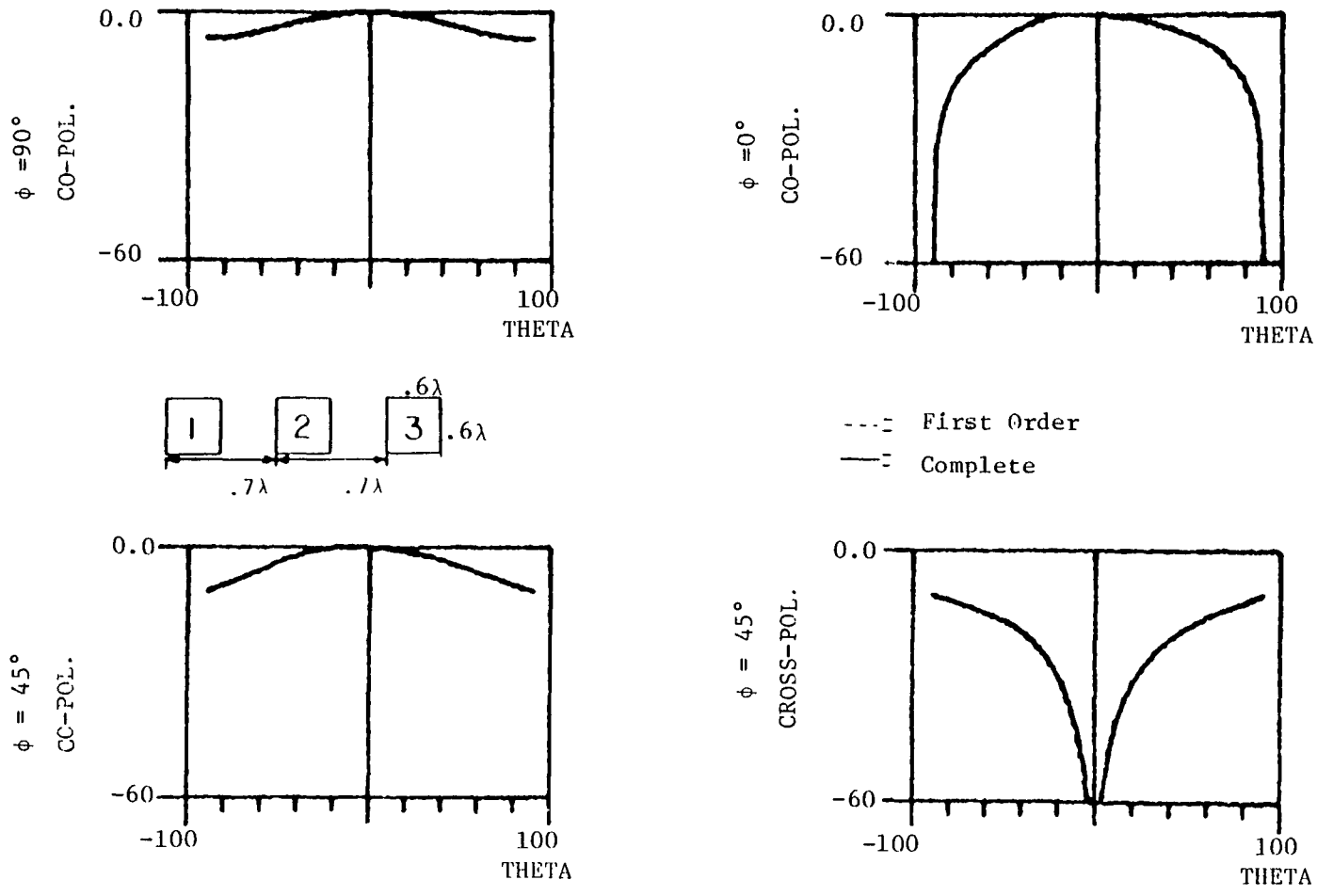

Figure 3.32 Comparison of Radiation Patterns with #1 Driven (dB).

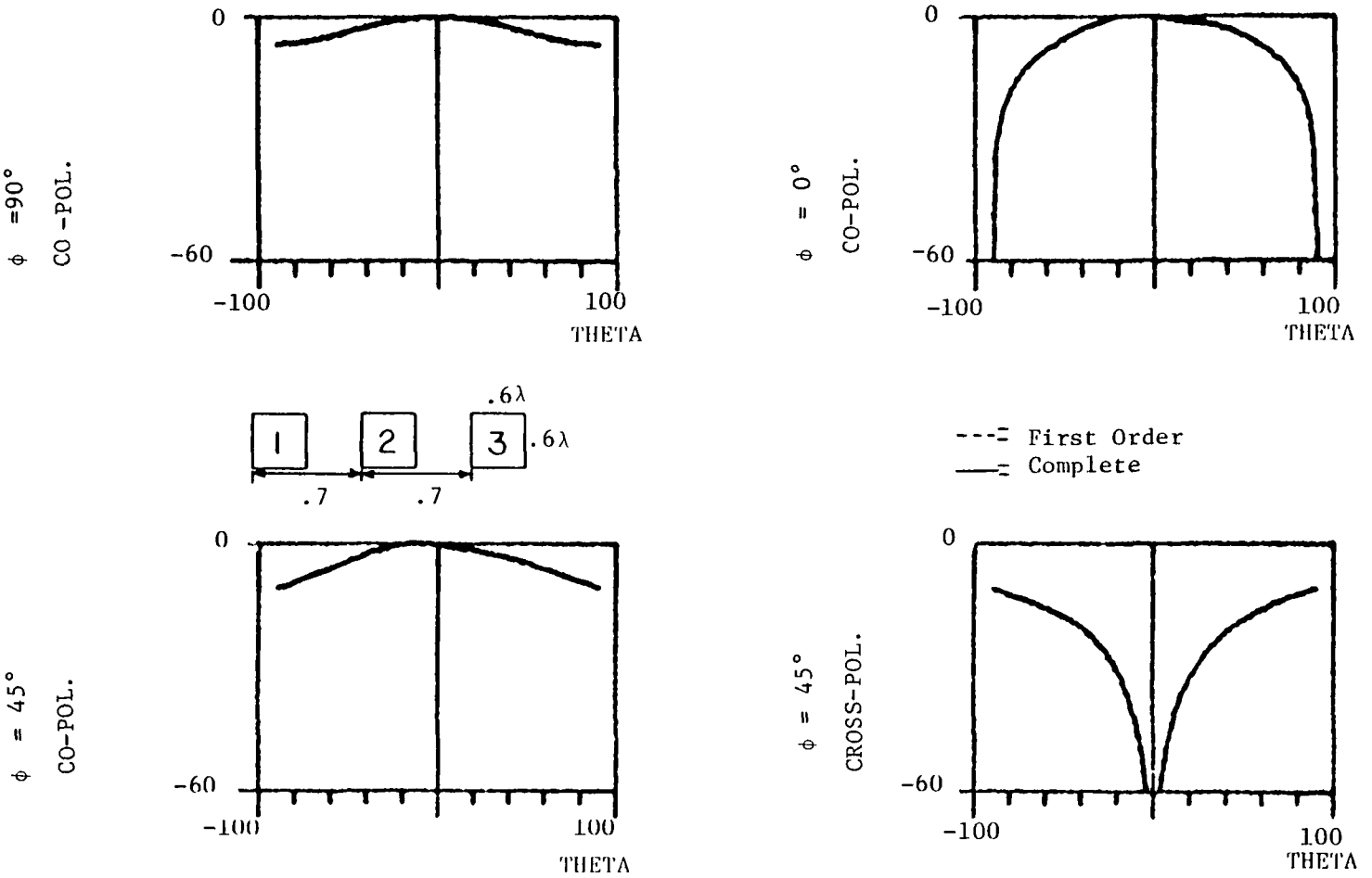

Figure 3.33 Comparison of Radiation Patterns with #2 Driven (dB).

more work on formulating a viable way to apply it to the types of antenna problems encountered today.

The final set of plots in this section are examples of the beam scanning properties of a three element array. The proper phase shifts in the driving modes of each aperture were entered to give 10° and 20° scans for a colinear array of three apertures at three different spacings. The results are shown in Fig's. 3.34 to 3.39 (again the 4-mode solution was used here). The plots are for $\phi = 45°$ and $\phi = 0°$ (each normalized by it's own largest value). Since there is only a single row of apertures the change in the shape of the patterns for the $\phi = 90°$ was slight. There was an overall reduction in level, but the shape didn't change with change in scan angle. So these patterns will not be presented here.

Before leaving scanned beams a look at the patterns show some interesting, even though expected results. First it's easy to see the super-imposed single aperture radiation patterns. These are products of the array factor, and can be seen in Fig's. 3.4, 3.5, and 3.6. The characteristic three aperture array factor can also be seen with it's single side lobe between main and grating lobes. Due to the large spacings necessary in an aperture antenna the grating lobe becomes sizable with very small scans of the beam. Therefore the resulting patterns do exhibit the general behavior of array antennas.

This concludes the three aperture results and the first order coupling computer testing. As was stated, the first order theory appears to provide an adequate approximation to the mutual coupling and should be studied further.

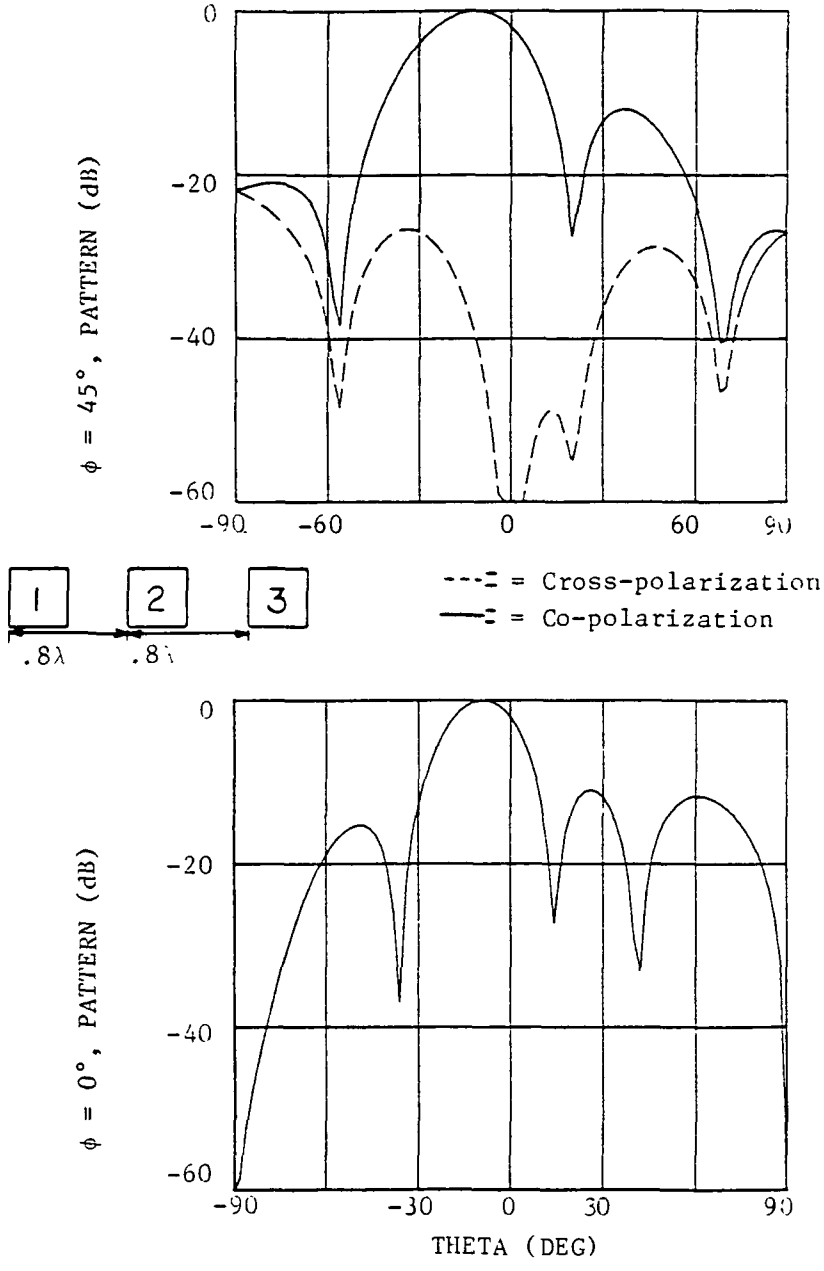

Figure 3.34 10° Scan of Beam.

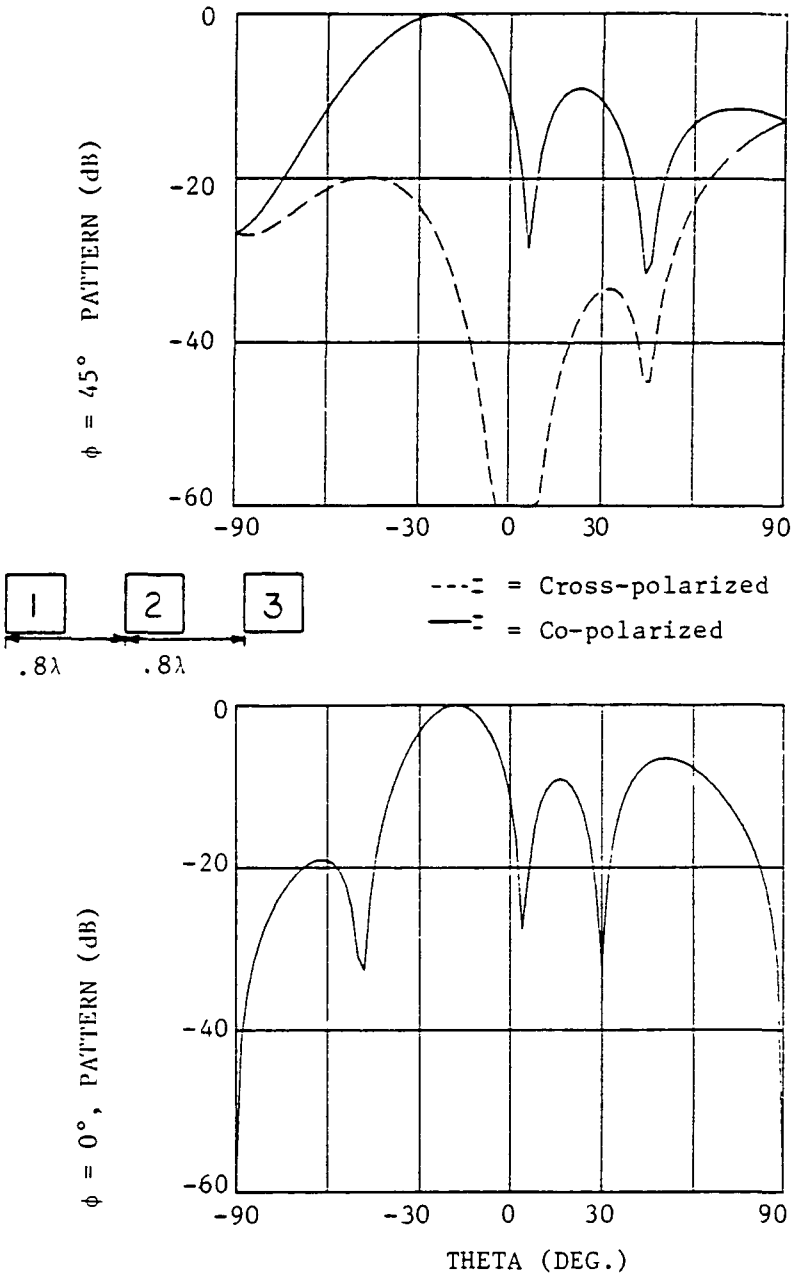

Figure 3.35 20° Scan of Beam.

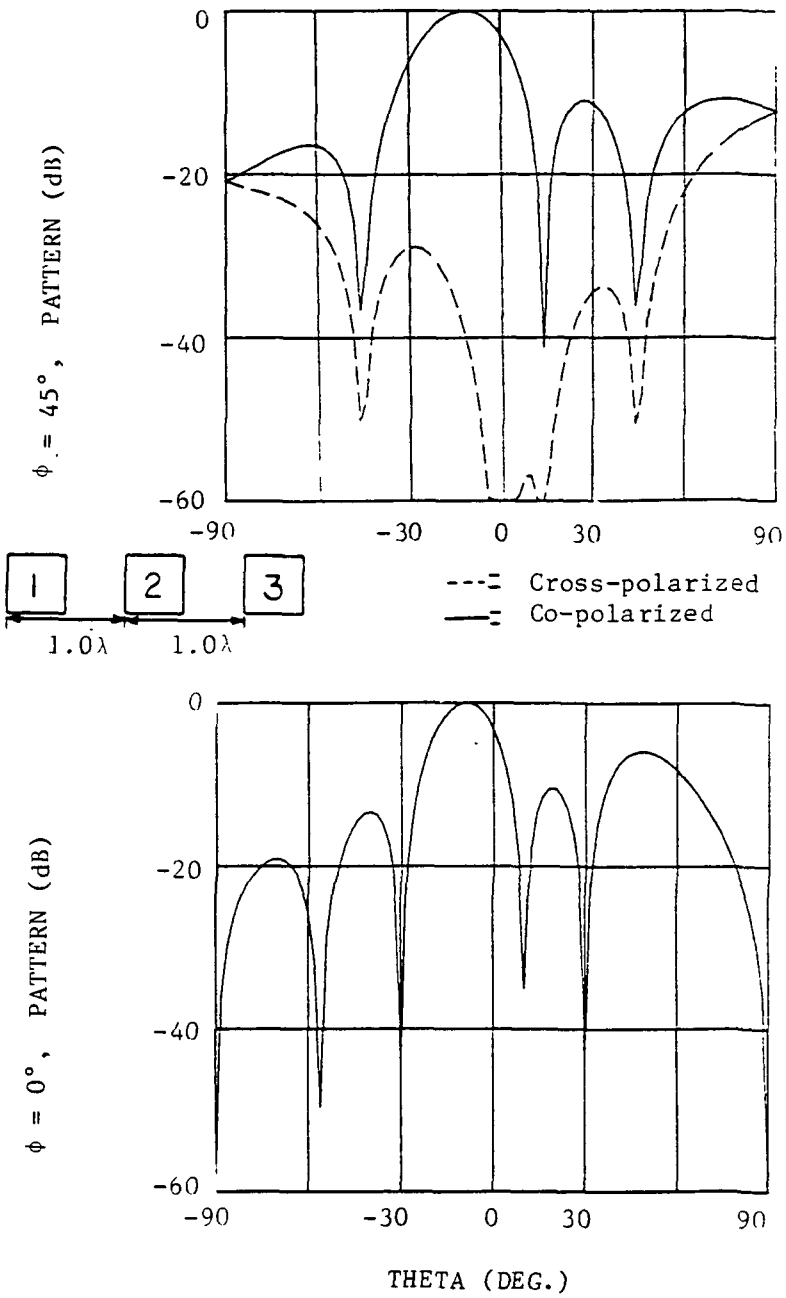

Figure 3.36 10° Scan of Beam.

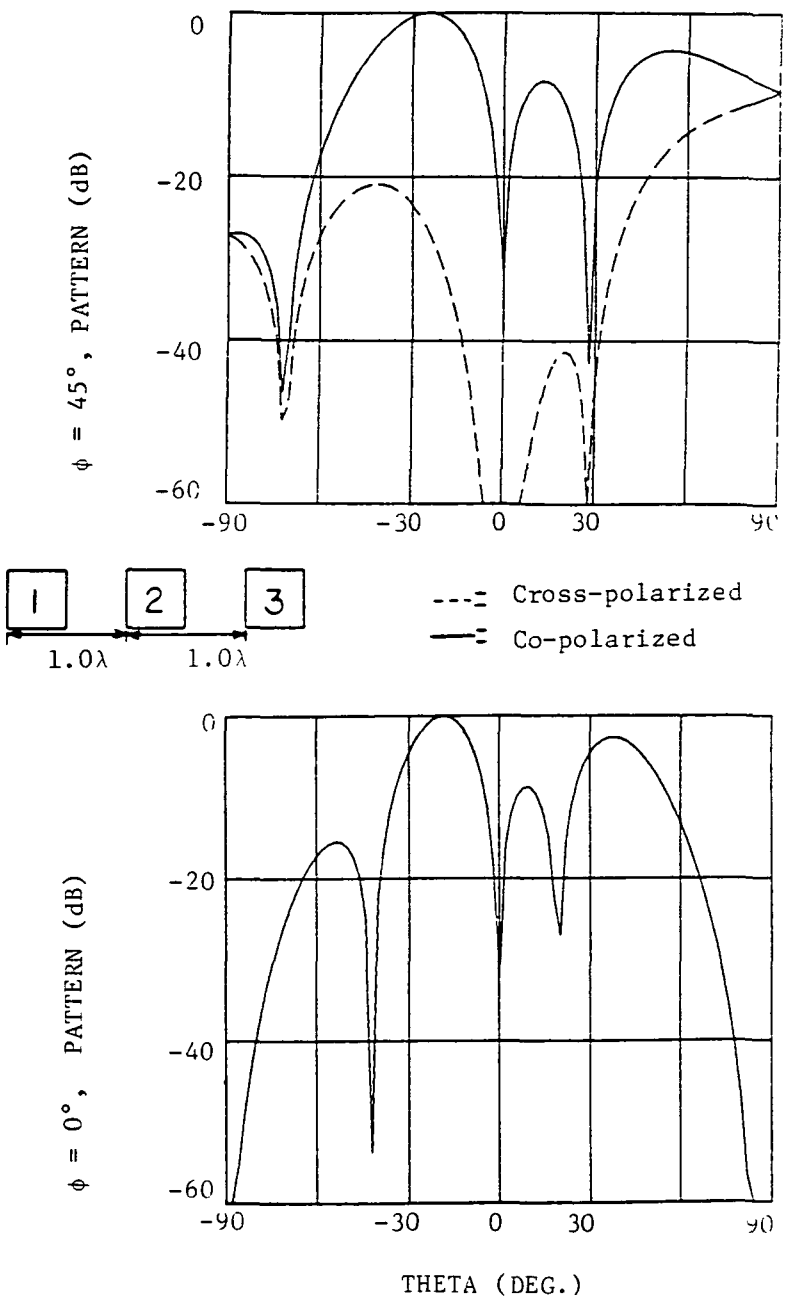

Figure 3.37 20° Scan of Beam.

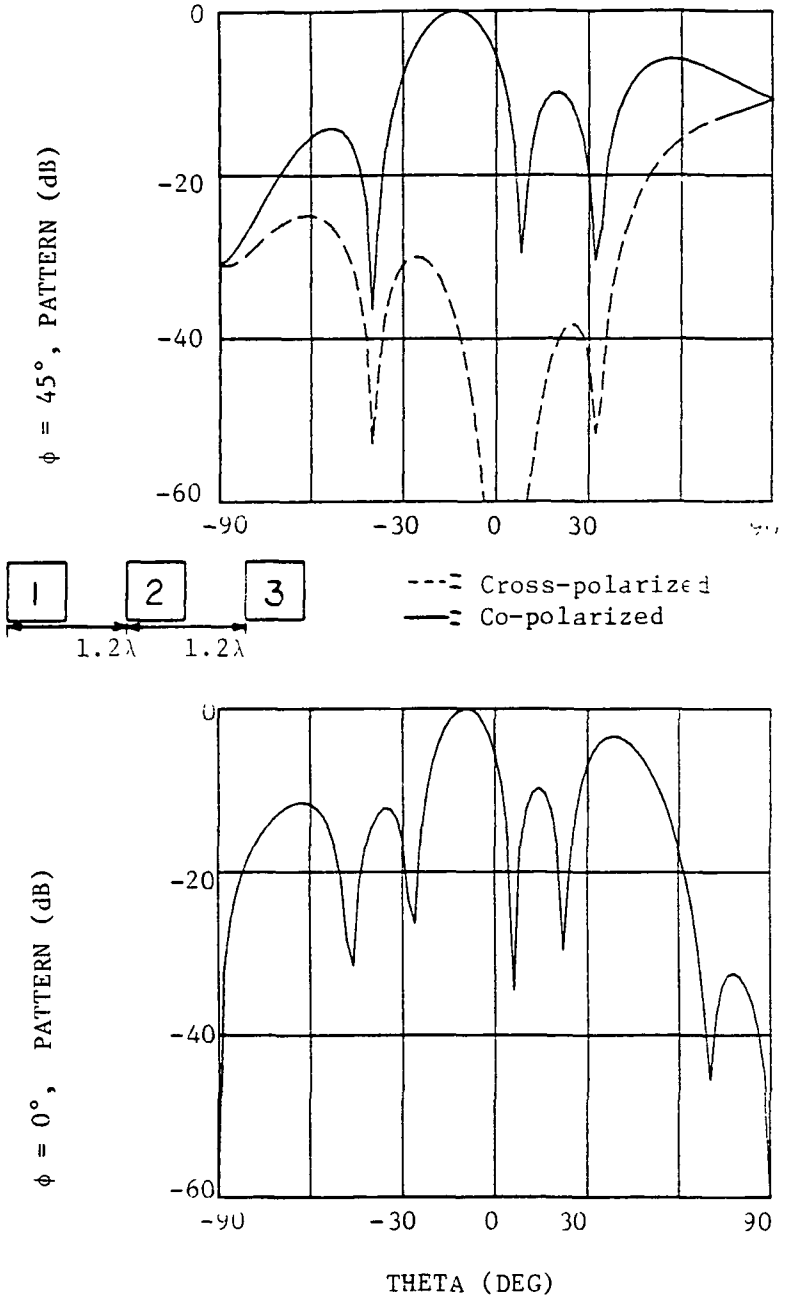

Figure 3.38 10° Scan of Beam.

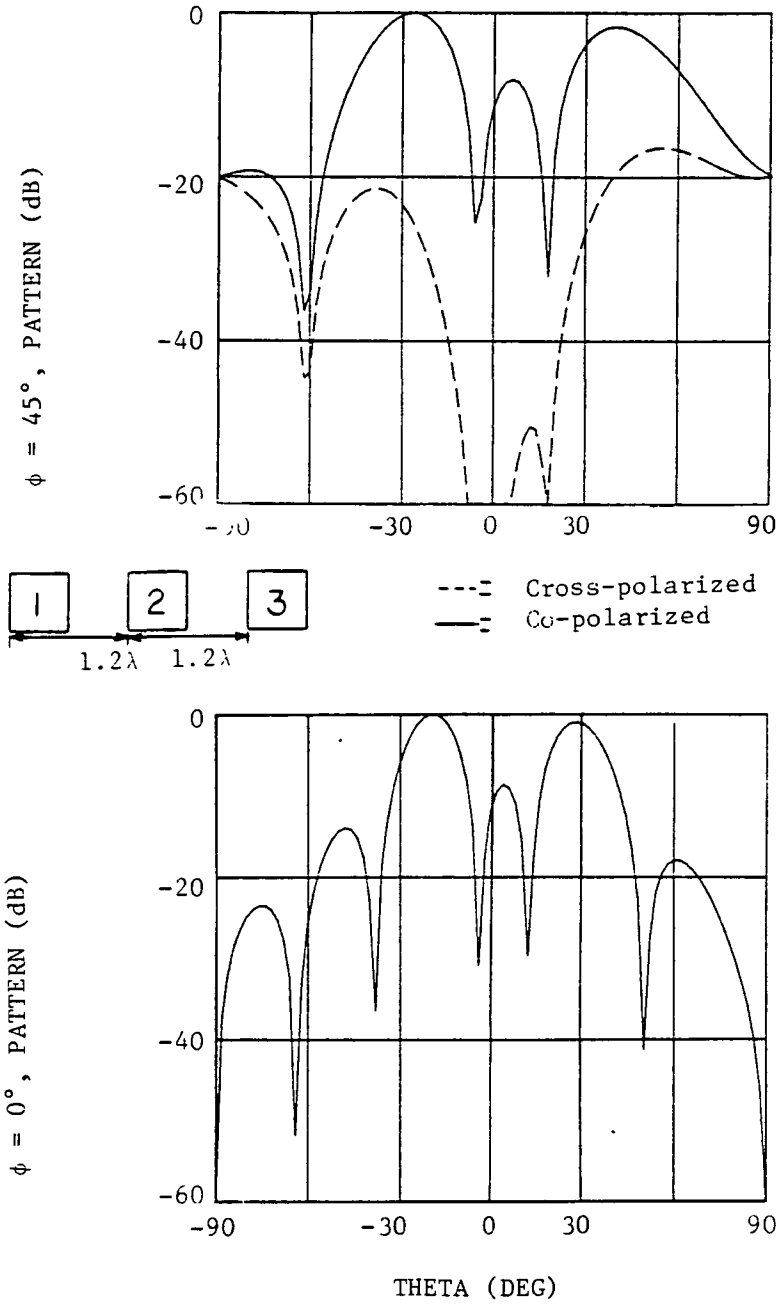

Figure 3.39 20° Scan of Beam.

3.5 Modest Sized Arrays

The results to be presented in this section are patterns of modestly sized arrays. The purpose is to compare the ideal array patterns with ones that include mutual coupling. These comparisons will help to show the necessity of including mutual coupling in larger arrays. A final note on edge effects will complete the discussion.

The first set of plots is the radation patterns of a 3 x 3 array of square apertures (0.6λ x 0.6λ) in a rectangular lattice with 0.7λ row and column spacings. The plots show a comparison of the ideally derived patterns (no coupling present) with the patterns found using the mutual coupling. These are shown in Fig's. 3.40, 3.41 and 3.42. Figures 3.43, 3.44 and 3.45 are the patterns for a 5 x 5 array of square apertures with like spacings. The 7 x 7 array case is shown in Fig's.3.46, 3.47 and 3.48. For the 3 x 3 and 5 x 5 array cases, a 5 mode solution (ψ_{10}, ψ_{12}, ψ_{30}, Φ_{01} and Φ_{12}) was used. For the 7 x 7 array only, a single mode, the dominant TE_{10} mode was used due to the limited matrix size of the program. All of the patterns are for the case of all the apertures equally driven with equal phases and amplitudes.

In looking at these plots the first conclusion to be drawn is that the coupling between columns must be smaller than the coupling between rows. This is seen in the fact that all of the $\phi = 0°$ (H-plane) comparisons show little difference between the patterns with and without coupling. There is a slight difference, but it didn't

always show up when the two sets of plots were superimposed. In looking at the data presented in Sec. 3.3 at Figures such as 3.7 or 3.9 it can in fact, be seen that coupling is smaller into an aperture next to the driven element then into one directly above it. So these patterns bear that out.

It can also be seen in these figures that the effect on the co-polarized main lobe and the first side lobe (in the larger cases) seem to be small. It wasn't until the second and higher side lobes that there seemed to be a difference. So the mutual coupling affects seem to be greater on the sidelobes that are at modest angles from the main lobe. The effect on the cross-polarized signal (ϕ = 45°) though was considerable. The coupling not only caused amplitude changes, but also shifted the position of the nulls. This result is due to the fact that the mutual coupling terms allow for additional energy in orthogonally directed fields to be present in the apertures that are cross-polarized in nature (of different symmetry than the incident fields). This additional energy, unaccounted for in the ideal case, then caused the large changes. It also seems that the differences in the 7 x 7 case are small. This is due to the fact that only one mode was used in the computer solution, thus not accurately predicting all of the coupling present. This shows the need for including more than just the dominant TE_{10} mode in the aperture field approximations.

The next comparison is that of the E-plane (ϕ = 90°) pattern of a single aperture radiating in various sized arrays, where all other elements are terminated in matching loads but not driven. Figure 3.49

shows these patterns for three array sizes. The first is that of a single element array. The other two are for a 5 x 5 and an 11 x 11 array where the center element is the driven aperture. These are all square apertures with the arrays in a rectangular lattice with 0.7λ row and column spacings. For the single and 5 x 5 array case, the 5 mode solution discussed above was used while a single mode was used in the 11 x 11 array case.

It is easy to see the effects that mutual coupling has on the patterns as more apertures are added. These additional apertures absorb energy that would normally be present in the pattern and scatter energy that then interacts with the original radiated fields. These two effects then account for the changes seen. It is interesting to note that as more elements are added, the pattern gets slightly more directive.

The analysis of the E-plane patterns of the center element of a large array was also looked into by Amitay, Galindo and Wu (Amitay, Galindo and Wu, 1972). They experimentally measured this pattern for the center element of a 19 x 19 array of square apertures. The array had slightly closer spacings than that used above. Their results show that at approximately 30° and 70° a sharp null appears in the pattern. The beginnings of this null can be seen in the 11 x 11 plot shown in the figure. While not as sharp, there are dips in the pattern that are 4 dB below the single aperture pattern. So it seems that the computer derived patterns do in fact give a fairly accurate picture of the true patterns.

Turning to the topic of edge effects, it is necessary to look at the early work on mutual coupling. In the early analysis the finite arrays were approximated by arrays with an infinite number of rows and columns. This allowed the radiated fields to be represented by Floquet modes and was thus easier to analyze. (see Amitay, Galindo and Wu, 1972 for complete analysis). The problem with this type of solution is that it predicts the effects on central elements in a large array fairly well, but it doesn't give accurate results for elements closer to the edge. This difference between coupling affects of center verses edge elements is known as the edge effect. It can be explained intuitively by considering the neighboring apertures that an element "sees". Center elements are surrounded on all sides by apertures while edge elements "see" fewer closely spaced apertures. To illustrate this point the patterns of the center element and the upper right hand corner element of a 5 x 5 arrays are compared in Fig's. 3.50 and 3.51. The elements are square (0.6λ x 0.6λ) with $.7\lambda$ row and column spacings in a rectangular lattice. A single mode approximation was used here. From these plots it can be seen that the edge element's patterns are shifted to one side due to the fact that it doesn't have neighboring elements on two of it's sides. So it can be concluded that due to the edge effects, the finite array type of analysis performed here is necessary to insure proper results.

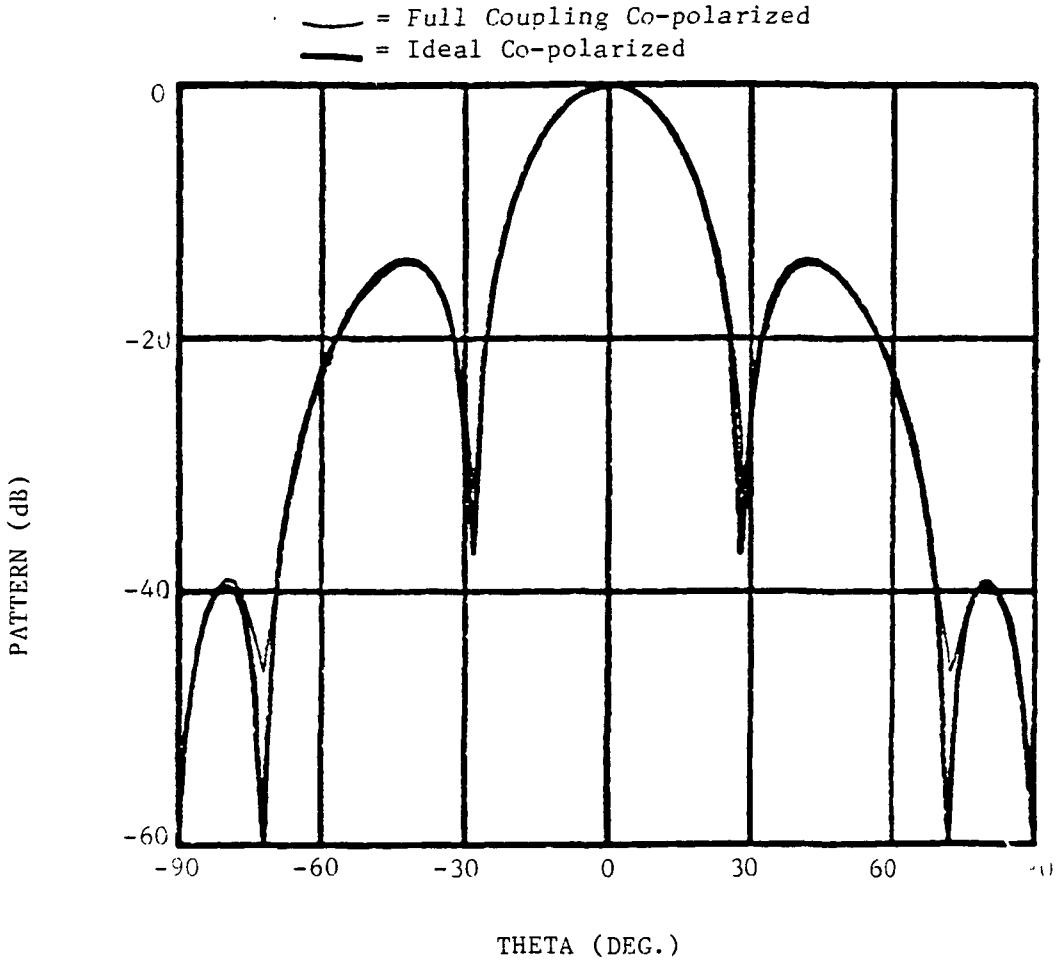

Figure 3.40 Comparison of Patterns of a 3 x 3 Array; $\phi = 0°$.

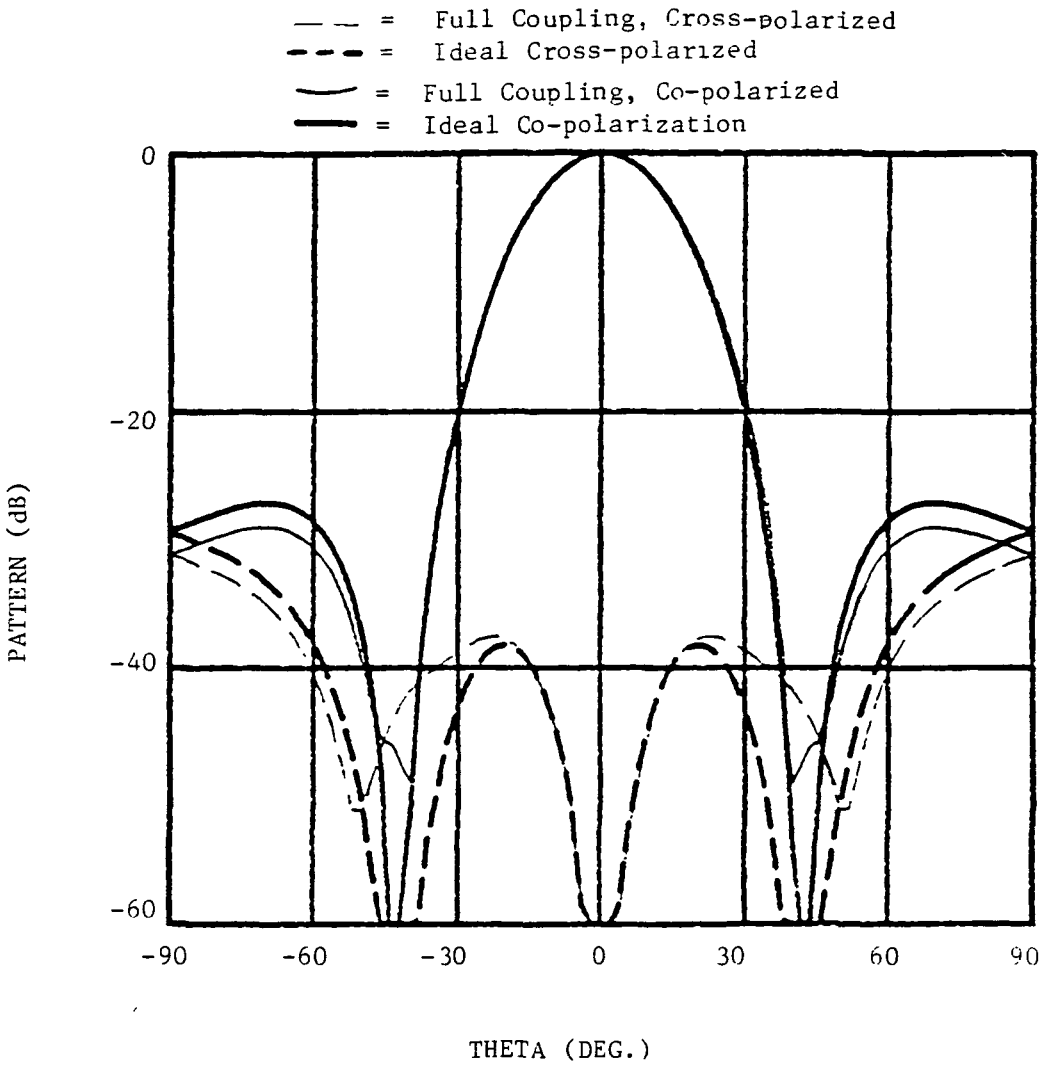

Figure 3.41 Comparisons of Patterns of a 3 x 3 Array; $\phi = 45°$

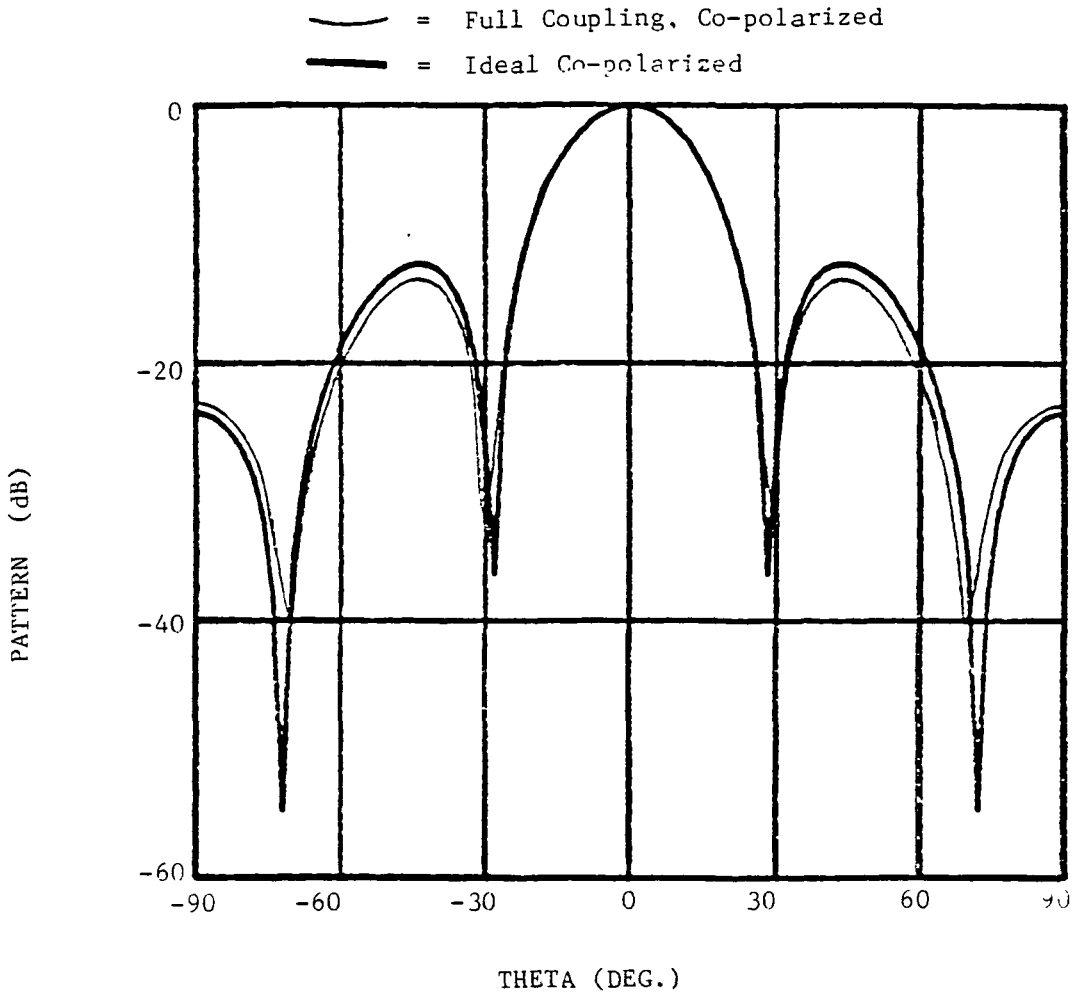

Figure 3.42 Comparison of Patterns of a 3 x 3 Array, $\phi = 90°$

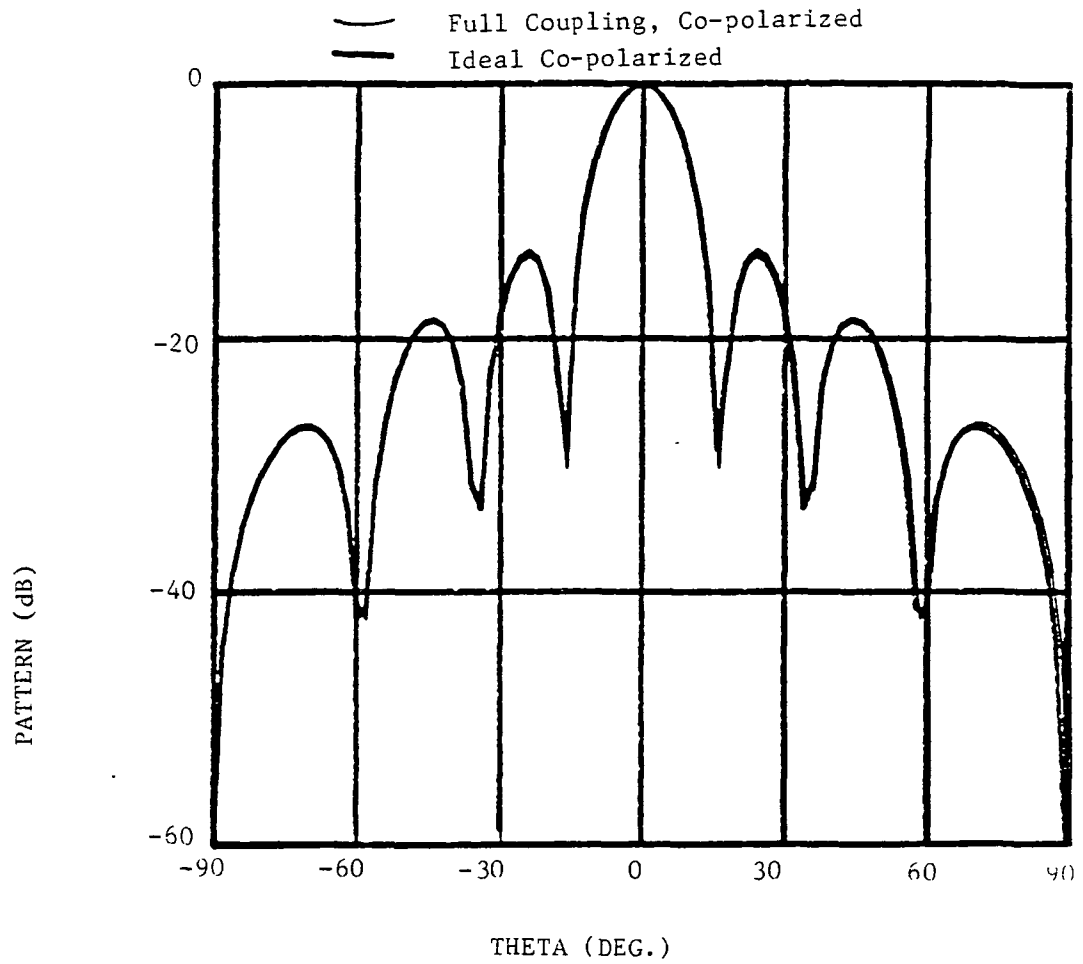

Figure 3.43 Comparison of Patterns of a 5 x 5 Array, $\varphi = 0^{\circ}$

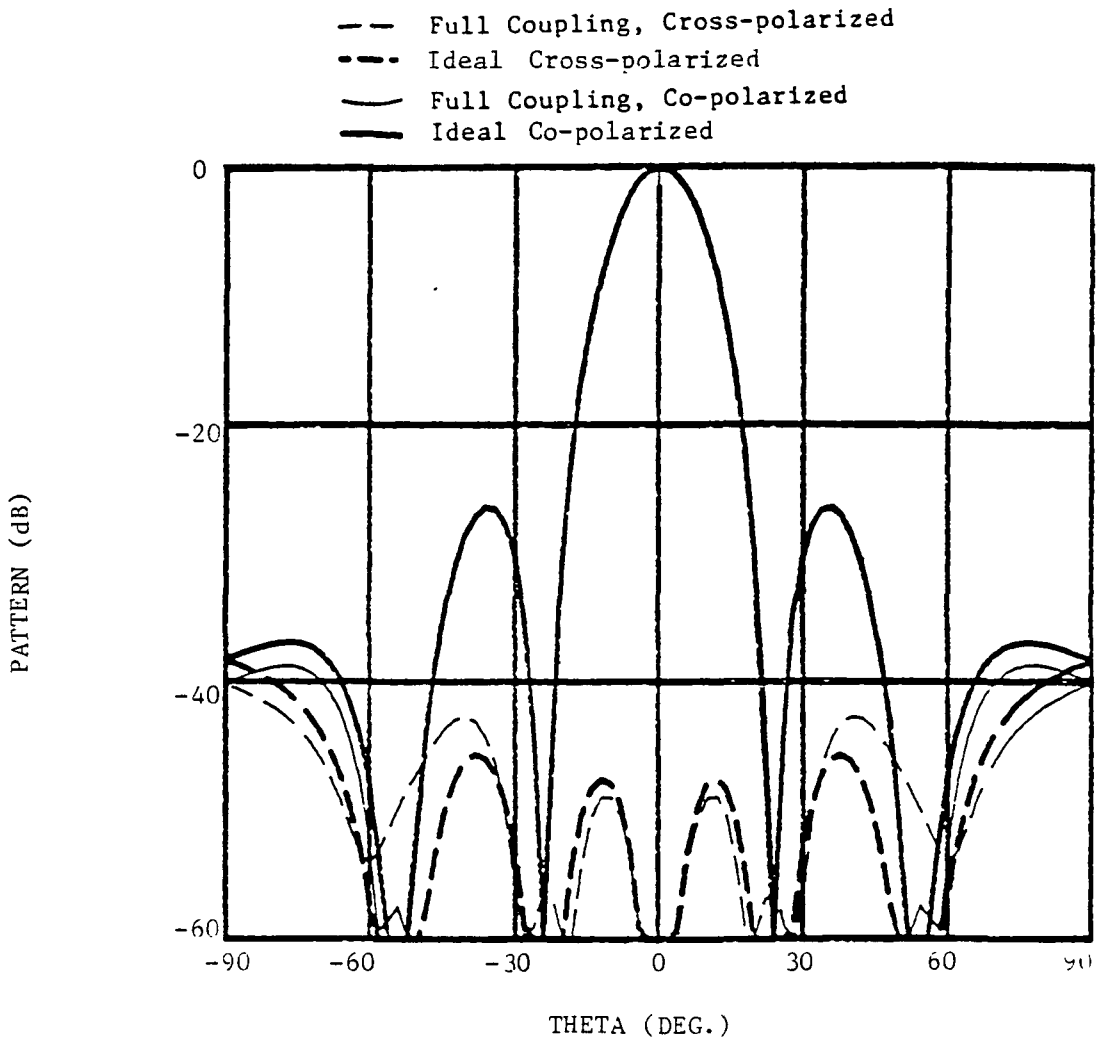

Figure 3.44 Comparison of Patterns of a 5 x 5 Array, $\phi = 45°$

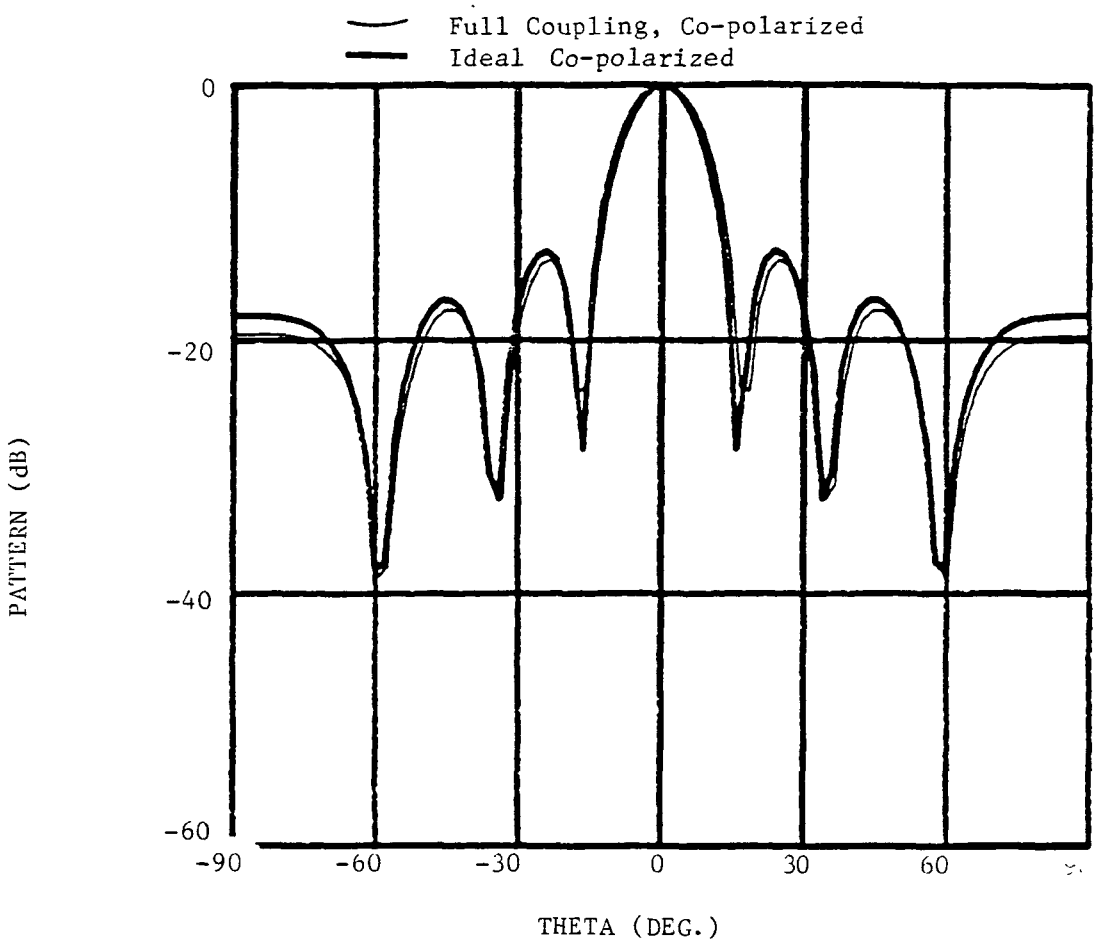

Figure 3.45 Comparison of Patterns of a 5 x 5 Array, ϕ = 30°

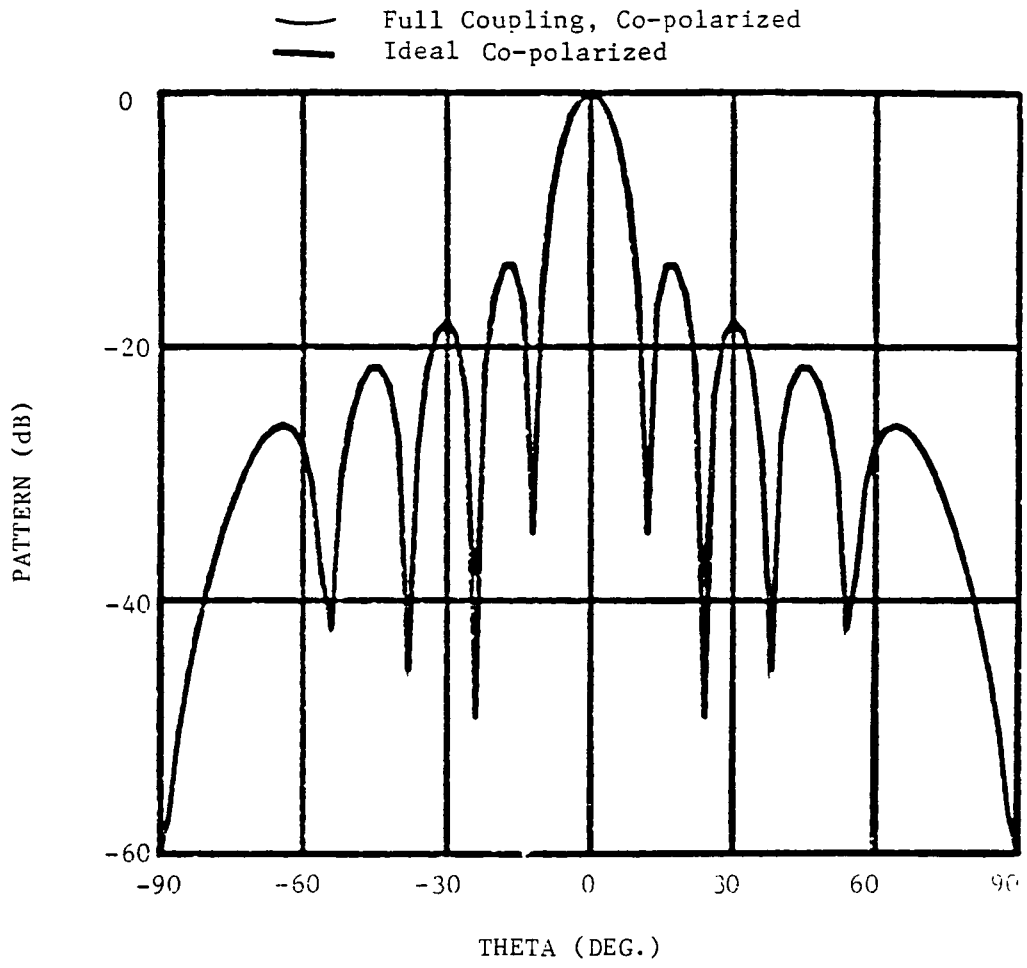

Figure 3.46 Comparison of Patterns of a 7 x 7 Array, $\phi = 0°$

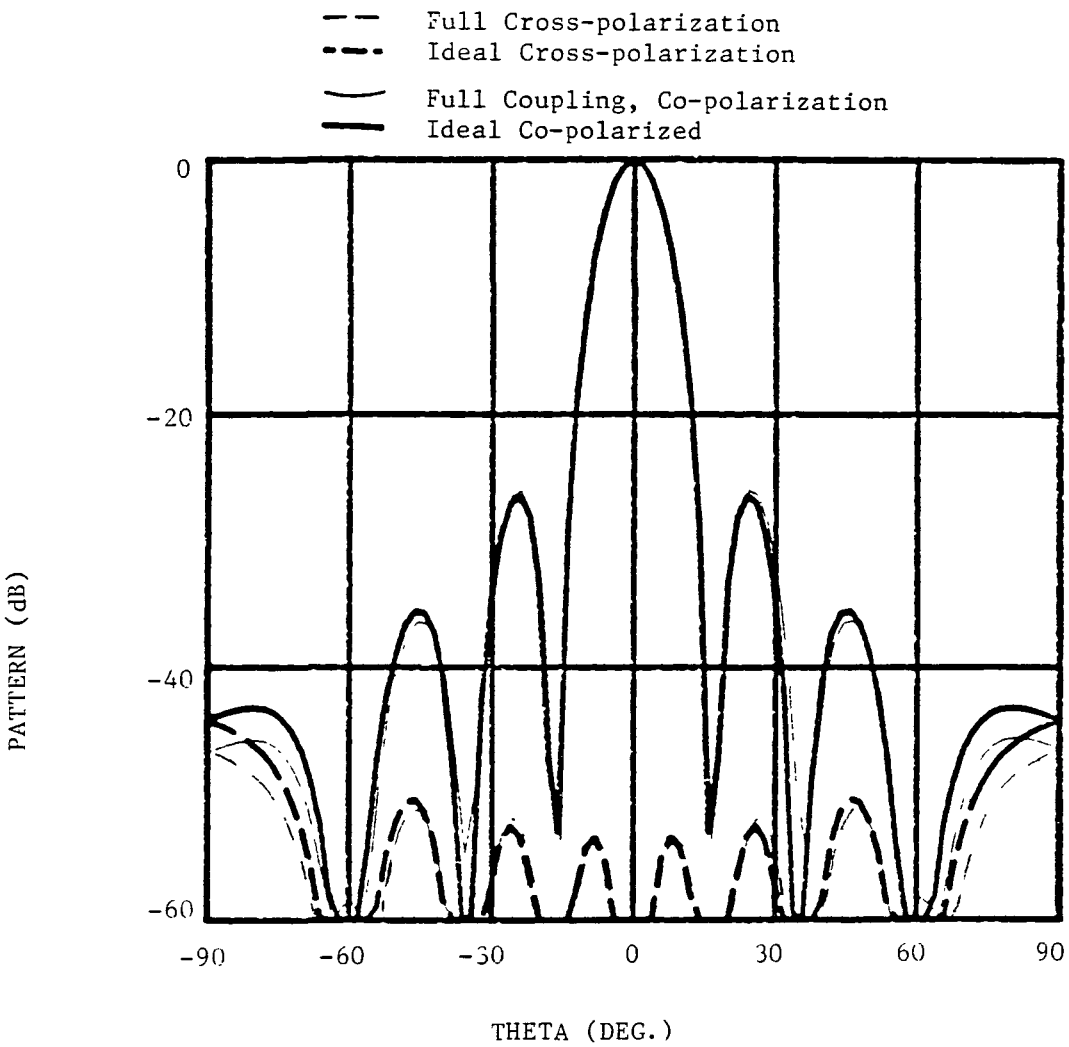

Figure 3.47 Comparison of Patterns of a 7 x 7 Array, $\phi = 45°$

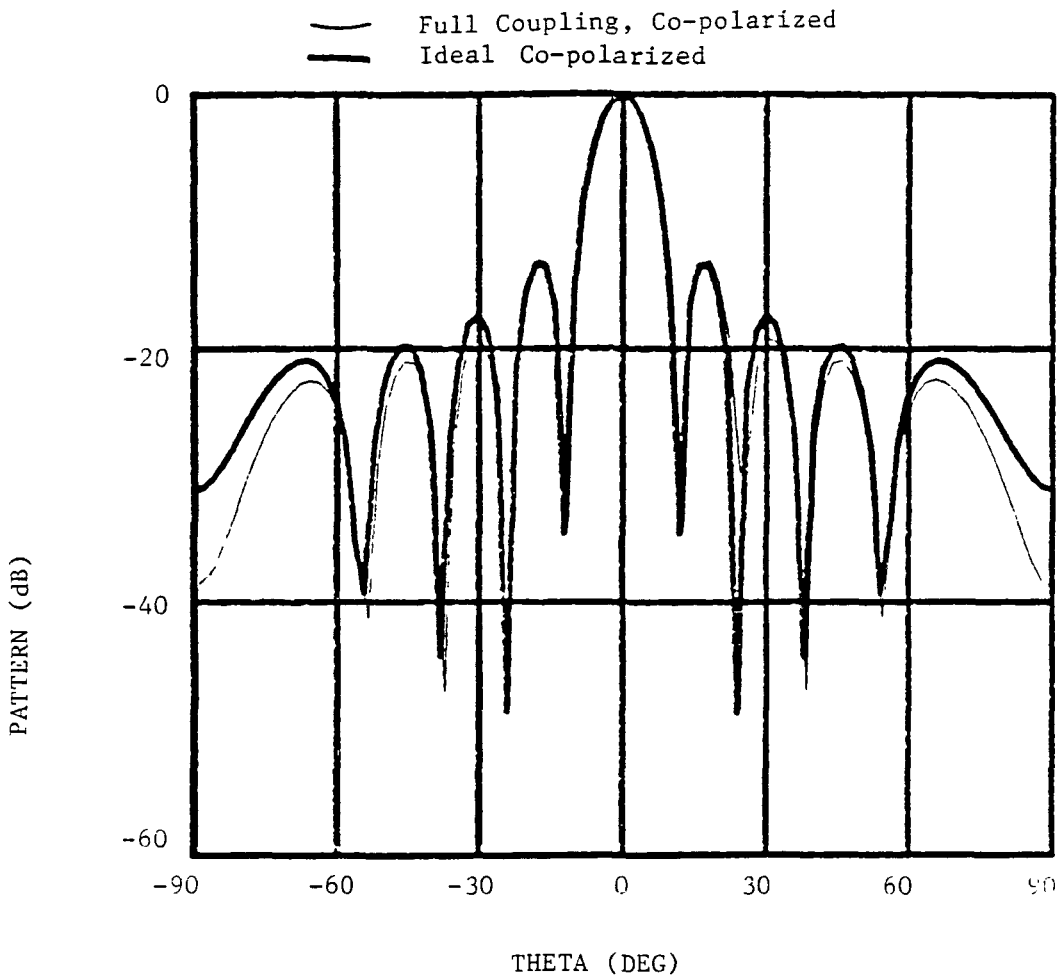

Figure 3.48 Comparison of Patterns of a 7 x 7 Array, $\phi = 90°$

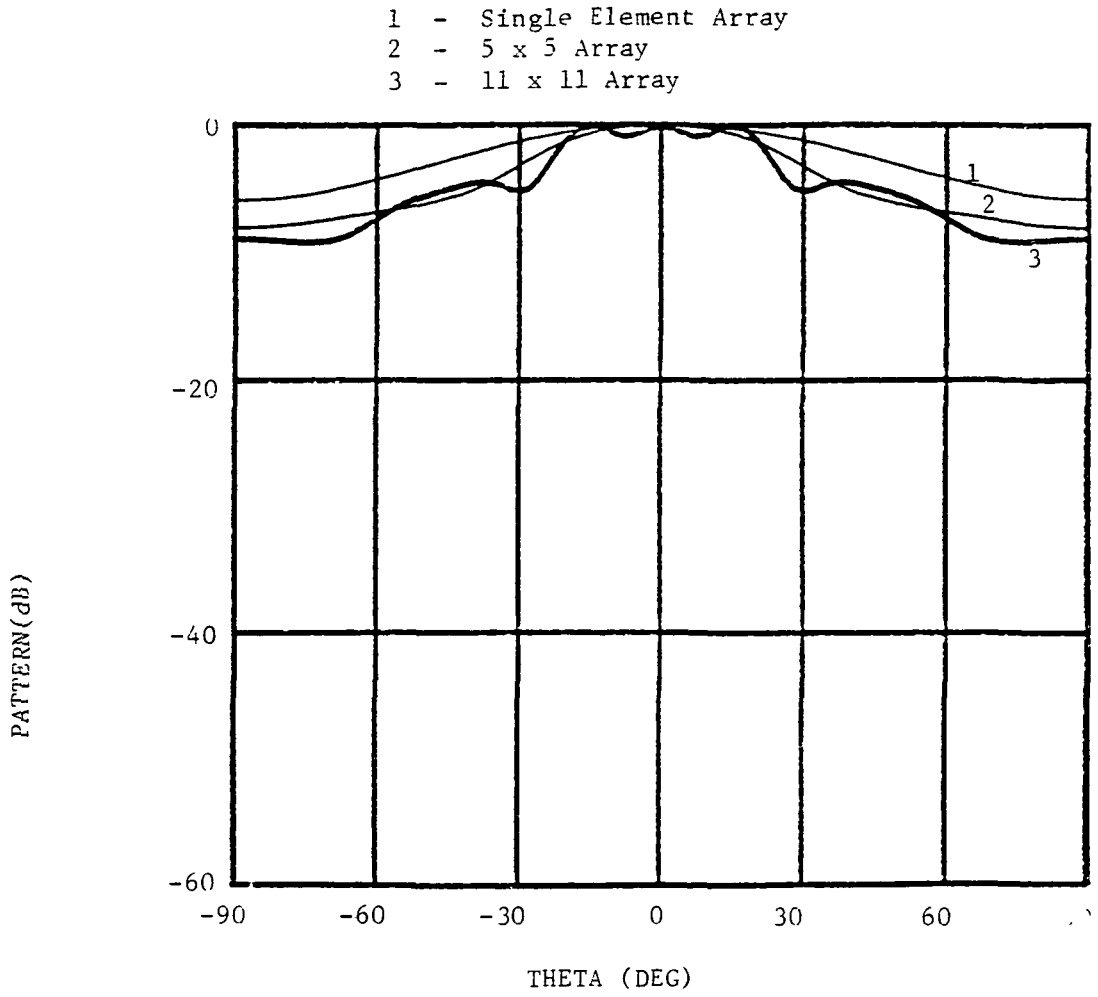

Figure 3.49 Comparison of E-plane Co-polarized Patterns for Center Element of Three Different Sized Arrays.

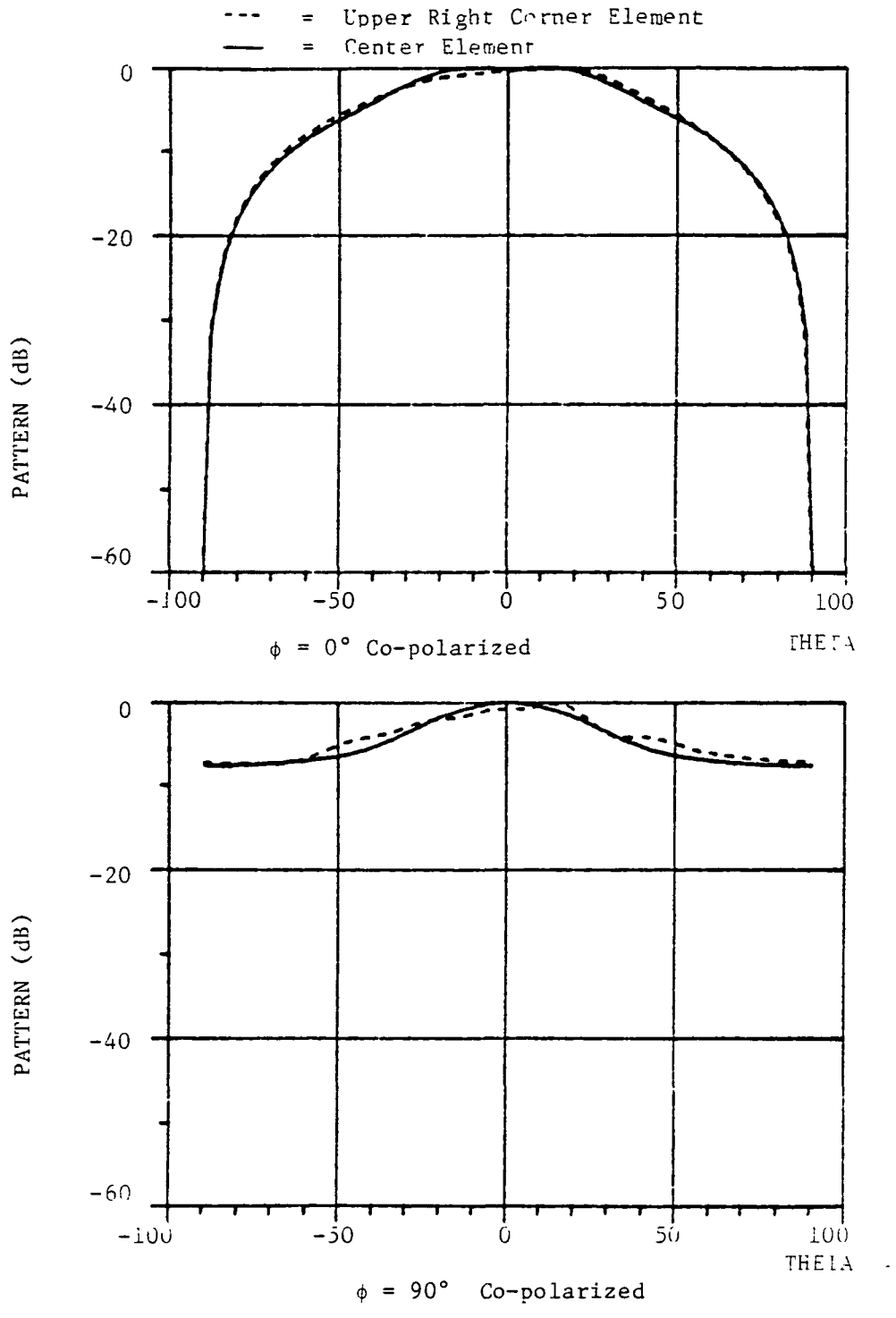

Figure 3.50 Comparison of Patterns of Elements in a 5 x 5 Array.

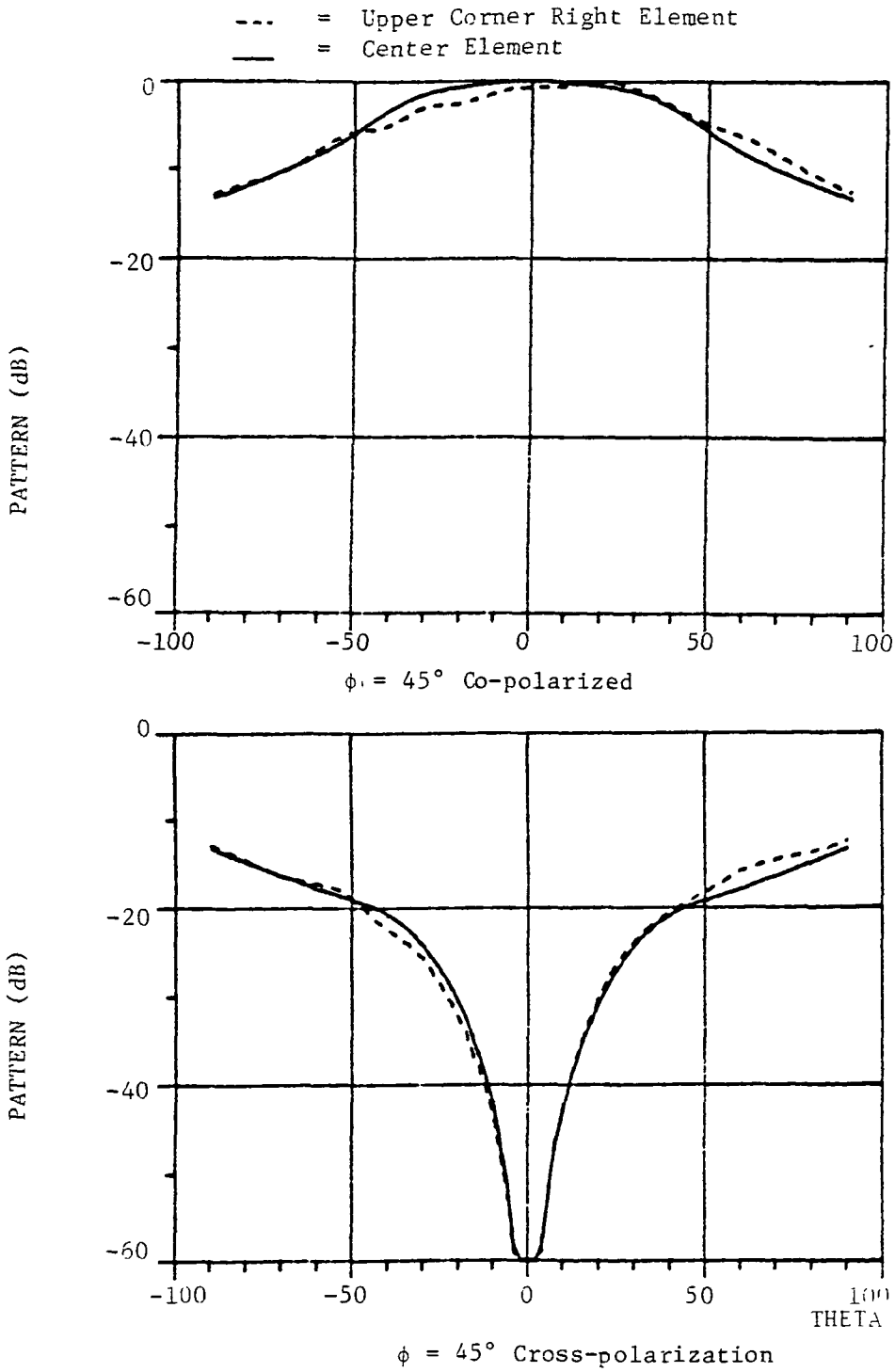

Figure 3.5i Comparison of Patterns of Elements in a 5 x 5 Array.

3.6 Conclusion

In this chapter various computer derived data, found using the vector potential approach, were presented. These results helped to shed some light on the mutual coupling problem by looking at it from several points of view.

First the single aperture array data was used to determine the proper approximation to use in the later analysis. After this, the validity of the computer model was established by comparing the results with those of several published articles. These comparisons along with the data to be presented in the next chapter show that the model is in fact reasonably accurate.

Some preliminary testing of the first order coupling idea was then presented. The two and three aperture tests showed that the first order coupling approximation did yield valid results. The testing, while incomplete, was sufficient to warrant further study on this idea.

The rest of the chapter dealt with various sized arrays and how mutual coupling affected their performance. This included a look at the beam scanning properties of small arrays and concluded with a discussion on edge effects.

Finally, a word regarding the radiation patterns presented here. The patterns were each normalized by their own largest value. That means that the $\phi = 90°$, $\phi = 0°$ and $\phi = 45°$ patterns were each normalized by their own peak values. The co- and cross-polarized patterns for $\phi = 45°$ were both normalized by the same value. This shouldn't cause any problems for the non-scanned plots as the peaks for all three coincide at $\theta = 0$.

In the scanned plots of Fig.'s 3.34-3.39 though this is not the case. If the $\phi = 45°$ and $\phi = 0°$ plots of each figure were normalized by the same value, the overall level of the $\phi = 45°$ plots would be slightly lower. The shapes of the patterns wouldn't change though, so the effect of scanning the beams is still properly illustrated by these plots.

CHAPTER 4

EXPERIMENTAL VERIFICATION

An experiment was conducted to test the accuracy of the computer derived results. The tests measured the coupling (S_{21}) between two apertures in various configurations on a large copper plate. The measurements were made with a Hewlett Packard 8409B Automatic Network Analyzer with version 11863D software. The test stand was a 2 ft. square ground plate with the waveguide fed apertures radiating to a room covered with absorber material.

To facilitate ease of manufacture and to reduce set-up times, a general purpose test stand was constructed. A 1/4" copper plate 2 feet square was milled so as to allow 5 X-band waveguides to be soldered directly to it. The hole configuration is shown in Fig. 4.1. The spacings were chosen by taking into consideration the waveguide flange sizes and the amount of material necessary to assure a strong plate that wouldn't warp during soldering.

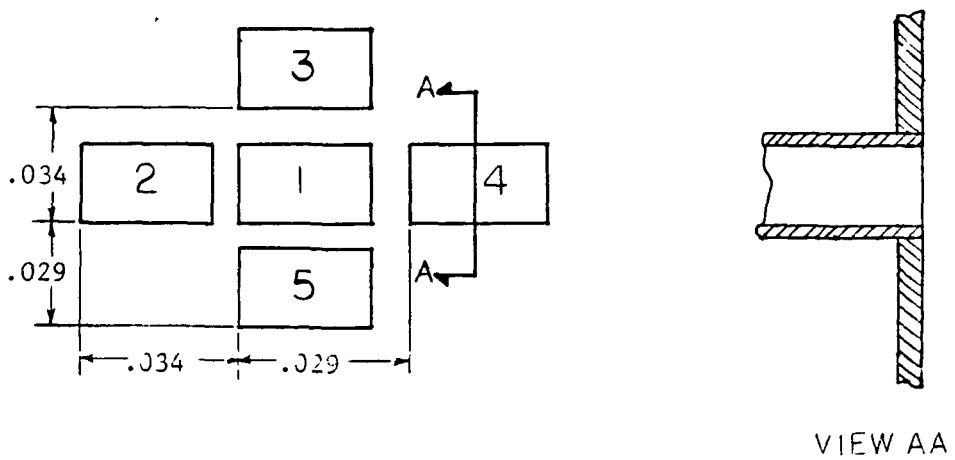

Figure 4.1 Test Set-up. Distance in Meters.

Two tests were run on this set-up. The first measured the coupling between two apertures at various spacings and angles in terms of S_{21}, for direct comparison against the computer data. The second was a test of first order coupling. The S_{21} and S_{11} was measured between two apertures with a third aperture present. This third aperture's waveguide was terminated in a matched load. These measured scattering parameters were then compared against the parameters measured for the coupling with no third aperture present. The difference then would be the re-radiated third aperture fields and thus the relative effects of the re-radiated fields could be determined.

In all these tests the unused apertures in the plate were covered with foil, so as not to interfere with the coupling between the two apertures being tested. For example to test the coupling between two apertures side by side at .034m spacing, the analyzer would be connected to the guides for apertures 1 and 2. Apertures 3, 4, and 5 would then be covered with foil.

The first set of data is shown in Fig's. 4.2 and 4.3. It compares the experimental results for two co-linear apertures, mounted side by side at 3 different spacings, against data from the computer. The computer results for the tests in this section used the four mode approximation discussed in Sec. 3.2 (ψ_{10}, ψ_{12}, ψ_{30} and Φ_{12}). Figures 4.4, 4.5, 4.6 and 4.7 show the same comparison but for two other aperture configurations. In these tests the frequency was scanned from 8 to 12 GHz to give a set of data points for each arrangement. By doing this, the size of the apertures and their spacings would increase in terms of wavelength with each increase in frequency.

The test data seemed to deviate from the computer results most at 9-10 GHz. At first it was thought that resonances in the set-up might be responsible, but after a more complete run was made, the true cause became apparent. Figures 4.8 and 4.9 show the S_{21} and S_{11} magnitude plots taken directly off the network analyzer for runs with very small spacing between data points. The experimental curves are seen to oscillate about the drawn in computer derived lines. The vertical axis is dB of loss so they are in fact negative quantities.

The cause of the oscillations is probably due to the irregularities in the system. One possible reason being the fact that the ground plane wasn't infinite. This could account for part of the oscillations since the amount of interference would depend on the distance between the source and the diffracting edge in wavelengths. This would then vary as the testing frequency is scanned. A second source of error is the test set-up itself. It was calibrated for a given location of the cables and their connections. These cables are then moved and connected to the test stand, destroying the calibration. This would explain the fact that the plots in Fig's. 4.8 and 4.9 give slightly different numbers then the data shown in Fig's. 4.2-4.7 at specific frequencies. While the average line for the experimental data was always about the same the overriding noise seemed to move up and down this line, depending on the day the test was run. Tests run on the same day with the same calibration didn't show this variation. If the noise could be averaged or filtered out of the experimental data, it would produce a set of curves that appears to be close to the computer derived data. So it seems possible

at this point to say that the tests agree with the computer data within the limits of the system noise.

The second test was performed for two co-linear apertures with a third undriven one present. The result for two different aperture arrangements are shown in Fig's. 4.10 and 4.11. The data measured with a third aperture present is compared against that found in the previous test. These plots are consistent with the first order computer tests presented in the last chapter. The presence of the third aperture seemed to have little affect on the S_{21} and S_{11} in Fig. 4.10, while the variation in S_{11} in Fig. 4.11 could be explained by the irregularities seen at 9-10 GHz discussed above.

The final measurements made tested the level of the analyzer's internal noise. It was measured by terminating the analyzer's outputs in matched loads and measuring the amount of signal present. The tests showed the worst case noise to be at approximately -60dB. This would explain the large differences seen in the d = .063 side-by-side test (Fig's. 4.2 and 4.3). It's magnitudes were approaching the point where the analyzer noise was large enough to have an effect. Also tested was the amount of reflected signal from the absorber in the measuring room. It showed that the reflection was buried in the level of the analyzer noise. So these two noise sources are small enough not to have much effect on the results.

This concludes the experimental analysis of mutual coupling between apertures in a ground plane. The results for the most part are consistent with the data found by the computer using a 4 mode solution. While the test results were slightly irregular, they were sufficient

enough to verify the accuracy of the analytical model.

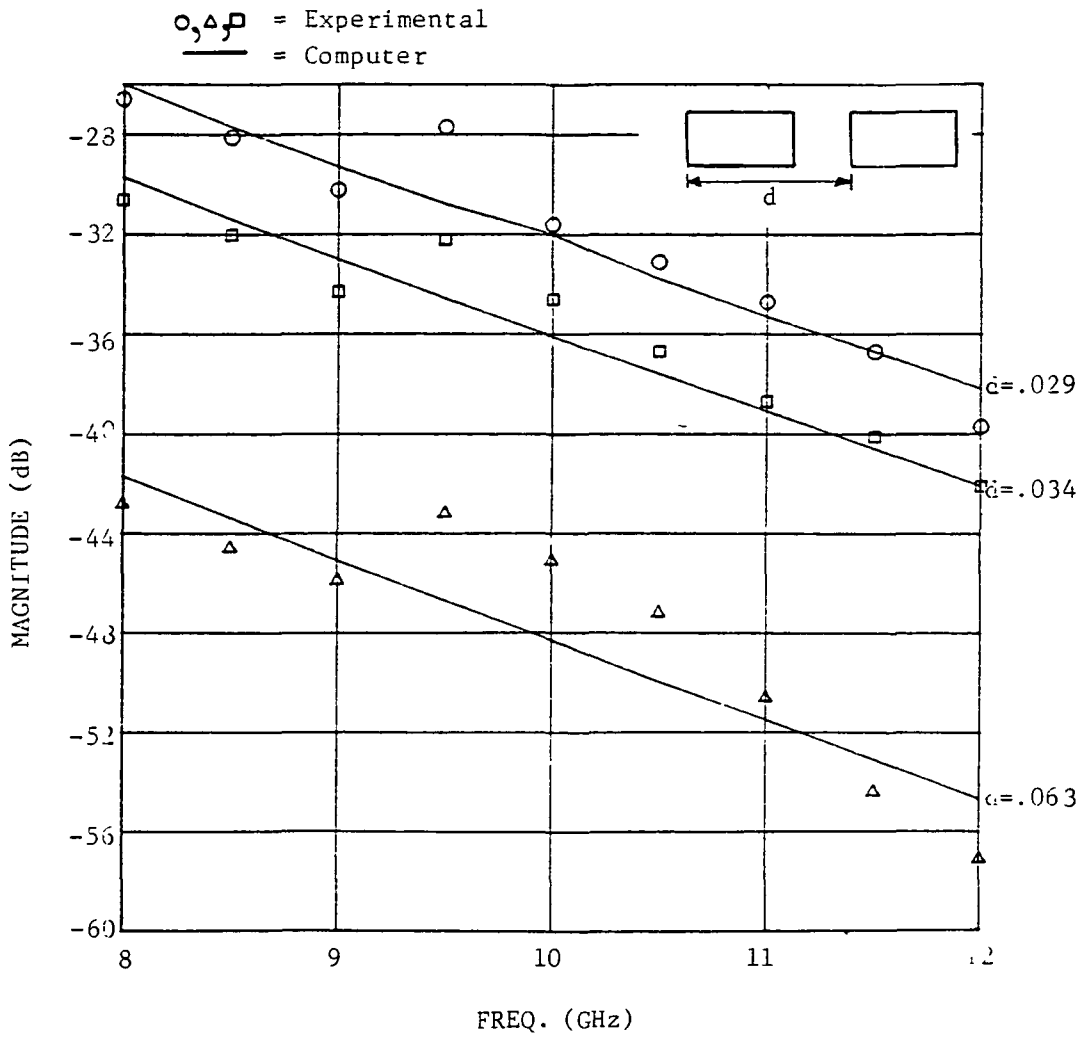

Figure 4.2 Experimental vs. Computer. S_{21} (d in Meters).

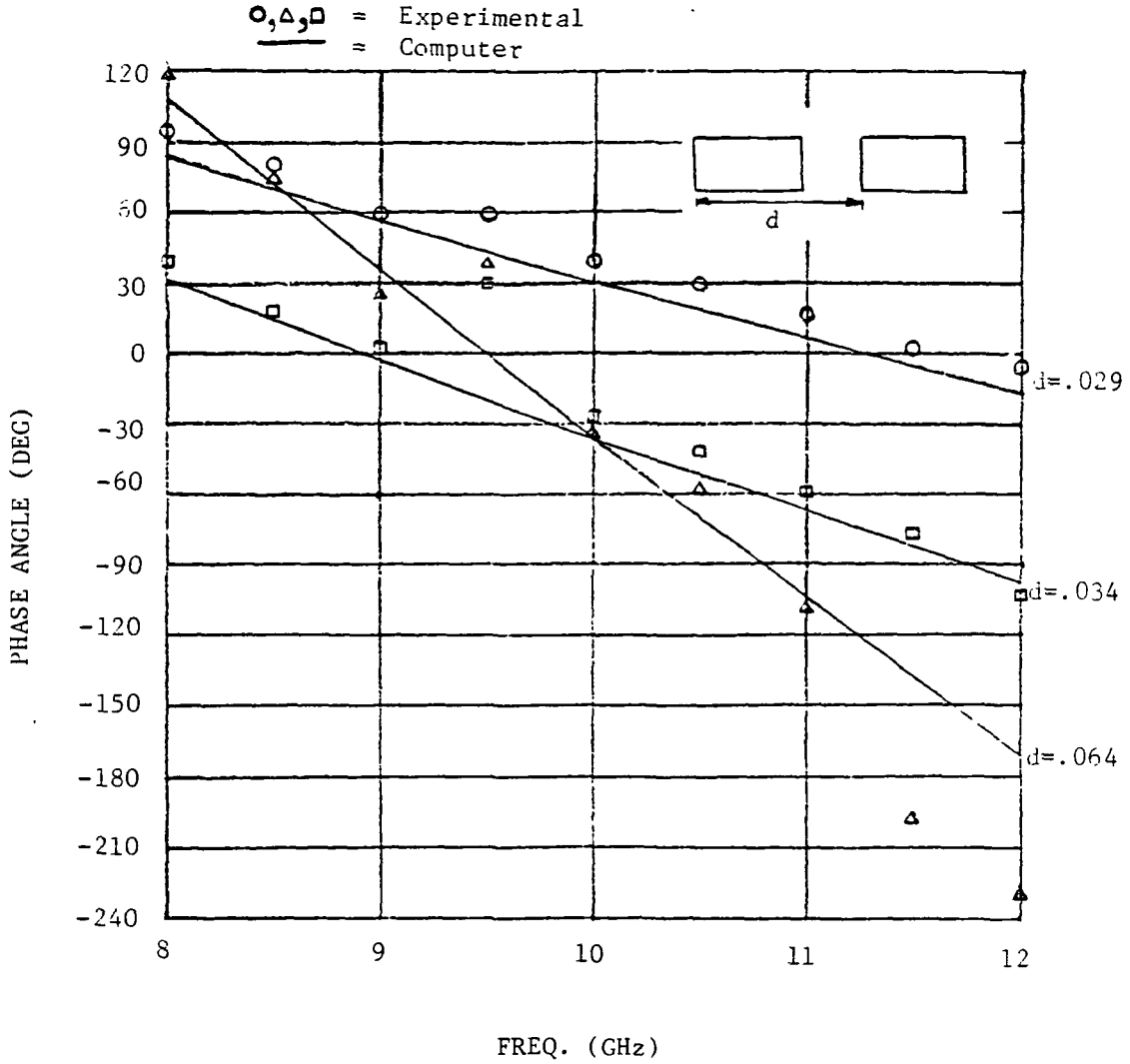

Figure 4.3 Experimental vs. Computer. S_{21} (d in Meters).

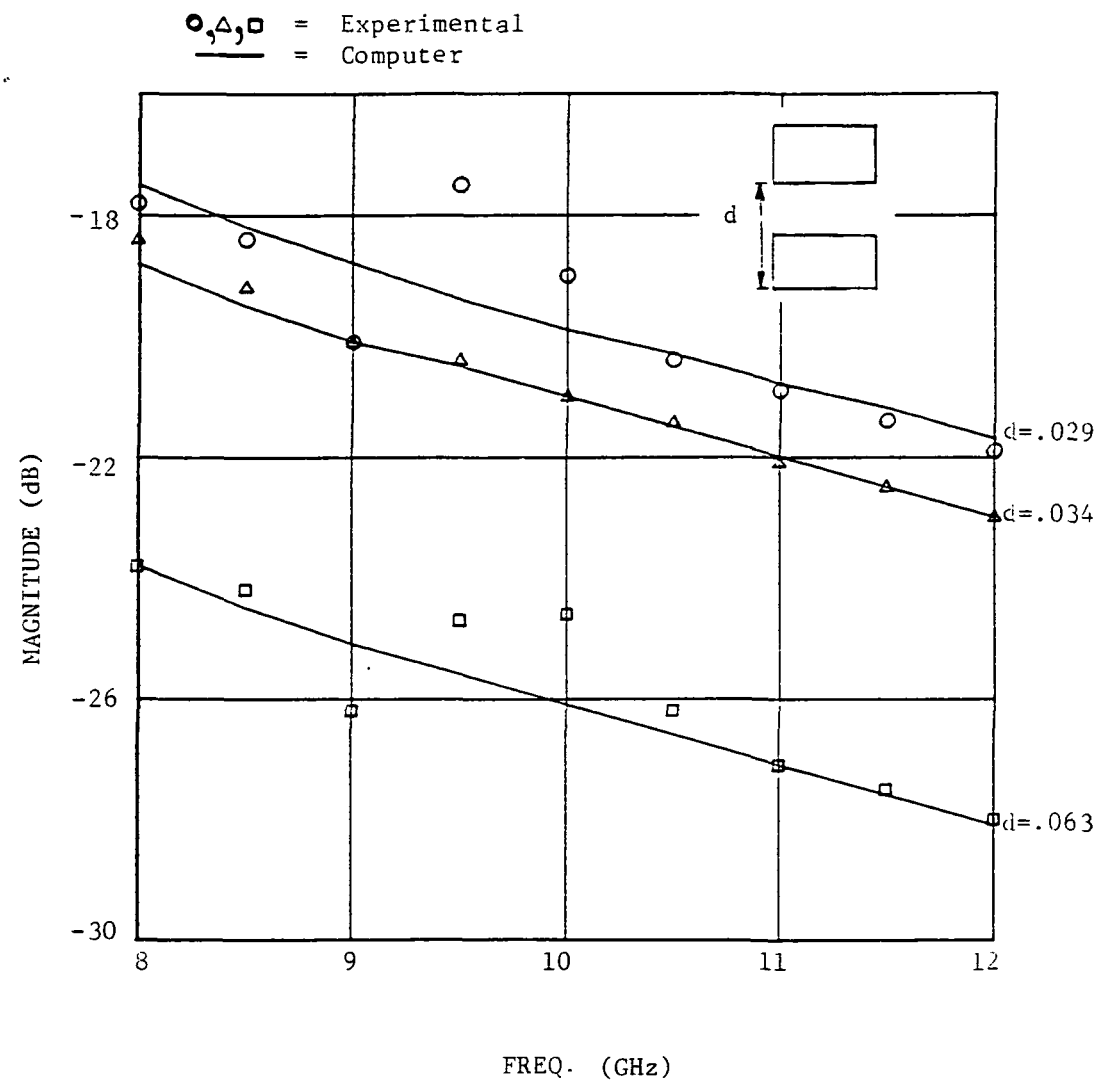

Figure 4.4 Experimental vs. Computer, S_{21} (d in Meters).

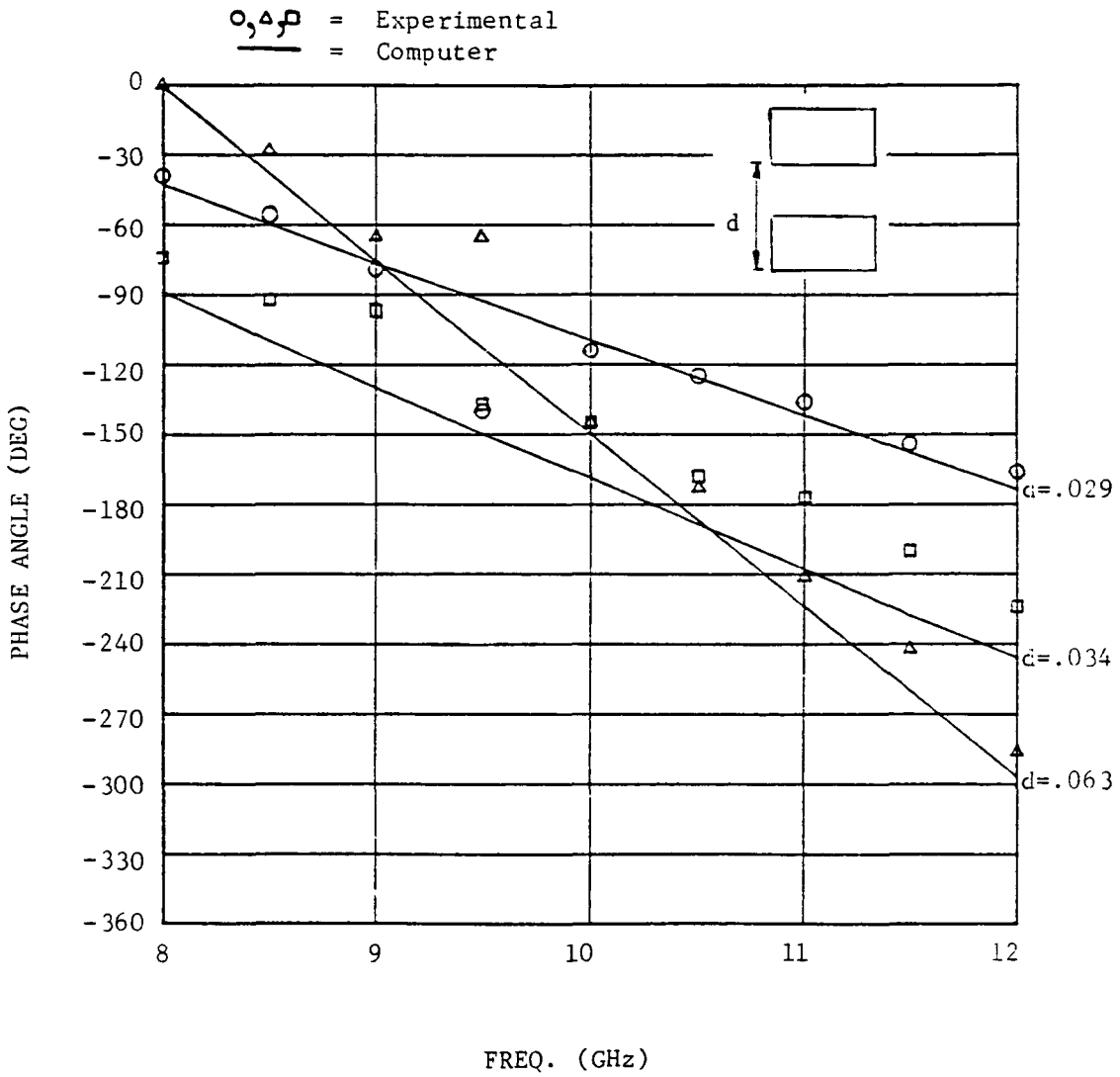

Figure 4.5 Experimental vs. Computer Results. S_{21} (d in Meters).

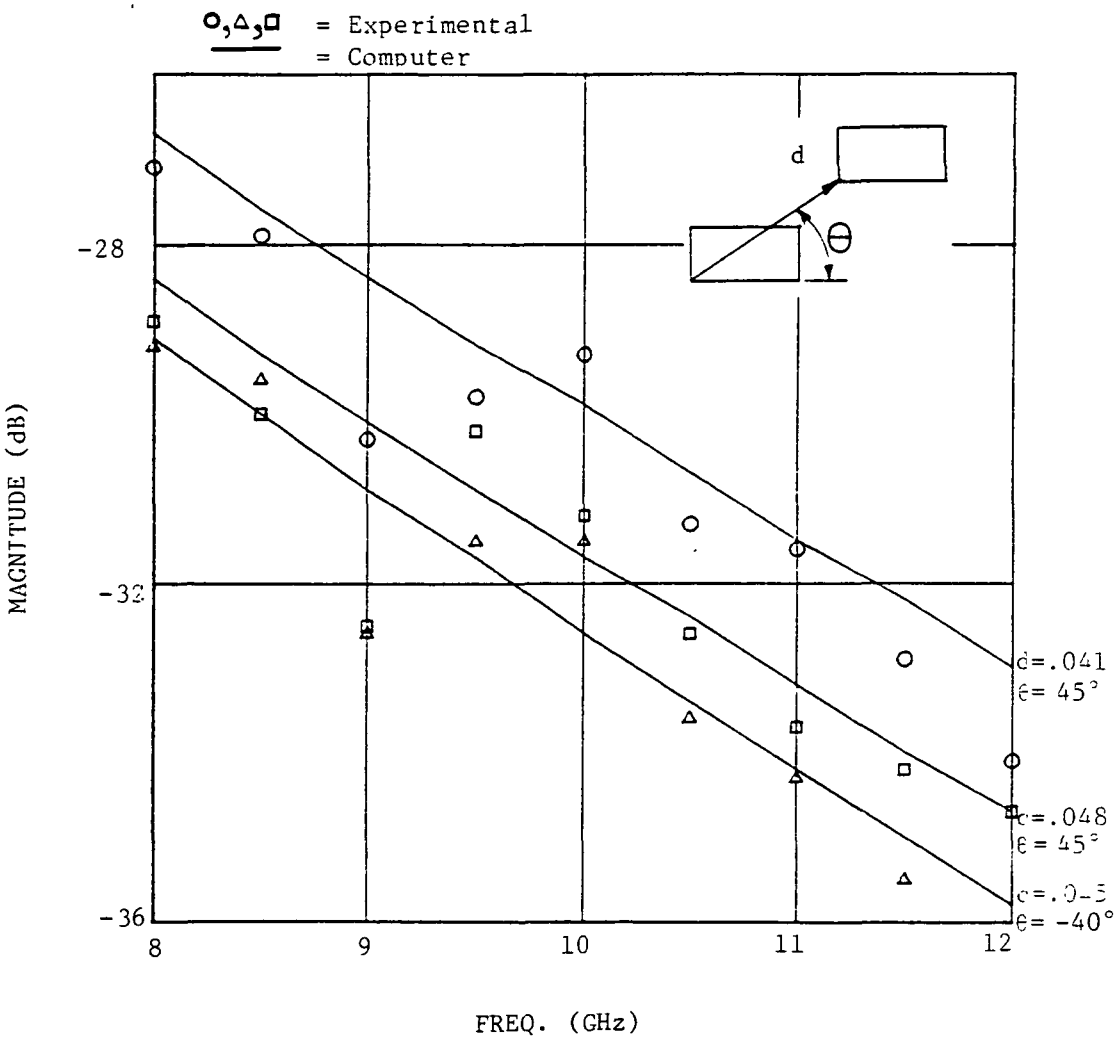

Figure 4.6 Experimental vs. Computer S_{21} (d in Meters).

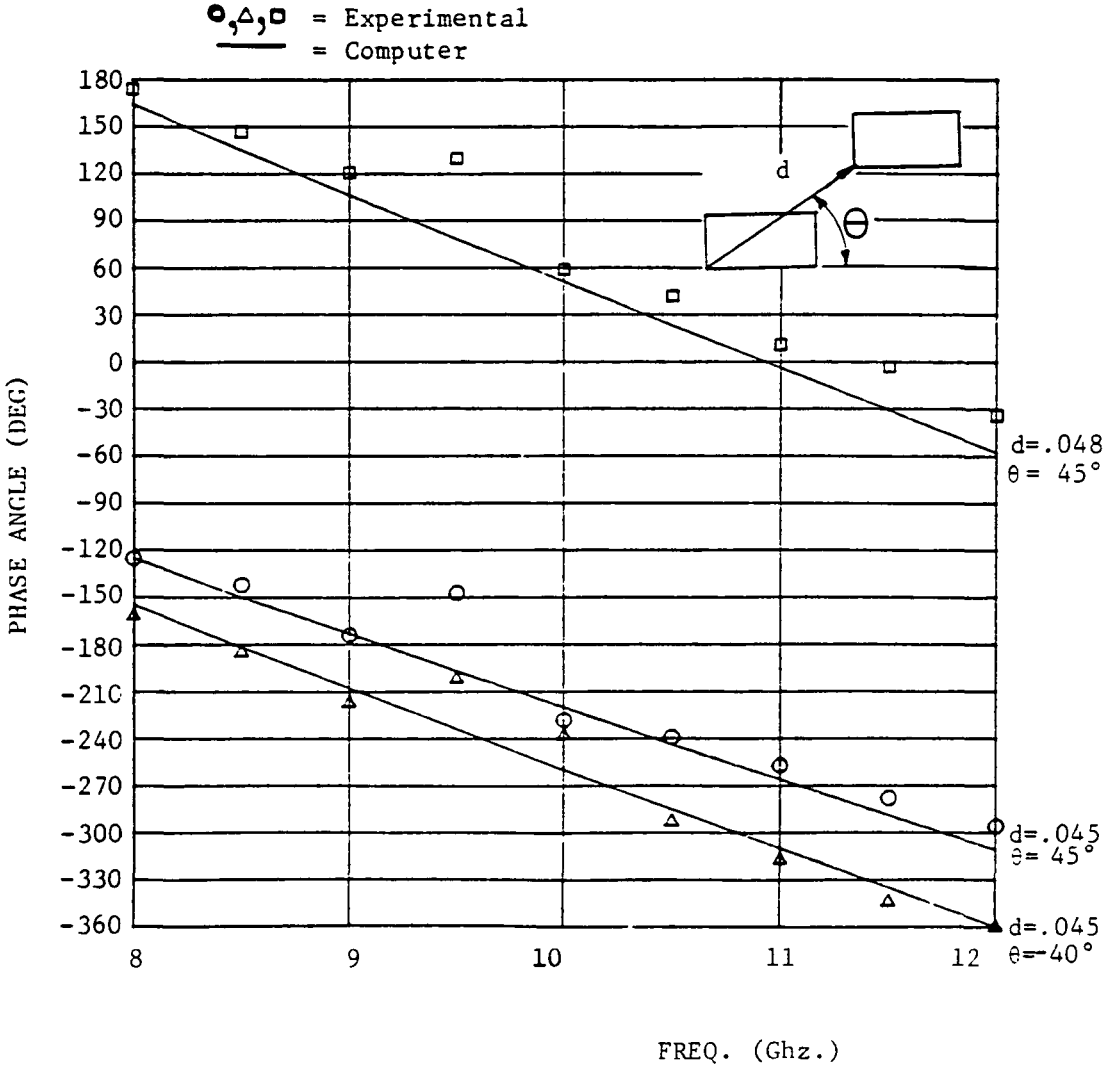

Figure 4.7 Experimental vs. Computer S_{21} (d in Meters).

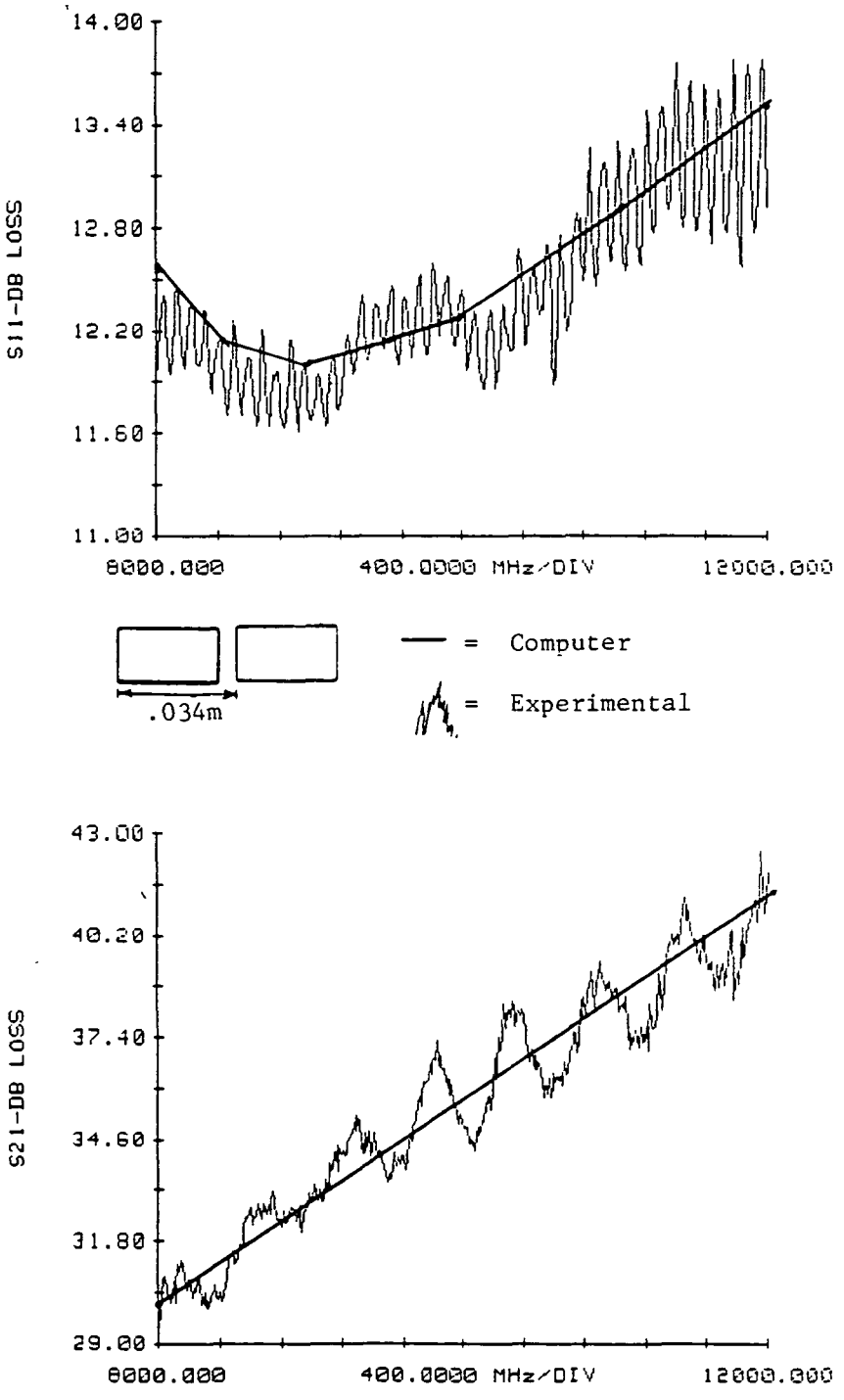

Figure 4.8 Experimental Results

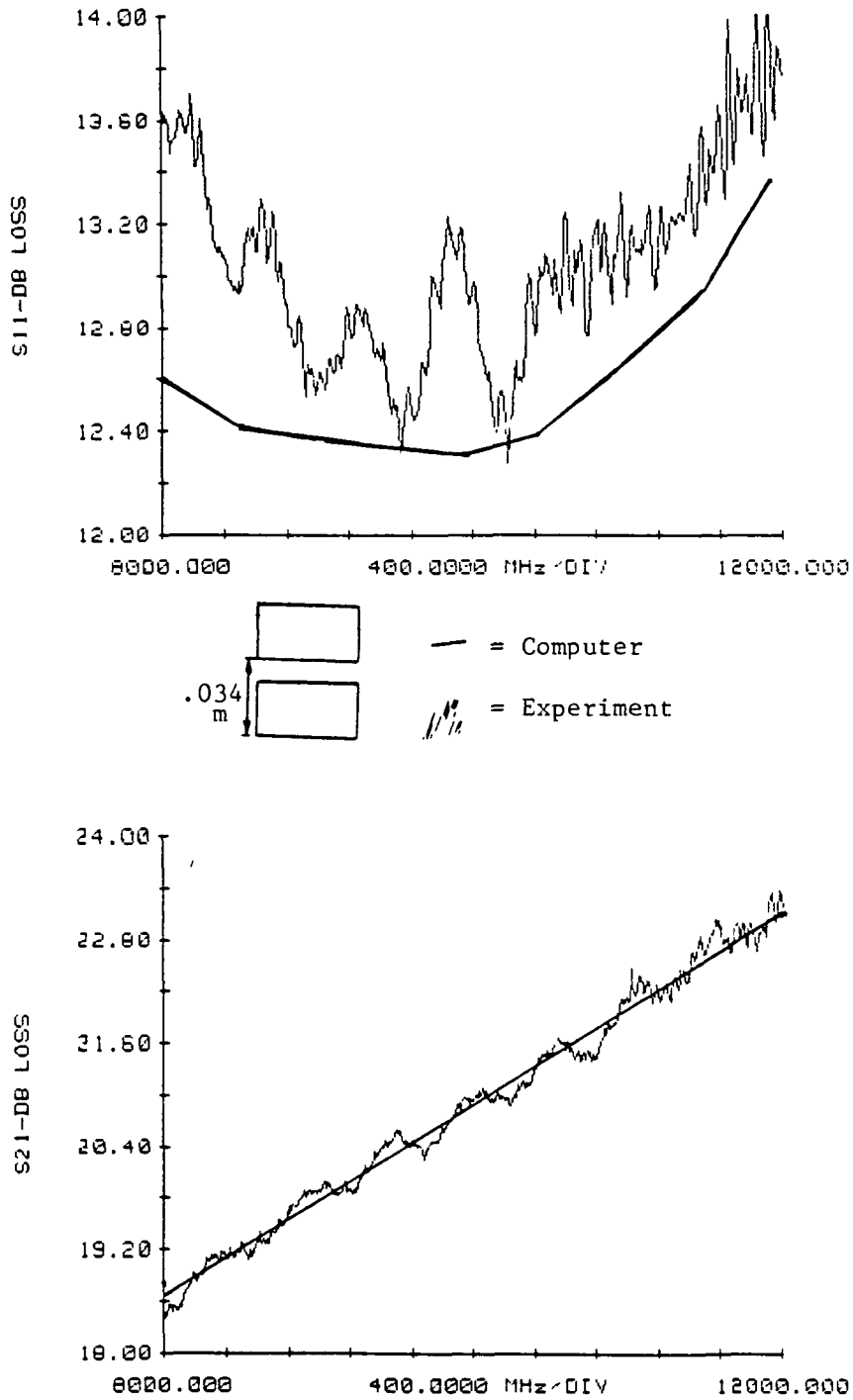

Figure 4.9 Experimental Results

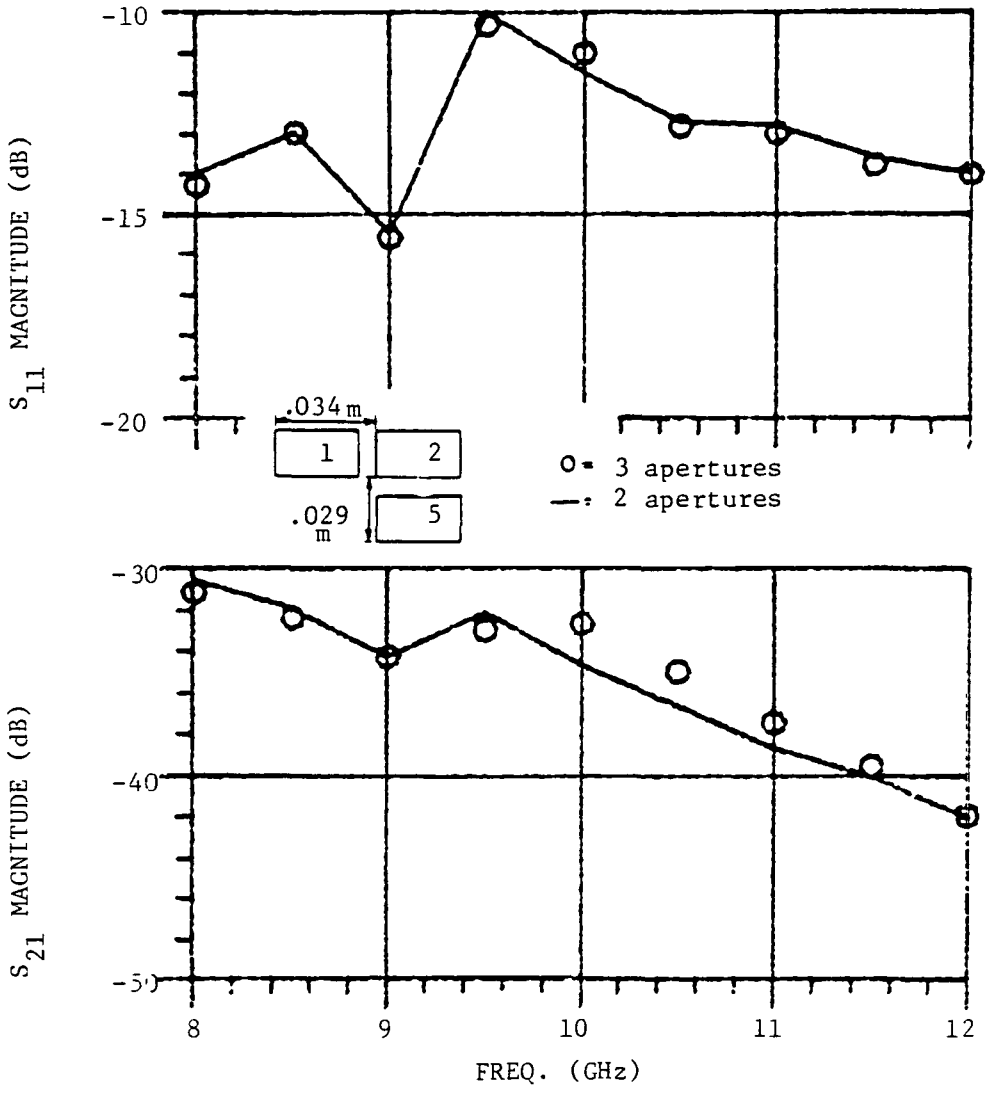

Figure 4.10 Comparisons of Results With and Without Third Aperture Present. (coupling is between 1 and 2)

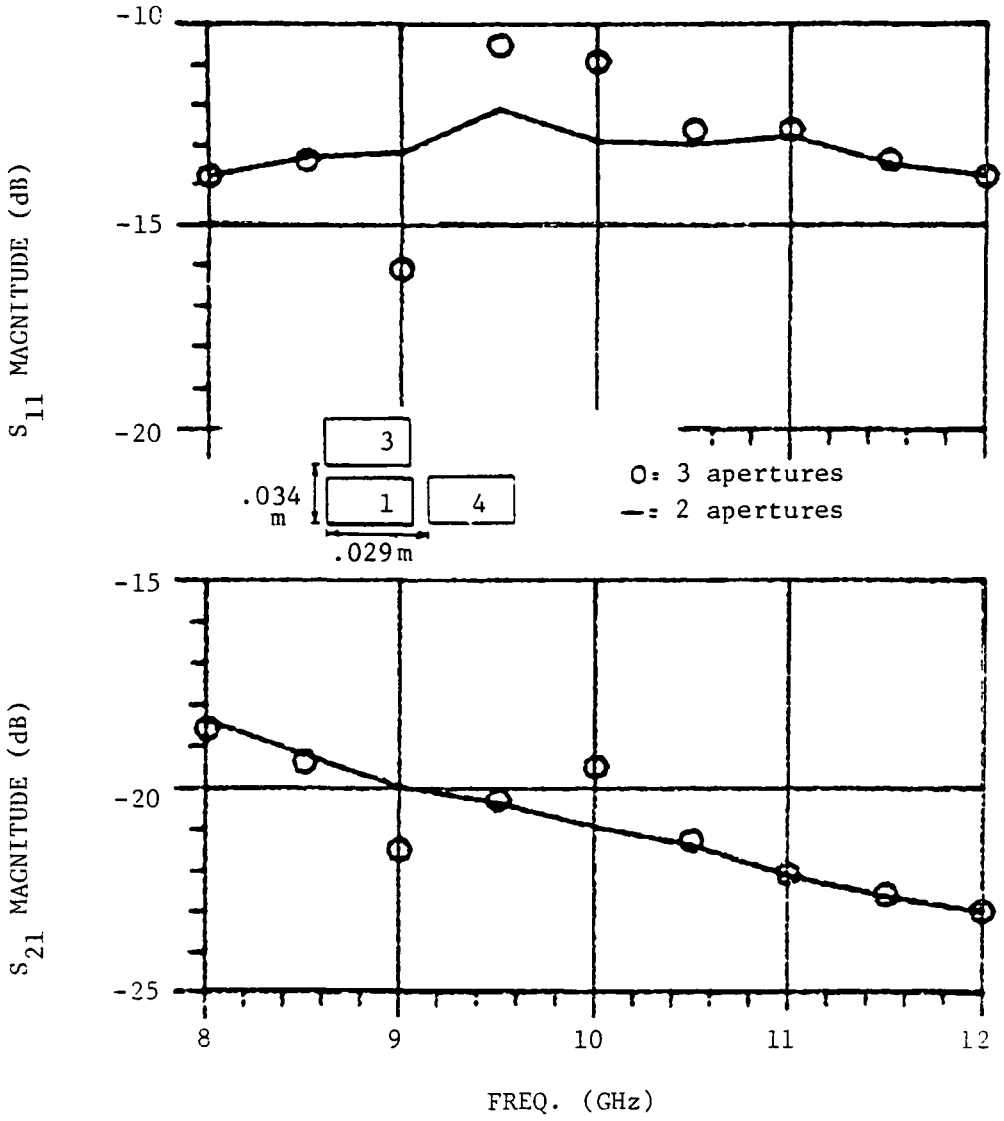

Figure 4.11 Comparisons of Results With and Without a Third Aperture Present. (Coupling is between 1 and 3)

CHAPTER 5

CONCLUSIONS AND RECOMMENDATIONS

5.1 Conclusion

The work described dealt with the analysis of mutual coupling in finite arrays of rectangular apertures. The analysis started with a discussion of the theoretical nature of the problem. It followed that with a look at the coupling effects in various arrays, which included comparisons against both published and experimental results. The conclusion to be drawn from this work is that the analysis and approximations used do in fact yield accurate results for the mutual coupling problem.

The various methods used to analyze the mutual coupling in arrays were discussed. From this discussion it was concluded that the vector potential approach was the best one to use for the type of array being analyzed. The required mathematical manipulations used in deriving the computer program are also included.

Using the computer programs, results were obtained for various sized arrays. The single element array data determined the best modal approximations to use. The two aperture case compared the computer data against published data. The other configurations looked at presented results that showed the effects of mutual coupling on larger arrays. It also looked at beam scanning in the three aperture antennas. Included with all this analysis was a considerable amount of data for testing the first order coupling theory. This data showed that the first order coupling theory could be used to approximate the coupling in arrays fairly accurately. It was included here for use in future

studies on antenna arrays in the hopes of reducing the computational time needed to solve large arrays.

Finally, in the last chapter the results from an experiment that was carried out was compared against computer derived data. While the experimental data was affected by system irregularities it did seem to show that the computer-derived results were correct.

5.2 Recommendations

Future study on the mutual coupling problem should:

1) include the non-matched source to waveguide case.
2) study arrays of circular apertures.
3) look at flared horns, both circular and rectangular.
4) consider the no-ground plane case.
5) look at possibly formulating a viable technique that uses the first order coupling.

The non-matched load case is one that can be easily included in the current computer model. If the waveguide is ℓ meters long and the guide to source interface has a known reflection coefficient (Γ), then to include it's affect a factor $(1 + \Gamma T e^{-j\beta_{10} 2\ell})$ must be multiplied by the Green's Function term for the TE_{10} part of the waveguide field (G_{xx} for nm = 10 in eqn. 2.36). In this factor, T is the total amplitude of the dominant mode excited in the guide due to reflection at the aperture and coupling from all the other guides. Once this has been done, tests could be run to see if the effect of this on the system results is large enough to warrant the inclusion of this type of mismatch in future studies.

The other problems are much more involved and would require con-

siderable amounts of work. The no-ground plane analysis should be conducted to determine if the affects of removing it are large enough to require that they be accounted for in antennas where the ground plane isn't present. If the effects are small enough, then the easier to solve infinite ground plane case could be used as an acceptable model. The circular aperture and flared horn elements in arrays should also be analyzed since these are also common array elements in use today. The final topic, the first order coupling theory, is one that needs further computer testing and much theoretical analysis before it can be considered complete. This analysis should be performed since it may lead to more efficient numerical procedures for analyzing mutual coupling effects in large arrays.

REFERENCES

Amitay, N., V. Galindo and C.P. Wu, Theory and Analysis of Phased Array Antennas, Wiley, New York, 1972.

Bailey, M.C., Near Field Coupling Between Elements of a Finite Planar Array of Circular Apertures, Ph.D. Thesis, Virginia Polytecnic Institute, Dec. 1972.

Borgiotti, V.V., "A Novel Expression for the Mutual Admittance of Planar Radiating Elements",IEEE Trans. on Ant. and Prop., Vol. AP-16, pp. 329-33, May, 1968.

Borgiotti, G.V., "Modal Analysis of Periodic Planar Phased Arrays of Apertures", Proceedings of the IEEE, Vol. 56, pp. 1881-1982, Nov. 1968.

Cha, A.C. and J.H. Hsiao, "A Matrix Formulation for Large Scale Numerical Computation of the Finite Planar Waveguide Array Problem", IEEE Trans. on Ant. and Prop., Vol. AP-22, pp. 106-108, Jan. 1974.

Cheney W. and D. Kincaid, Numerical Mathematics and Computing, Monterey, Brooks/Cole, Monterey, 1980.

Collin, R.E. Field Theory of Guided Waves, McGraw-Hill, New York, 1960.

Collin, R.E. and F.J. Zucker, Antenna Theory, Part I, McGraw-Hill, New York, 1969.

Fenn, A.J., G.A. Thiele and B.A. Munk, "Moment Method Analysis of Finite Rectangular Waveguide Phased Arrays", IEEE Trans. on Ant. and Prop., Vol. AP-30, pp. 554-564, July 1982.

Harrington, R.F., Time-Harmonic Electromagnetic Fields, McGraw-Hill, New York, 1961.

Harrington, R.F., Field Computations by Moment Methods , MacMillan, New York, 1968.

Harrington, R.F. and J.R. Mantz, "A General Network Formulation for Aperture Problems", IEEE Trans. on Ant. and Prop., Vol. AP-24, pp. 870-872, Nov. 1976.

Ludwig, A.C., "The Definition of Cross Polarization", IEEE Trans. on Ant. and Prop., Vol. AP-21, pp. 116-119, Jan. 1973.

Luzwick, J. and R.F. Harrington," Mutual Coupling Analysis in a Finite Planar Rectangular Waveguide Antenna Array", Electromagnetics, Vol. 2, pp. 25-42, Jan.-Mar. 1982.

Mailloux, R.J., "Radiation and Near-Field Coupling Between Two Co-linear Open Ended Waveguides", IEEE Trans. and Prop., Vol. AP-17. pp. 49-55, Jan. 1969.

Mailloux. R.J. , "First Order Solutions for Mutual Coupling Between Waveguides Which Propagate Two Orthogonal Modes", IEEE Trans. on Ant. and Prop., Vol. AP-17, pp. 740-746, Nov. 1969.

Steyskal, H., "Mutual Coupling Analysis of a Finite Planar Waveguide Array, IEEE Trans. on Ant. and Prop., Vol. AP-22, pp. 594-597, July 1974.

Stutzman, W.L. and G.A. Thiele, Antenna Theory and Design, John Wiley and Sons, New York, 1981.

APPENDIX A

PROGRAM LISTING

```
C       SOLUTION OF MUTUAL COUPLING IN ANTENNA ARRAYS
C       OF RECTANGULAR APERTURES.  MATRIX OF 360X360
C       ALLOWED.
        REAL A,B,LA,LAM,PI,E0,TP,E,REM,WA(180),IER,RP,DX,DY,K,IM
        REAL D,EF,S,DXP(180),DYP(180),DT,LB,DEL1,DEL2
        REAL X(91),Y2(91),Y3(91),MX1,MX2,RT(360,4),MX3,MX4
        REAL PP(180),PHR,ID,PR,PHG,D3,Y4(91),Y5(91)
        REAL Y11(91),Y12(91),Y13(91),Y14(91),MXT
        COMPLEX BT,BETA,DBLINT,Z1,Z2,Z3,Z4,Y1,H1,H2,I1,I2,I3,I4
        COMPLEX I5,I6,C,G,EM1,EM2,JMX,JMY,EM3,EM4,RC,V1,NORM1,V15
        COMPLEX*16 AM(360,360),V(360),NV(360,360),VI(360)
        CHARACTER*1 ANS,TEST,TEST2
        INTEGER CM(6,2),P,Q,N,M,ND,NA,NC,NT,NR,NAP,VP(180),RTP
        EXTERNAL TP,Y1,H1,H2,I1,I2,I3,I4,I5,I6,RP,G
        COMMON P,Q,N,M,A,B,K,E,D,DX,DY
C       SET UP NV AS AN IDENTITY MATRIX
        DO 10 M19=1,60
          NV(M19,M19)=(1.0,0)
10      CONTINUE
20      FORMAT (A1)
30      FORMAT (1X,'REFLECT COEFF OF GUIDE#',1X,I2,1X,'IS:')
40      FORMAT (2X,'INPUT THE # OF APP. IN ROW#',2X,I2,2X,
        1 'AND THE ROW OFFSET')
C       SET UP THE NEEDED CONSTANTS
        TYPE*,'SOLVES MULTI-APPERTURE PROBLEM '
        TYPE*,' USING THE VECTOR POTENTIAL APPROACH'
        TYPE*,'INPUT THE # PSI AND PHI FUNCTIONS'
        ACCEPT*,NC,ND
        NT=NC+ND
        RTP=0
        DO 50 J22=1,NC
          TYPE*,'INPUT THE',J22,'PSI COEFF.:'
          ACCEPT*,CM(J22,1),CM(J22,2)
50      CONTINUE
        DO 60 J23=1,ND
          TYPE*,'INPUT THE',J23,'PHI COEFF.:'
          ACCEPT*,CM(NC+J23,1),CM(NC+J23,2)
60      CONTINUE
        TYPE*,'INPUT A/LAMBDA ,B/LAMBDA AND LAMBDA'
        ACCEPT*,LA,LB,LAM
C       CM=THE PHI &PSI COEFFS  ND=#PHI  NC=#PSI  NT=TOTAL#
        A=LA*LAM
        B=LB*LAM
        TEST='Y'
        PI=3.1415926
        E0=8.854E-12
        AL=(A*.001)**2
        K=2*PI/LAM
        REM=4.0*(B*LOG((A+SQRT(A**2+B**2))/B)+A*LOG((B+SQRT(A**2
        1 +B**2))/A))
        NA=0
        TYPE*,'ALL SPACINGS ARE TO BE GIVEN IN FRACTIONS OF LAMBDA'
        TYPE*,'INPUT THE # OF ROWS AND SPACING BETWEEN THE ROWS'
        ACCEPT*,NR,DEL1
        TYPE*,'INPUT THE SPACING BETWEEN ELEMENTS WITHIN A ROW'
        ACCEPT*,DT
        DT=DT*LAM
C       NR=#ROWS  DT=ELEMENT SPACING   DEL1=ROW SPACING
        NAPE=0
        TYPE*,'REGULAR LATTICE ARRAY? (Y/N)'
        ACCEPT20,TEST2
        IF (TEST2.EQ.'Y') THEN
          TYPE*,'INPUT THE EVEN ROWS # OF GUIDES & ROW OFFSET'
          ACCEPT*,NAPE,DEL2E
          TYPE*,'INPUT THE ODD ROWS # OF GUIDES & ROW OFFSET'
          ACCEPT*,NAPO,DEL2O
          DO 90 J50=1,NR
            IF (MOD(J50,2).EQ.0) THEN
              DO 70 J55=1,NAPE
                DXP(J55+NA)=(J55-1)*DT+DEL2E*LAM
                DYP(J55+NA)=(J50-1)*LAM*DEL1
70            CONTINUE
              NA=NA+NAPE
            ELSE
C         NAPE,DEL2E=#&SPACING IN EVEN ROWS   NAPO,DEL2O=ODD ROWS
              DO 80 J60=1,NAPO
                DXP(J60+NA)=(J60-1)*DT+DEL2O*LAM
                DYP(J60+NA)=(J50-1)*LAM*DEL1
80            CONTINUE
              NA=NA+NAPO
            END IF
```

```
 820    90         CONTINUE
 830             ELSE
 840               DO 110 J30=1,NR
 850                 TYPE40,J30
 860                 ACCEPT*,NAP,DEL2
 870                 DO 100 J31=1,NAP
 880                   DXP(NA+J31)=DEL2*LAM+DT*(J31-1)
 890                   DYP(NA+J31)=DEL1*LAM*(J30-1)
 900    100          CONTINUE
 910                 NA=NA+NAP
 920    C        NA=TOTAL# APERTURES
 930    110        CONTINUE
 940             END IF
 950             DO 120 J75=1,NA
 960               TYPE*,'DX,DY',J75,DXP(J75),DYP(J75)
 970    120      CONTINUE
 980    C        THE APPERTURE ROWS
 990             DO 310 K1=1,NA
1000    C        THE APPERTURE COLUMNS
1010               DO 300 K2=K1,NA
1020                 IF (K1.EQ.K2) THEN
1030                   IF (K1.EQ.1) THEN
1040                     DO 150 J=1,NC
1050                       P=CM(J,1)
1060                       Q=CM(J,2)
1070    C        THE COLUMNS WITH PSI@S
1080                       DO 130 J1=1,NC
1090                         N=CM(J1,1)
1100                         M=CM(J1,2)
1110                         E=EF(P,Q,N,M)
1120                         BETA=BT(N)
1130                         D=1.0
1140                         Z3=(0,-1.0)*(K**2-(N*PI/A)**2)/BETA
1150                         Z1=DBLINT(0,A,0,B,Y1)
1160                         Z2=DBLINT(0,A,0,B,H1)
1170                         Z2=Z2*P*E/(2*A*A)
1180                         IF (P.EQ.N .AND. Q.EQ.M) THEN
1190                           Z1=(K**2-(P*PI/A)**2)*(Z1+REM)/(2*PI)+Z3
1200                         ELSE
1210                           Z1=Z1*(K**2-(P*PI/A)**2)/(2*PI)
1220                         END IF
1230                         AM(J,J1)=Z1+Z2
1240    130                CONTINUE
1250    C        THE PHI COLUMNS
1260                       DO 140 K4=1,ND
1270                         N=CM(NC+K4,1)
1280                         M=CM(NC+K4,2)
1290                         E=EF(P,Q,N,M)
1300                         D=-1.0
1310                         BETA=BT(N)
1320                         Z1=DBLINT(0,A,0,B,Y1)
1330                         Z3=(0,1.0)*N*M*PI**2/(BETA*A*B)
1340                         IF (P.EQ.N .AND. Q.EQ.M) THEN
1350                           Z1=(-P*Q*PI/(2*A*B))*(Z1+REM)+Z3
1360                         ELSE
1370                           Z1=-P*Q*PI*Z1/(2*A*B)
1380                         END IF
1390                         Z2=DBLINT(0,A,0,B,H2)
1400                         Z2=E*P*Z2/(2*A*B)
1410                         AM(J,NC+K4)=Z1+Z2
1420    140                CONTINUE
1430    150              CONTINUE
1440    C        THE PHI TESTING FUNCTION ROWS
1450                     DO 180 K8=1,ND
1460                       P=CM(NC+K8,1)
1470                       Q=CM(NC+K8,2)
1480    C        THE Y Y1,X1 TERMS
1490                       DO 160 J3=1,NC
1500                         D=1.0
1510                         N=CM(J3,1)
1520                         M=CM(J3,2)
1530                         E=EF(P,Q,N,M)
1540                         BETA=BT(N)
1550                         Z3=(0,1.0)*N*M*PI**2/(A*B*BETA)
1560                         Z1=DBLINT(0,A,0,B,Y1)
1570                         IF(P.EQ.N .AND. Q.EQ.M) THEN
1580                           Z1=(-P*Q*PI/(2*A*B))*(Z1+REM)+Z3
1590                         ELSE
1600                           Z1=(-P*Q*PI/(2*A*B))*Z1
1610                         END IF
1620                         Z2=DBLINT(0,A,0,B,H1)
```

```
1630                          Z2=Z2*E*Q/(A*B*2)
1640                          AM(NC+K8,J3)=Z1+Z2
1650    160                 CONTINUE
1660    C         THE I Y1,Y1 TERMS
1670                        DO 170 K9=1,ND
1680                          N=CM(NC+K9,1)
1690                          M=CM(NC+K9,2)
1700                          D=-1.0
1710                          E=EF(P,Q,N,M)
1720                          BETA=BT(N)
1730                          Z3=(0,-1.0)*(K**2-(M*PI/B)**2)/BETA
1740                          Z1=DBLINT(0,A,0,B,Y1)
1750                          IF (M.EQ.Q .AND. P.EQ.N) THEN
1760                            Z1=(K**2-(Q*PI/B)**2)*(Z1+REM)/(2*PI)+Z3
1770                          ELSE
1780                            Z1=(K**2-(Q*PI/B)**2)*Z1/(2*PI)
1790                          END IF
1800                          Z2=DBLINT(0,A,0,B,H2)
1810                          Z2=Z2*E*Q/(2*B*B)
1820                          AM(NC+K8,NC+K9)=Z1+Z2
1830    170                 CONTINUE
1840    180               CONTINUE
1850                    ELSE
1860                      DO 200 K5=1,NT
1870                        DO 190 K6=1,NT
1880                          AM(K5+(K1-1)*NT,K6+(K1-1)*NT)=AM(K5,K6)
1890    190                 CONTINUE
1900    200               CONTINUE
1910                    END IF
1920                  ELSE
1930    C         FIND NEXT DX,DY AND IF ALREADY SOLVED FOR LOAD IN AND CONTINUE
1940                    DX=DXP(K2)-DXP(K1)
1950                    DY=DYP(K2)-DYP(K1)
1960                    OPT=0
1970                    DO 230 J19=1,RTP
1980                      IF (ABS(DX-RT(J19,1)).LT..00001 .AND.
1990          1 ABS(DY-RT(J19,2)).LT..00001) THEN
2000                        DO 220 J59=1,NT
2010                          DO 210 J60=1,NT
2020                            AM((K1-1)*NT+J59,(K2-1)*NT+J60)=AM((RT(J19,3)-1)
2030          1 *NT+J59, (RT(J19,4)-1)*NT+J60)
2040                            AM((K2-1)*NT+J59,(K1-1)*NT+J60)=AM((K1-1)*NT+J59,
2050          1 (K2-1)*NT+J60)
2060    210                   CONTINUE
2070    220                 CONTINUE
2080                        OPT=1.0
2090                      END IF
2100    230               CONTINUE
2110    C         IF NEW DX,DY SOLVE FOR COUPLING VALUES
2120                    IF (OPT.EQ.0) THEN
2130                      IF (RTP.LT.180) THEN
2140                        RTP=RTP+1
2150                        RT(RTP,1)=(DX)
2160                        RT(RTP,2)=(DY)
2170                        RT(RTP,3)=K1
2180                        RT(RTP,4)=K2
2190                      END IF
2200    C         THE ROW #S
2210                      DO 260 J6=1,NC
2220                        P=CM(J6,1)
2230                        Q=CM(J6,2)
2240    C         THE COLUMN #S
2250                        DO 240 J16=1,NC
2260                          N=CM(J16,1)
2270                          M=CM(J16,2)
2280    C          Y X1,X2
2290                          E=EF(P,Q,N,M)
2300                          Z1=DBLINT(-A,A,-B,B,I1)*(K**2-(P*PI/A)**2)
2310                          Z2=DBLINT(0,A,-B,B,I3)
2320                          AM((K1-1)*NT+J6,(K2-1)*NT+J16)=(Z1+Z2)*E
2330                          AM((K2-1)*NT+J6,(K1-1)*NT+J16)=(Z1+Z2)*E
2340    240                 CONTINUE
2350    C         Y X1,Y2
2360                        DO 250 J26=1,ND
2370                          N=CM(J26+NC,1)
2380                          M=CM(J26+NC,2)
2390                          E=EF(P,Q,N,M)
2400                          Z1=(DBLINT(-A,A,-B,B,I2))*(-P*Q*PI**2)/(A*B)
2410                          Z2=DBLINT(-A,A,0,B,I4)
2420                          AM((K1-1)*NT+J6,(K2-1)*NT+J26+NC)=(Z1+Z2)*E
2430                          AM((K2-1)*NT+J6,(K1-1)*NT+J26+NC)=(Z1+Z2)*E
```

```
2440    250               CONTINUE
2450    260             CONTINUE
2460                    DO 290 L2=1,ND
2470                      P=CM(L2+NC,1)
2480                      Q=CM(L2+NC,2)
2490    C       Y Y1,X2
2500                      DO 270 L3=1,NC
2510                        N=CM(L3,1)
2520                        M=CM(L3,2)
2530                        E=EF(P,Q,N,M)
2540                        Z1=(DBLINT(-A,A,-B,B,I1))*(-P*Q*PI**2)/(A*B)
2550                        Z2=DBLINT(0,A,-B,B,I5)
2560                        AM((K1-1)*NT+L2+NC,(K2-1)*NT+L3)=(Z1+Z2)*E
2570                        AM((K2-1)*NT+L2+NC,(K1-1)*NT+L3)=(Z1+Z2)*E
2580    270               CONTINUE
2590    C       Y Y1,Y2
2600                      DO 280 L4=1,ND
2610                        N=CM(NC+L4,1)
2620                        M=CM(NC+L4,2)
2630                        E=EF(P,Q,N,M)
2640                        Z1=(DBLINT(-A,A,-B,B,I2))*(K**2-(Q*PI/B)**2)
2650                        Z2=DBLINT(-A,A,0,B,I6)
2660                        AM((K1-1)*NT+L2+NC,(K2-1)*NT+NC+L4)=E*(Z1+Z2)
2670                        AM((K2-1)*NT+L2+NC,(K1-1)*NT+NC+L4)=E*(Z1+Z2)
2680    280               CONTINUE
2690    290             CONTINUE
2700                  END IF
2710                END IF
2720    300         CONTINUE
2730    310       CONTINUE
2740    C         MATRIX IS FULL
2750              NZ=NT*NA
2760    C         NZ=TOTAL # MODES IN ARRAY
2770              TYPE*,'PRINT MATRIX? (Y/N)'
2780              ACCEPT20,TEST2
2790              IF (TEST2.EQ.'Y') THEN
2800                DO 320 J26=1,NZ
2810                  DO 320 J27=1,NZ
2820                    TYPE*,'MATRIX',J26,J27,AM(J26,J27)
2830    320         CONTINUE
2840              END IF
2850    C         FIND THE INVERSE OF THE MATRIX AND CLR V & VI
2860              CALL LEQT1C(AM,NZ,360,NV,NZ,360,0,WA,IER)
2870    330       DO 340 J25=1,NZ
2880                V(J25)=(0,0)
2890                VI(J25)=(0,0)
2900    340       CONTINUE
2910    C         INPUT THE # OF DRIVEN ARRAYS, IF EQUALS TOTAL # OF APERTURES
2920    C         THEN ALLOW FOR EASE OF ENTRY OF PHASE SHIFTS
2930              TYPE*,'INPUT THE # OF DRIVEN GUIDES'
2940              ACCEPT*,NDM
2950              ID=(2.*((PI/A)**2-K**2)/E0)
2960              D3=0
2970              IF (NDM.EQ.NA) THEN
2980                TYPE*,'CONSTANT PHASE FOR EACH? (Y/N)'
2990                ACCEPT20,TEST2
3000                IF (TEST2.EQ.'Y') THEN
3010                  DO 350 L7=1,NA
3020                    VI((L7-1)*NT+1)=ID
3030    350             CONTINUE
3040                    D3=1.
3050                ELSE
3060                  IF (NAPE.NE.0) THEN
3070                    TYPE*,'INPUT THE PHASE SHIFT BETWEEN ELEMENTS IN A ROW'
3080                    ACCEPT*,PHG
3090                    TYPE*,'INPUT THE PHASE SHIFT BETWEEN ROWS'
3100                    ACCEPT*,PHR
3110                    NPH=0
3120                    D3=1.
3130                    DO 360 L71=1,NR
3140                      PR=(L71-1)*PHR*PI/180
3150                      IF (MOD(L71,2).EQ.0) THEN
3160                        DO 360 L72=1,NAPE
3170                          L100=NPH+1+(L72-1)*NT
3180                          VI(L100)=ID*CEXP((0,1.)*(PR+(PHG*PI/180)*(L72-1)))
3190    360                   CONTINUE
3200                          NPH=NPH+NAPE*NT
3210                      ELSE
3220                        DO 370 L73=1,NAPO
3230                          L110=NPH+1+(L73-1)*NT
3240                          VI(L110)=ID*CEXP((0,1.)*(PR+(PHG*PI/180)*(L73-1)))
```

```
3250    370               CONTINUE
3260                      NPH=NPH+NAPO*NT
3270                    END IF
3280    380           CONTINUE
3290                ENDIF
3300              END IF
3310            END IF
3320    C       IF ALL NOT DRIVEN THEN INPUT # AND PHASE OF EACH DRIVEN GUIDE
3330            IF (D3.EQ.0) THEN
3340              TYPE*,'INPUT THE GUIDE #@S THAT ARE DRIVEN &IT@S PHASE(DEG)'
3350              DO 390 L6=1,NDM
3360                ACCEPT*,VP(L6),PP(L6)
3370    390         CONTINUE
3380              TYPE*,'WILL ASSUME 1&10 MODE IN EACH'
3390              DO 400 L8=1,NDM
3400                VI((VP(L8)-1)*NT+1)=ID*CEXP((0,1.0)*(PP(L8)*PI/180.))
3410    400         CONTINUE
3420            END IF
3430            TYPE*,'PRINT COLUMN  MATRIX? (Y/N)'
3440            ACCEPT20,TEST
3450            IF (TEST.EQ.'Y') THEN
3460              DO 410 J50=1,NT*NA
3470                TYPE*,'VI:',VI(J50)
3480    410         CONTINUE
3490              NZ=NT*NA
3500            END IF
3510    C       USING THE RESULTS AND THE INVERTED MATRIX
3520    C       SOLVE FOR V
3530            DO 430 L20=1,NZ
3540              DO 420 L21=1,NZ
3550                V(L20)=V(L20)+NV(L20,L21)*VI(L21)
3560    420         CONTINUE
3570    430       CONTINUE
3580            NORM1=(0,1.)*E0/SQRT(K**2-(PI/A)**2)
3590            TYPE*,'THE NORMALIZED OUTPUT VECTOR IS:'
3600            DO 440 L15=1,NZ
3610              V15=V(L15)*NORM1
3620              TYPE*,'V(',L15,')=',V15,',',SQRT(REAL(V15)**2+AIMAG(V15)**2),
3630            1 ATAN(AIMAG(V15)/REAL(V15))*180/PI
3640    440       CONTINUE
3650            D5=0
3660            MX1=0
3670            MX2=0
3680            MX3=0
3690            MX4=0
3700    C       CALCULATE THE VALUES OF THE PATTERNS,0 & 90 DEG.
3710    C       THIS DOESN'T WORK FOR A 01 MODE!!!!!!!!!!
3720            DO 490 M10=1,91
3730              TH=PI*((M10-1)*2-90)/180
3740              EM1=0
3750              EM2=0
3760              EM3=0
3770              EM4=0
3780              DO 460 M11=1,NA
3790                DO 450 M12=1,NC
3800                  EM1=EM1-JMX(TH,PI/2,CM(M12,1),CM(M12,2))*V((M11-1)*NT
3810            1 +M12)*CEXP((0,1.0)*K*SIN(TH)*DYP(M11))
3820                  EM2=EM2-JMX(TH,0,CM(M12,1),CM(M12,2))*V((M11-1)*NT+M12)
3830            1 *CEXP((0,1.0)*K*SIN(TH)*DXP(M11))*COS(TH)
3840    C       E/CO 45 DEG.
3850                  EM3=EM3-JMX(TH,PI/4,CM(M12,1),CM(M12,2))*V((M11-1)*NT
3860            1 +M12)*(CEXP((0,1.)*K*SIN(TH)*(DYP(M11)+DXP(M11))/
3870            2 SQRT(2.)))*(1+COS(TH))/2.
3880                  EM4=EM4+JMX(TH,PI/4,CM(M12,1),CM(M12,2))*V((M11-1)*NT
3890            1 +M12)*(CEXP((0,1.)*K*SIN(TH)*(DYP(M11)+DXP(M11))/
3900            2 SQRT(2.)))*(COS(TH)-1)/2.
3910    C       THIS WAS THE E/CROSS 45 DEG.
3920    450           CONTINUE
3930    460         CONTINUE
3940                DO 480 M21=1,NA
3950                  DO 470 M22=NC+1,NT
3960                    EM3=EM3+JMY(TH,PI/4,CM(M22,1),CM(M22,2))*V((M21-1)*NT
3970            1 +M22)*(CEXP((0,1.)*K*SIN(TH)*(DYP(M21)+DXP(M21))/
3980            2 SQRT(2.)))*(1-COS(TH))/2.
3990                    EM4=EM4+JMY(TH,PI/4,CM(M22,1),CM(M22,2))*V((M21-1)*NT
4000            1 +M22)*(CEXP((0,1.)*K*SIN(TH)*(DYP(M21)+DXP(M21))/
4010            2 SQRT(2.)))*(1+COS(TH))/2.
4020    470           CONTINUE
4030    480         CONTINUE
4040                Y2(M10)=SQRT((REAL(EM1))**2+(AIMAG(EM1))**2)
4050                Y3(M10)=SQRT((REAL(EM2))**2+(AIMAG(EM2))**2)
```

```
4060              Y4(M10)=SQRT((REAL(EM3))**2+(AIMAG(EM3))**2)
4070              Y5(M10)=SQRT((REAL(EM4))**2+(AIMAG(EM4))**2)
4080              X(M10)=(M10-1)*2-90
4090              IF (MX1.LT.Y2(M10)) MX1=Y2(M10)
4100              IF (MX2.LT.Y3(M10)) MX2=Y3(M10)
4110              IF(MX3.LT.Y4(M10)) MX3=Y4(M10)
4120              IF (MX4.LT.Y5(M10)) MX4=Y5(M10)
4130     490      CONTINUE
4140              TYPE*,'PLOT? (Y/N)'
4150              ACCEPT20,ANS
4160              MXT=MX2
4170              IF (MX1.GT.MX2) MXT=MX1
4180              DO 500 M15=1,91
4190                Y2(M15)=DBCON(Y2(M15),MXT)
4200                Y3(M15)=DBCON(Y3(M15),MXT)
4210                Y4(M15)=DBCON(Y4(M15),MXT)
4220                Y5(M15)=DBCON(Y5(M15),MXT)
4230     500      CONTINUE
4240     CCC      CALL AG2(X,Y2,91,0)
4250     C        PLOT THE PATERNS:
4260              IF (ANS.EQ.'Y') THEN
4270     C        PLOT THE 4 PATTERNS:
4280                CALL PLOT(X,Y2)
4290                CALL PLOT(X,Y3)
4300                CALL PLOT(X,Y4)
4310                CALL PLOT(X,Y5)
4320              END IF
4330              TYPE*,'ANOTHER SET OF INPUT VALUES? (Y/N)'
4340              ACCEPT20,ANS
4350     C        ANOTHER SET OF INPUT DATA FOR THE SAME INVERTED MATRIX?
4360              IF (ANS.EQ.'Y') GO TO 330
4370              END
4380     C        THE SUBROUTINES
4390              COMPLEX FUNCTION BT(L)
4400              REAL A,B,K,E,D,BP,PI,L
4410              INTEGER P,Q,N,M
4420              COMMON P,Q,N,M,A,B,K,E,D,DX,DY
4430              PI=3.1415926
4440              BP=K**2-((N*PI/A)**2+(M*PI/B)**2)
4450              IF (BP.LT.0) THEN
4460                BT=(0,-1.0)*SQRT(ABS(BP))
4470              ELSE
4480                BT=SQRT(BP)
4490              END IF
4500              RETURN
4510              END
4520              REAL FUNCTION TP(P,N,G,PM,T1)
4530              REAL G,PM,SP,SM,PI,G2,AL,DM,T,T1
4540              INTEGER P,N
4550              AL=(.001*G)**2
4560              PI=3.1415926
4570              SP=P+N
4580              SM=P-N
4590              G2=2.0*G
4600              DM=0
4610              T=ABS(T1)
4620              IF (SM.EQ.0) DM=1.0
4630              IF (SP.EQ.0) THEN
4640                TP=2*(G-T)*(1-PM)/G2
4650              ELSE
4660                TP=(PM*COS(SM*PI*T/G2)*(1+COS(SP*PI))*
4670     1 SIN(SP*PI*T/G2)/(SP*PI/G2)-
4680     2 COS(SP*PI*T/G2)*(1+COS(SM*PI))*
4690     3 (SIN(SM*PI*T/G2)/(SM*PI/G2+AL)+DM*(T-G)))/G2
4700              END IF
4710              RETURN
4720              END
4730              REAL FUNCTION RP(P,N,G,PM,T)
4740              REAL G,PM,T,PM,PI,AL
4750              INTEGER P,N
4760              PI=3.1415926
4770              AL=(.001*G)**2
4780              RP=(G/2.0)*(PM*(SIN(P*PI*T/G)-SIN(N*PI*T/G))*
4790     1 (1-COS((P+N)*PI))/((P+N)*PI+AL)-
4800     2 (SIN(P*PI*T/G)+SIN(N*PI*T/G))*
4810     3 (1-COS((P-N)*PI))/((P-N)*PI+AL))/G
4820              RETURN
4830              END
4840              COMPLEX FUNCTION DBLINT(AX,AY,BX,BY,F)
4850              REAL AX,AY,BX,BY,H2,S(21),X,I,HI
4860              INTEGER N
```

```
4870            COMPLEX F,DP
4880            DATA S/1,4,2,4,2,4,2,4,2,4,2,4,2,4,2,4,2,4,2,4,1/
4890            N=20
4900            H1=(AY-AX)/N
4910            H2=(BY-BX)/N
4920            DP=0
4930            DO 20 L1=0,N
4940              DO 10 L2=0,N
4950                X=L1*H1+AX
4960                Y=L2*H2+BX
4970                DP=DP+F(X,Y)*S(L1+1)*S(L2+1)
4980    10        CONTINUE
4990    20      CONTINUE
5000            DBLINT=DP*H1*H2/9.0
5010            RETURN
5020            END
5030            COMPLEX FUNCTION Y1(U,W)
5040            REAL U,W,A,B,E,K,D,AL,TP
5050            COMPLEX YP
5060            INTEGER P,Q,N,M
5070            COMMON P,Q,N,M,A,B,K,E,D,DX,DY
5080            AL=(A*.001)**2
5090            YP=CEXP((0,-1.0)*K*SQRT(U**2+W**2))/SQRT(U**2+W**2+AL)
5100            YP=YP*TP(P,N,A,D,U)*TP(Q,M,B,-1.0*D,W)*E
5110            IF (P.EQ.N .AND. Q.EQ.M) THEN
5120              Y1=YP-4.0/SQRT(U**2+W**2+AL)
5130            ELSE
5140              Y1=YP
5150            END IF
5160            RETURN
5170            END
5180            COMPLEX FUNCTION H1(X,W)
5190            REAL D,A,B,K,E,X,W,AL,TP,PI
5200            COMPLEX HP
5210            INTEGER P,Q,N,M
5220            COMMON P,Q,N,M,A,B,K,E,D,DX,DY
5230            AL=(A*.001)**2
5240            PI=3.1415926
5250            HP=CEXP((0,-1.0)*K*SQRT(W**2+X**2))/SQRT(X**2+W**2+AL)
5260            1 -COS(P*PI)*CEXP((0,-1.0)*K*SQRT((A-X)**2+W**2))/
5270            2 SQRT((A-X)**2+W**2+AL)
5280            HP=HP*SIN(N*PI*X/A)
5290            H1=HP*TP(Q,M,B,-1.0,W)
5300            RETURN
5310            END
5320            COMPLEX FUNCTION H2(U,Y)
5330            REAL U,Y,D,K,A,B,E,AL,TP,PI
5340            INTEGER P,Q,N,M
5350            COMPLEX HP
5360            COMMON P,Q,N,M,A,B,K,E,D,DX,DY
5370            AL=(A*.001)**2
5380            PI=3.1415926
5390            HP=CEXP((0,-1.0)*K*SQRT(U**2+Y**2))/SQRT(U**2+Y**2+AL)-
5400            1 COS(Q*PI)*CEXP((0,-1.0)*K*SQRT(U**2+(B-Y)**2))/
5410            2 SQRT(U**2+(B-Y)**2+AL)
5420            HP=HP*SIN(M*PI*Y/B)
5430            H2=HP*TP(P,N,A,-1.0,U)
5440            RETURN
5450            END
5460            COMPLEX FUNCTION G(X,Y)
5470            REAL X,Y,PI,K,R,AL
5480            COMMON P,Q,N,M,A,B,K,E,D,DX,DY
5490            PI=3.1415926
5500            R=SQRT(X**2+Y**2)
5510            G=CEXP((0,-1.0)*K*R)/(2*PI*R)
5520            RETURN
5530            END
5540            COMPLEX FUNCTION I1(U,W)
5550            REAL U,W,TP,HP,A,B,K,D,DX,DY
5560            COMPLEX G,IP
5570            INTEGER P,Q,N,M
5580            COMMON P,Q,N,M,A,B,K,E,D,DX,DY
5590            IP=(1/4.0)*(TP(P,N,A,1.0,U)+HP(P,N,A,1.0,U))*
5600            1 (TP(Q,M,B,-1.0,W)+HP(Q,M,B,-1.0,W))*
5610            2 G(U-DX,W-DY)
5620            I1=IP
5630            RETURN
5640            END
5650            COMPLEX FUNCTION I2(U,W)
5660            REAL U,W,TP,HP,A,B,K,D,DX,DY
5670            COMPLEX G,IP
```

```
5680            INTEGER P,Q,N,M
5690            COMMON P,Q,N,M,A,B,K,E,D,DX,DY
5700            IP=(1/4.0)*(IP(P,N,A,-1.0,U)+RP(P,N,A,-1.0,U))*
5710           1 (IP(Q,M,B,1.0,W)+RP(Q,M,B,1.0,W))*
5720           2 G(U-DX,W-DY)
5730            I2=IP
5740            RETURN
5750            END
5760            COMPLEX FUNCTION I3(X,W)
5770            REAL X,W,TP,RP,A,B,K,D,DX,DY,PI,E
5780            COMPLEX G,IP
5790            INTEGER P,Q,N,M
5800            COMMON P,Q,N,M,A,B,K,E,D,DX,DY
5810            PI=3.1415926
5820            IP=(P*PI/(A*A*2))*SIN(N*PI*X/A)
5830            IP=IP*(G(Q-X-DX,W-DY)-COS(P*PI)*G(A-X-DX,W-DY))
5840            I3=IP*(IP(Q,M,B,-1.0,W)+RP(Q,M,B,-1.0,W))
5850            RETURN
5860            END
5870            COMPLEX FUNCTION I5(X,W)
5880            REAL X,W,IP,RP,A,B,K,D,DX,DY,PI,E
5890            COMPLEX G,IP
5900            INTEGER P,Q,N,M
5910            COMMON P,Q,N,M,A,B,K,E,D,DX,DY
5920            PI=3.1415926
5930            IP=(Q*PI/(B*A*2))*SIN(N*PI*X/A)
5940            IP=IP*(G(Q-X-DX,W-DY)-COS(P*PI)*G(A-X-DX,W-DY))
5950            I5=IP*(IP(Q,M,B,-1.0,W)+RP(Q,M,B,-1.0,W))
5960            RETURN
5970            END
5980            COMPLEX FUNCTION I4(U,Y)
5990            REAL U,Y,TP,RP,A,B,K,D,DX,DY,PI,E
6000            COMPLEX G,IP
6010            INTEGER P,Q,N,M
6020            COMMON P,Q,N,M,A,B,K,E,D,DX,DY
6030            PI=3.1415926
6040            IP=(P*PI/(2.0*A*B))*SIN(M*PI*Y/B)
6050            IP=IP*(G(U-DX,Q-Y-DY)-COS(Q*PI)*G(U-DX,B-Y-DY))
6060            I4=IP*(IP(P,N,A,-1.0,U)+RP(P,N,A,-1.0,U))
6070            RETURN
6080            END
6090            COMPLEX FUNCTION I6(U,Y)
6100            REAL U,Y,TP,RP,A,B,K,D,DX,DY,PI,E
6110            COMPLEX G,IP
6120            INTEGER P,Q,N,M
6130            COMMON P,Q,N,M,A,B,K,E,D,DX,DY
6140            PI=3.1415926
6150            IP=(Q*PI/(2.0*B*B))*SIN(M*PI*Y/B)
6160            IP=IP*(G(U-DX,Q-Y-DY)-COS(Q*PI)*G(U-DX,B-Y-DY))
6170            I6=IP*(IP(P,N,A,-1.0,U)+RP(P,N,A,-1.0,U))
6180            RETURN
6190            END
6200            REAL FUNCTION EF(P,Q,N,M)
6210            REAL E
6220            INTEGER P,Q,N,M
6230            E=16.0
6240            IF (Q.EQ.0) E=E/2.0
6250            IF (M.EQ.0) E=E/2.0
6260            IF (P.EQ.0) E=E/2.0
6270            IF (N.EQ.0) E=E/2.0
6280            EF=SQRT(E)
6290            RETURN
6300            END
6310            COMPLEX FUNCTION JMX(T,PH,N1,M1)
6320            REAL T,PH,E1,PI,KX,KY,K,A,B,G1
6330            INTEGER N1,M1
6340            COMMON P,Q,N,M,A,B,K,E,D,DX,DY
6350            PI=3.1415926
6360            G1=(.001*A)**2
6370            E1=4.0
6380            IF (N1.EQ.0) E1=E1/2
6390            IF (M1.EQ.0) E1=E1/2
6400            E1=SQRT(E1)
6410            KX=SIN(T)*COS(PH)*K
6420            KY=SIN(T)*SIN(PH)*K
6430            IF (PH.EQ.0) THEN
6440              IF (M1.EQ.0) THEN
6450                JMX=E1*(N1*PI)*(1-COS(N1*PI)*CEXP((0,1.0)*KX*A))/((N1*PI/A)
6460           1 **2-KX**2)
6470              ELSE
6480                JMX=0
```

```
6490              END IF
6500            ELSE
6510              IF (M1.EQ.0 .AND. T.EQ.0) THEN
6520                JMX=-E1*(1-COS(N1*PI))*B/(N1*PI/A)
6530              ELSE
6540                JMX=E1*(N1*PI/A)*((0,1.0)*KY)*(1-COS(N1*PI)*
6550           1 CEXP((0,1.0)*KX*A))*(CEXP((0,1.0)*KY*B)*COS(M1*PI)-1)/
6560           2 (((N1*PI/A)**2-KX**2+G1)*((M1*PI/B)**2-KY**2+G1))
6570              END IF
6580            END IF
6590            RETURN
6600            END
6610      C     ADD SYMMETRIC MATRIX PART
6620      C     ADD EASIER PHASE ENTRY
6630            COMPLEX FUNCTION JMY(T,PH,N1,M1)
6640            REAL T,PH,E1,PI,KX,KY,K,A,B,G1
6650            INTEGER N1,M1
6660            COMMON P,Q,N,M,A,B,K,E,D,DX,DY
6670            PI=3.1415926
6680            G1=(.001*A)**2
6690            E1=4.
6700            IF(N1.EQ.0) E1=E1/2.
6710            IF(M1.EQ.0) E1=E1/2.
6720            E1=SQRT(E1)
6730            KX=K*SIN(T)*COS(PH)
6740            KY=K*SIN(T)*SIN(PH)
6750            IF (T.EQ.0) THEN
6760              JMY=0
6770            ELSE
6780              JMY=E1*(M1*PI/B)*(1-COS(N1*PI)*CEXP((0,1.)*KX*A))*
6790           1 (0,1.)*KX*(COS(M1*PI)*CEXP((0,1.)*KY*B)-1)/((
6800           2 (N1*PI/A)**2-KX**2)*((M1*PI/B)**2-KY**2)+G1)
6810            END IF
6820            RETURN
6830            END
6840            SUBROUTINE PLOT(X,Y)
6850            REAL X(91),Y(91)
6860            CALL INITT(240)
6870            CALL BINITT
6880            CALL DLIMY(-60.,0)
6890            CALL NPTS(91)
6900            CALL CHECK(X,Y)
6910            CALL DSPLAY(X,Y)
6920            CALL TKPAUSE
6930            CALL INITT(240)
6940            CALL FINITT(0,767)
6950            RETURN
6960            END
6970      C     THIS INCLUDES THE 45 DEG. PLOTS
6980            REAL FUNCTION DBCON(X,Y)
6990            REAL X,Y
7000            X=X/Y
7010            IF (X.LE.0.001) X=.001
7020            DBCON=20*LOG10(X)
7030            RETURN
7040            END
```

APPENDIX B

USER INSTRUCTIONS

The computer program discussed in this report and presented in Appendix A is currently on the Research Computer Labs VAX under the file name: MCOUPL. It is written in FORTRAN and can handle large matrices, on the order of 300 x 300 (the user is warned that tests of matrices larger than 125 x 125 have never been done and round-off error may be a problem). The following is the user instructions, and before proceeding the notation used must be explained. In the examples shown, the underlined terms are the user entered responses, while the rest are the computer generated phrases and questions. The * signifies a return. The examples to be discussed are presented at the end of this section, with added circled numbers signifying the step numbers referred to in the text.

The program is written so that the computer will prompt the user for the necessary data. There are a few factors that are held constant throughout the array and they are entered first. The constant factors are the a and b dimensions of the apertures entered in wavelengths, the spacing between each row and between each element in each row again in wavelengths, the wavelength entered in meters and finally the number of and type of ψ_{nm} and Φ_{nm} to be used in the approximation. These are values that typically remain constant throughout standard waveguide arrays. In the sample runs, shown at the end of this section, steps 1-3 are the ones where the above mentioned data is entered. In step 1, after inputting the number of ψ and Φ the computer will ask for the mode index nm one at a time. The order that these are entered

should be remembered because it will be important later. The ψ_{10} must always be the first modal function entered. Steps 2 and 3 are self explanatory.

Step 4 is the point where the user has the choice of whether to take advantage of an array configuration entry system that is designed specifically for arrays of rectangular or triangular lattice or to use the general entry system. In the steps that will follow, the user enters the array configuration and if it is one of the regular lattices it can be entered much easier under the system mentioned above. As we will see later, this approach will also allow for easier entry of regular phase shifts in the driven fields used when scanning the beam. The regular lattice approach will be looked at first and the general method will be discussed in a later example (see steps 12 and 13) The array must have at least 2 rows to use the regular lattice method.

After a "Y" is entered (note: in all the Y/N questions, the Y must be upper case) the computer is in the regular lattice mode. Under this system the user enters the number of apertures and the row off-set (in λ) for the even numbered rows and for the odd numbered rows once each. The way the computer numbers rows and apertures is shown in Fig. A.1 The rows always count up and the apertures from left to right. The configuration entered in step 4 is the one shown in Fig. A.1a. Figure A.1b shows what is meant by a row off-set and as to how it allows for entry of triangular lattice arrays. If the array of Fig. A.1b were entered instead, 3 rows would have been entered in step 3 and for the odd numbered rows an offset of .5 would have been entered. Figure A.1 also illustrates the types of arrays that can be

handled by each configuration entry system.

After this, the computer will print out the D_x and D_y of each aperture in meters in the order of the aperture numbers. The first number is the aperture number, the next the D_x and the last the D_y. After this the computer will calculate the admittance parameters. Once this is complete, the user has the opportunity to view them by entering a "Y" in step 5. The computer will then print first the column number and then the row number of each parameter's location in the admittance matrix. The value of the admittance is given in standard FORTRAN complex number representation (the real part comes first, followed by the imaginary part, seperated by a comma). If a "N" is entered the computer would go directly to Step 6.

Step 6 is where the user tells the computer how to drive the array in calculating the modal amplitudes and then the radiation patterns. The user must enter how many elements, and if it's less than the total number which elements are to be driven. Also the phase of the driving field of the elements must be entered. The computer always drives the first ψ_{nm} of each driven aperture with a TE_{10} mode, so the user must make sure to always enter the 10 mode first in step 1 as was done here. Under the regular lattice system the user has 3 different ways to enter the driven element data. The first is shown in steps 6 and 7. If the number of driven elements equals the total number of elements then the computer will ask if a constant phase for each should be used. If "Y" is entered here, then all will be equally driven with zero phase. The case of "N" entered under con-

stant phase is shown in step 11. Here the computer asks for the phase shift between each element in a row (call it β here) and the phase shift between each row (call it α here), both entered in degrees. The added phase for each aperture then equals $(n-1)\beta + (m-1)\alpha$ where n is the column number and m is the row number of the aperture. This way, aperture #1 will always have 0° of added phase shift. For rectangular lattices this allows the user to easily scan the beam. There is a problem with this system when using a triangular lattice. Since the computer always assigns the first aperture of each row to column #1 and since the apertures aren't co-linear in the vertical direction this will cause problems in these cases. This will be corrected in the next update of the software, but for now if you wish to scan beams in a triangular lattice use the general approach and enter the phase of each aperture one at a time. The third and final situation is shown in step 10. If less than the total number of elements is entered then the user must enter the element number and it's added phase for each element to be driven. After each element number and it's corresponding phase, a return must be entered as shown here or else the computer will not input the data properly. The steps that follow each of these situations are the same and will be discussed next, using the example steps 7-10.

Shown after step 7 is the next question: That of whether to view the tested incident magnetic field column matrix (see page 27.) If a "Y" is entered, the elements are printed out in order, as shown. Notice how it's the first modal function of each aperture that is driven and with zero phase in this example. Directly after this, or

after a "N" is entered above, the computer prints out the normalized modal amplitudes of each modal function. The order of these amplitudes is the order of the apertures (as numbered before), where within each aperture the order of the modal functions is the same order as entered in Step 1. In this example, there were 4 modes per aperture so the first 4 amplitudes are the ones of aperture #1, the next 4 for aperture #2 and so on. The modes of each aperture then are in the order of ψ_{10}, ψ_{12}, ψ_{30}, and Φ_{12} as entered in Step # 1. So the first amplitude is the ψ_{10} of aperture #1, the second ψ_{12} and so on.

In Step 9, the user decides whether to view the plots of the radiation pattern. If a "Y" is entered, then the patterns will appear one at a time in the following order. 1) $\phi = 90°$ co-polarized, 2) $\phi = 0°$ co-polarized, 3) $\phi = 45°$ co-polarized and, 4) $\phi = 45°$ cross-polarized. After each plot has been viewed, hitting the return will bring up the next pattern until the last plot. Hitting the return after viewing the last plot brings back the program.

After the plot question, the user has a choice, to input a new set of values for the driven elements or to exit the program (see Step 10). A "N" entered here and the program exists. A "Y" and the computer returns to Step 6 and proceeds exactly as before. In the example shown, a "Y" was entered in Steps 10, and right before Step 11 in order to enter different sets of driven elements for the same array. This way the user can scan the beam or change the number of driven elements several times on the same array configuration without going through the redundant procedure of having the computer recompute the admittance parameters.

Finally Steps 12 and 13 show how the general array configuration entry system works. If a "N" was entered when the computer asked if the regular lattice approach was to be used, the user will be prompted to input the number of elements and row offset for each row in the array one at a time. The example shown in 12 and 13 is the array of Figure A.1b. After these steps the computer proceeds exactly as before with one exception. When the user drives all the elements as in Step 6 he has the choice to drive all with constant phase, as before, but if a "N" is entered there the user then must enter the element numbers and their phases one at a time similar to what was done in Step 10. The user does not have the option to use the phase method shown in Step 11. If less then the total number are driven, it is handled exactly as before.

As a final comment, the meaning of the normalized modal amplitudes will be discussed. The printed values are the normalized equivalent magnetic current amplitudes ($\underline{J}_m$), not the normalized aperture field amplitudes (see Appendix C for the differences between the two). The currents are always normalized by an incident ψ_{10} term of 0° added phase, so when entering the phases of the driven modes always make the reference phase 0°. The usefulness of this type of result is readily apparent (see App. C). If only aperture i is driven (with 0° phase), then the resulting values of the normalized ψ_{10} amplitude term of aperture j is the $S_{TE_{10}i,\ TE_{10}j}$ term. For arrays of square apertures the value of the normalized modal amplitude of the ψ_{01} term in aperture j then is the $S_{TE_{10}i,\ TE_{01}j}$. Finally, the normalized value of the driven aperture's ψ_{10} amplitude gives $1 + \Gamma_i$ for

that guide. So by driving only one guide with zero phase the computer will output the scattering parameters for coupling between the driven guide and it's neighboring undriven guides and the reflection coefficient of the driven aperture.

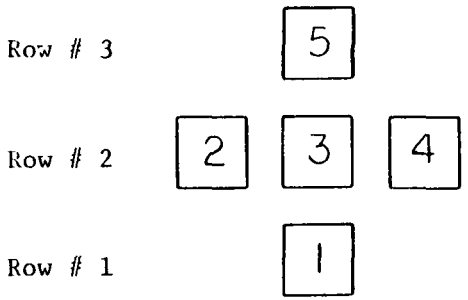

Figure A.1c Both

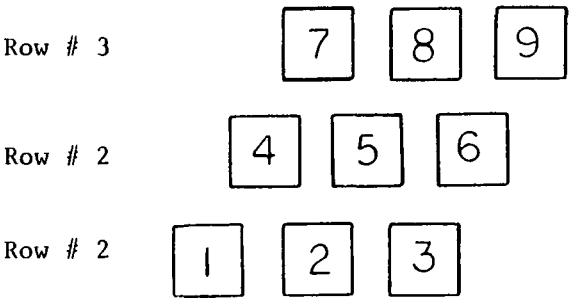

Figure A.1d General Only

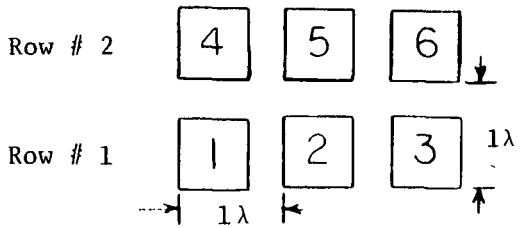

Figure A.1a Both

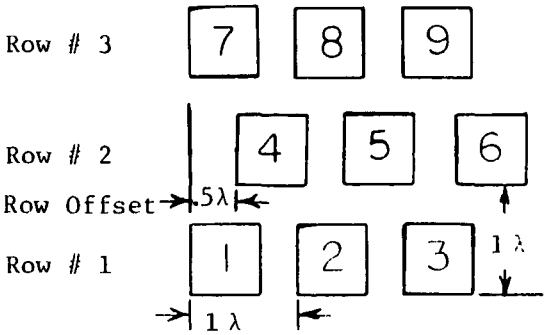

Figure A.1b Both

Figure A.1a-d Different Arrays and Which Entry System Can Be Used.

```
INPUT THE # PSI AND PHI FUNCTIONS
3,1*                                                              (1)
INPUT THE            1PSI COEFF.:
1,0*
INPUT THE            2PSI COEFF.:
1,2*
INPUT THE            3PSI COEFF.:
3,0*
INPUT THE            1PHI COEFF.:
1,2*
INPUT A/LAMBDA ,B/LAMBDA AND LAMBDA                               (2)
.6,.6,.015*
ALL SPACINGS ARE TO BE GIVEN IN FRACTIONS OF LAMBDA               (3)
INPUT THE # OF ROWS AND SPACING BETWEEN THE ROWS
2,1.*
INPUT THE SPACING BETWEEN ELEMENTS WITHIN A ROW
1.*
REGULAR LATTICE ARRAY? (Y/N)                                      (4)
Y*
INPUT THE EVEN ROWS # OF GUIDES & ROW OFFSET
3,0*
INPUT THE ODD ROWS # OF GUIDES & ROW OFFSET
3,0*
DX,DY            1  0.0000000E+00  0.0000000E+00
DX,DY            2  1.5000000E-02  0.0000000E+00
DX,DY            3  2.9999999E-02  0.0000000E+00
DX,DY            4  0.0000000E+00  1.5000000E-02
DX,DY            5  1.5000000E-02  1.5000000E-02
DX,DY            6  2.9999999E-02  1.5000000E-02
PRINT MATPIX? (Y/N)                                               (5)
Y*
MATRIX           1           1 (12.27046966552734,-517.9987182617188)
MATRIX           1           2 (-30.51866722106934,54.47422790527344)
MATRIX           1           3 (53.73537826538086,-70.30246734619141)
MATRIX           1           4 (71.57903289794922,-26.94529342651367)
MATRIX           1           5 (1.308216094970703,19.72079849243164)
                                .
                                .
                                .
INPUT THE # OF DRIVEN GUIDES                                      (6)
6*
CONSTANT PHASE FOR EACH? (Y/N)                                    (7)
Y*
PRINT COLUMN  MATRIX? (Y/N)
Y*
VI: (-1.2110380771835904E+16,0.0000000000000000E+00)
VI: (0.0000000000000000E+00,0.0000000000000000E+00)
VI: (0.0000000000000000E+00,0.0000000000000000E+00)
VI: (0.0000000000000000E+00,0.0000000000000000E+00)
VI: (-1.2110380771835904E+16,0.0000000000000000E+00)
VI: (0.0000000000000000E+00,0.0000000000000000E+00)
VI: (0.0000000000000000E+00,0.0000000000000000E+00)
VI: (0.0000000000000000E+00,0.0000000000000000E+00)
VI: (-1.2110380771835904E+16,0.0000000000000000E+00)
VI: (0.0000000000000000E+00,0.0000000000000000E+00)
                                .
                                .
                                .
```

```
THE NORMALIZED OUTPUT VECTOR IS:                                          (8)
V(           1)= (0.9525498,-6.5083817E-02),  0.9547706      -3.908711
V(           2)= (0.1387619,-9.7904637E-02),  0.1698240      -35.20520
V(           3)= (2.6979776E-02,-4.0551741E-02),  4.8706800E-02  -56.36349
V(           4)= (-2.4122884E-02,6.4293578E-02),  6.8670064E-02  -69.43397
V(           5)= (0.9735299,-4.6621375E-02),  0.9746456      -2.741743
V(           6)= (0.1327942,-9.0362079E-02),  0.1606225      -34.23400
V(           7)= (2.4720680E-02,-4.1649926E-02),  4.8433751E-02  -59.30940
V(           8)= (-1.8278474E-02,7.0564717E-02),  7.2893634E-02  -75.47779
V(           9)= (0.9525498,-6.5083809E-02),  0.9547706      -3.908710
V(          10)= (0.1387620,-9.7904630E-02),  0.1698240      -35.20520
V(          11)= (2.6979776E-02,-4.0551744E-02),  4.8706800E-02  -56.36349
V(          12)= (-2.4122884E-02,6.4293578E-02),  6.8670064E-02  -69.43397
V(          13)= (0.9525498,-6.5083809E-02),  0.9547706      -3.908710
V(          14)= (0.1387620,-9.7904630E-02),  0.1698240      -35.20520
V(          15)= (2.6979776E-02,-4.0551744E-02),  4.8706800E-02  -56.36349
V(          16)= (-2.4122884E-02,6.4293578E-02),  6.8670064E-02  -69.43397
V(          17)= (0.9735299,-4.6621375E-02),  0.9746456      -2.741743
V(          18)= (0.1327942,-9.0362079E-02),  0.1606225      -34.23400
V(          19)= (2.4720680E-02,-4.1649926E-02),  4.8433751E-02  -59.30940
V(          20)= (-1.8278474E-02,7.0564717E-02),  7.2893634E-02  -75.47779
V(          21)= (0.9525498,-6.5083817E-02),  0.9547706      -3.908711
V(          22)= (0.1387619,-9.7904637E-02),  0.1698240      -35.20520
V(          23)= (2.6979776E-02,-4.0551741E-02),  4.8706800E-02  -56.36349
V(          24)= (-2.4122884E-02,6.4293578E-02),  6.8670064E-02  -69.43397
PLOT? (Y/N)
N                                                                         (9)
ANOTHER SET OF INPUT VALUES? (Y/N)                                        (10)
Y*
INPUT THE # OF DRIVEN GUIDES
3*
INPUT THE GUIDE #'S THAT ARE DRIVEN &IT'S PHASE(DEG)
1,0*
2,0*
3,0
WILL ASSUME TE10 MODE IN EACH
PRINT COLUMN  MATRIX? (Y/N)
N *
THE NORMALIZED OUTPUT VECTOR IS:
V(           1)= (0.9562839,-2.7126919E-02),  0.9566686      -1.624875
V(           2)= (0.1217258,-8.5655443E-02),  0.1488423      -35.13311
V(           3)= (2.2908077E-02,-3.8559444E-02),  4.4850983E-02  -59.28555
V(           4)= (-1.3244004E-03,5.0520133E-02),  5.0537493E-02  -88.49832
                          .
                          .
                          .

ANOTHER SET OF INPUT VALUES? (Y/N)
Y *
INPUT THE # OF DRIVEN GUIDES                                              (11)
6 *
CONSTANT PHASE FOR EACH? (Y/N)
N *
INPUT THE PHASE SHIFT BETWEEN ELEMENTS IN A ROW
30*
INPUT THE PHASE SHIFT BETWEEN ROWS
30 *
PRINT COLUMN  MATRIX? (Y/N)
```

```
ALL SPACINGS ARE TO BE GIVEN IN FRACTIONS OF LAMBDA                    (12)
INPUT THE # OF ROWS AND SPACING BETWEEN THE ROWS
3,1*
INPUT THE SPACING BETWEEN ELEMENTS WITHIN A ROW
1 *
REGULAR LATTICE ARRAY? (Y/N)
N *
 INPUT THE # OF APP. IN ROW#   1  AND THE ROW OFFSET                    (13)
3,0*
 INPUT THE # OF APP. IN ROW#   2  AND THE ROW OFFSET
3,0*
 INPUT THE # OF APP. IN ROW#   3  AND THE ROW OFFSET
3,0*
DX,DY            1  0.0000000E+00  0.0000000E+00
DX,DY            2  1.5000000E-02  0.0000000E+00
DX,DY            3  2.9999999E-02  0.0000000E+00
DX,DY            4  0.0000000E+00  1.5000000E-02
DX,DY            5  1.5000000E-02  1.5000000E-02
DX,DY            6  2.9999999E-02  1.5000000E-02
DX,DY            7  0.0000000E+00  2.9999999E-02
DX,DY            8  1.5000000E-02  2.9999999E-02
DX,DY            9  2.9999999E-02  2.9999999E-02
```

APPENDIX C

RESULT NORMALIZATION

The results shown in Chap. 3 are the normalized aperture electric field modal amplitudes, normalized by the incident field amplitude. The program, on the other hand, will output the normalized magnetic current ($\underline{J}_m$) modal amplitudes. The differences between the two and the reason for outputting the normalized currents is the topic of this appendix.

The computer model solves for the $\underline{J}_m$ modal amplitudes. Since $\underline{E}_{apert.} = \underline{a}_z \times \underline{J}_m$ and $\underline{J}_m = \sum_{n,m} C_{nm} \psi_{nm} \underline{a}_x + \sum_{n,m} D_{nm} \Phi_{nm} \underline{a}_y$

then $\underline{E}_{apert.} = - \sum_{n,m} C_{nm} \psi_{nm} \underline{a}_y + \sum_{n,m} D_{nm} \Phi_{nm} \underline{a}_x$.

The $\underline{E}^{INC}$ normalization term has an extra minus sign relative to the $\underline{J}_m$ normalization term. The difference between the normalized $\underline{J}_m$ and the normalized $\underline{E}_a$ is that the signs on the D_{nm} terms are changed and the $\underline{a}_x$ and $\underline{a}_y$'s interchanged. Thus taking the negative of the Φ_{nm} amplitude terms from the computer outputs and assigning the proper $\underline{a}_x$ and $\underline{a}_y$ is required to get the normalized $\underline{E}_a$ functions.

The reason for outputting the results in terms of normalized $\underline{J}_m$ is that this leads directly to the scattering parameters. Scattering matrix parameters are defined using the TE waveguide modal functions. These modal functions by definition have opposite signs for the $\underline{a}_x$ and $\underline{a}_y$ terms (see the modal function used by Harrington in Sec. 2.3 for example). This negative sign cancels the one needed to convert the currents to field quantities. So by leaving it this way, if only one aperture is driven in an array of square guides, the value of the

normalized Φ_{01} amplitude in a neighboring guide gives the scattering parameter for coupling between the TE_{10} of the driven guide and the TE_{01} of the undriven guide. If $\underline{E}_a$ terms were outputted it would equal the negative of this S parameter. The value of the normalized ψ_{10} amplitudes are the scattering parameters between the driven TE_{10} and the undriven TE_{10} in both cases. It must be remembered that this is only so if only one guide is driven in the array with zero degrees added phase.

The value of the amplitude used to normalize the $\underline{E}_a$ term is: $E^{INC} = -\frac{\beta_{10} A_{10}}{j\varepsilon_0}$.